The Role of Complement in Retinal Ganglion Cell Loss in Glaucoma

Stephen Daniel Cross

Thesis submitted to Cardiff University in accordance with the requirements for the degree of Doctor of Philosophy

Visual Neurosciences and Molecular Biology Group

School of Optometry and Vision Sciences

Cardiff University

September 2012

Contents

Acknowledgments

I would like to thank my supervisors Professor James Morgan and Professor Paul Morgan for their guidance and support.

I am grateful to Dr Claire Harris, Dr Meike Heurich and Dr Svetlana Hakobyan for the C3b/iC3b and C1-inhibitor antibodies which were crucial to my experiments.

I would like to express my gratitude to Dr Debbie Tudor, Dr Paulina Samsel, Dr Lillian Kisiswa, Dr Gill Smith and Dr Claudia Calder for their supervision and guidance throughout my PhD.

I would also like to thank fellow students Hannah Jones, Ed Pritchard, Rebecca Thirgood, Amanda Mui, Caroline Waters, Beth Flynn, James Tribble, Pete Williams and Chris Dillingham for their tireless support and bonhomie during my time here.

I am also grateful to my family and my partner Andrea Griffiths for supporting me through my life during this time.

Contributions

The majority of the work presented here is my own, however I recognise the following people for their contributions.

Dr Guy Jones, for the electron microscopy of the paramagnetic microspheres.

Dr Paulina Samsel and Dr Lillian Kisiswa for the protocols and tissue used in the early stages of the development of the bead model of glaucoma.

Dr Debbie Tudor for performing the microsphere MTT toxicity assay.

Dr Jon Erichsen for maintaining the project licence I used for all my work.

Dr Gill Smith and Mr Nick White for the protocols used to section tissue and image fluorescence with confocal microscopy respectively.

Andrew Rankmore, for the production of the Perspex chambers for the *in vitro* hydrostatic pressure elevation experiments.

Dr Claudia Calder, for the immunofluorescent detection of C1q in glaucomatous retinal sections.

Summary of Thesis

Glaucoma is an umbrella term for a number of related optic neuropathies which have the common pathology of a progressive, irreversible vision loss associated with atrophy of retinal ganglion cells. Together, the various forms of glaucoma constitute the second leading cause of vision loss in the developed world. Current therapies for the treatment of glaucoma focus on alleviating the primary risk factor, an elevation in intraocular pressure. These treatments are effective at mitigating the progression of vision loss however they cannot recover vision and do not completely halt vision loss, limiting their use as treatments. To better understand the biology underlying the loss of retinal ganglion cells in glaucoma, I have examined the role of complement in retinal ganglion cell loss. Complement is a network of cross-reacting serine proteases which form part of the humoral immune system and are primarily responsible for clearance of apoptotic cells and defence against pathogens.

To understand the role played by complement in glaucoma I used an inducible model of glaucoma to establish the complement activation occurs in the glaucomatous retina. I then used the inhibitor of the classical complement cascade, C1 inhibitor to protect the dendrites and cell bodies of retinal ganglion cells and found that this protection did not prevent axonal degeneration. Using *in vitro* and *in vivo* animal models of complement deficiency I established that deficiency in complement components C3 and C6 which are further down the cascade, exacerbates damage suffered in hypertensive glaucoma.

This study adds to the existing evidence that the role of complement in central nervous system degeneration is a complex, multifactorial process, with elements of the complement system being variously protective and damaging. It does, however, add hope to the prospect of developing a treatment for glaucomatous optic neuropathy based on manipulation of the complement system.

Chapter One: General Introduction

1.1 Glaucoma

Glaucoma is the collective term for a number of related optic neuropathies which are characterised by progressive, irreversible degeneration of the retinal ganglion cells and associated visual field loss. Globally, glaucoma is the second most common cause of blindness after age-related macular degeneration and it has been projected that, by 2020, more than 11 million people will suffer from bilateral blindness as a result of glaucoma (Resnikoff *et al*. 2004; Quigley & Broman 2006a; Cook & Foster 2012).

1.1.1 Risk factors

An elevation in intraocular pressure is the primary identified risk factor for glaucoma and the reduction in intraocular pressure is the primary focus of glaucoma treatment, this has been shown to be effective in mitigating the progression of glaucoma (Heijl et *al.* 2002; The Advanced Glaucoma Intervention Study, 2000). It is however a recurrent finding of glaucoma treatment that intraocular pressure reduction does not always correlate with a reduction in vision loss and does not halt the progressive decline in the visual field.

Primary open angle glaucoma is characterised by an elevation in intraocular pressure with no apparent underlying cause. Genetic factors have been identified which are strongly associated with an increased likelihood of developing the disease. The gene encoding for the protein myocilin (previously known as TIGR) has been identified as a significant risk factor for primary open angle glaucoma (Tamm 2002; Kim *et al*. 2001; Stone *et al.* 1997). Although the exact mechanism underlying this effect is unknown, it has been hypothesised that mutations in regulatory genes or exposure to certain steroids can redirect myocilin to accumulate in peroxisomes of

trabecular meshwork cells (Shepard *et al*. 2007). These cells then become enlarged and cease to function as an effective outflow for aqueous humour, causing an increase pressure within the eye. Numerous genetic factors have been identified which contribute to the risk of developing glaucoma, reviewed in Allingham, Liu, & Rhee, (2009).

Unlike primary open angle glaucoma, angle closure glaucoma is a secondary syndrome produced by an identifiable, structural/anatomical defect such as pigment dispersion from the iris or congenital malformation in the anterior chamber. Risk factors for glaucoma secondary to pigment dispersion are male gender, black race and high myopia (Farrar et *al*. 1989). Secondary glaucoma may also develop from malformations of the anterior chamber such as Peters anomaly or Axenfeld-Rieger syndrome (DeLuise & Anderson 1983). Secondary glaucomas typically cause bilateral presentation and an acute elevation in intraocular pressure (Lindberg 1989).

1.1.2 Pathophysiology

The pathophysiology of glaucoma is dependent on a number of factors, including age, race, gender, myopia and intraocular pressure. The typical pattern of progression in glaucoma is bilateral but asymmetric and corresponds to a thinning in the retinal nerve fibre layer (Bertuzzi *et al*. 2009). Visual field loss typically conforms to a specific topology which varies between species between a superior-inferior 'hourglass' pattern in humans (Quigley *et al*. 1982) and higher primates (Quigley & Addicks 1980a) and a preferential loss of nasal neurones in the DBA/2J mouse (Jakobs et *al.* 2005).

Glaucoma is marked by an increase in the expression of pro-apoptotic agents in the retina, including markers of physiological stress; adenosine triphosphate

synthase enzymes, caspases, and proteins of the classical complement cascade particularly the subcomponents of the initiator molecule; complement component 1 (C1) (Tezel *et al*. 2010; Yang *et al*. 2004a). This is accompanied by an increase in the inflammatory cytokines; IFN-γ, IL-1b, IL-6 and TNFα at the optic nerve head (Nikolskaya *et al*. 2009).

The initial site of neuronal injury in glaucoma is the optic nerve head, specifically the retinal ganglion cell axons at the myelination transition zone (Chidlow *et al*. 2011, Quigley & Anderson 1976, Weber *et al*. 1998a) however whether neurodegeneration is directly caused by the mechanical disruption of axons preventing axonal transport (Quigley *et al.*, 2000) or as a result of optic nerve head astrocytes activating in response to the increase in hydrostatic pressure(Hernandez, 2000, Hernandez, Agapova, & Yang, 2002, Nikolskaya *et al*., 2009) is unclear.

The progression of damage is well characterised, following sustained degeneration of retinal ganglion cell axons and associated vision loss there is degeneration and apoptosis of retinal ganglion cells (Figure 1.1) *(Quigley & Anderson, 1976; Weber et al*., 1998).

While axonal degeneration is undoubtedly the initiator of glaucomatous damage, the relative contributions of other cellular events is less clear. It may be the case that axonal degeneration can be counteracted and regenerating axons may be able to reattach at the same point as they did in a pre-disease state, using persistent structural supports (Crish *et al,.* 2010). It may also be the case that axonal degeneration, once it has occurred, cannot be reversed with the restoration of function due to the potential for mis-wiring of the regenerated axon terminals. It is therefore important to understand the mechanisms of retinal ganglion cell

degeneration so that function may be effectively protected and/or restored as early as possible during the progress of disease.

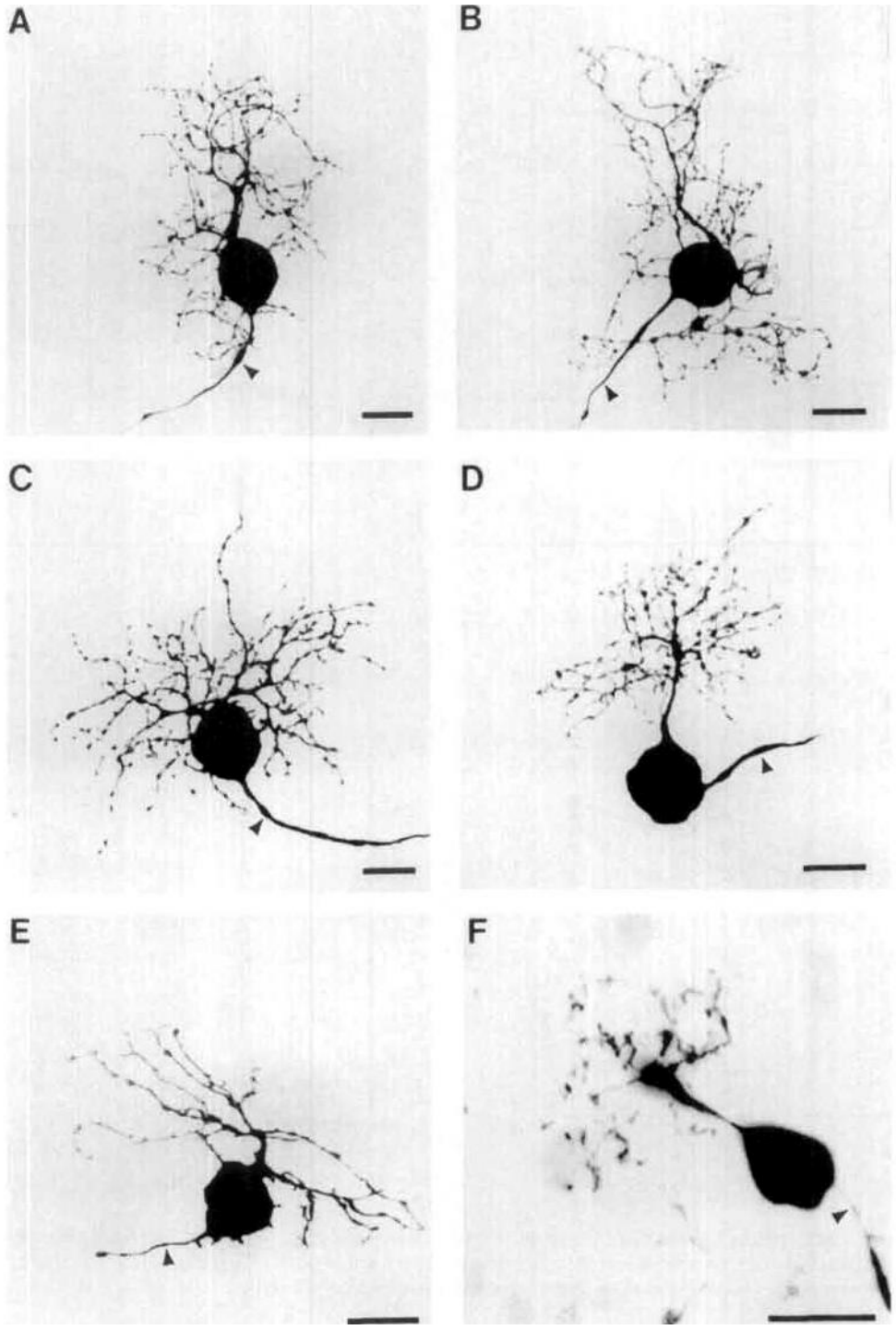

Figure 1.1 The degeneration of glaucomatous, midget retinal ganglion cells. Confocal images showing examples of midget RGS displaying mild degeneration (A and B), moderate degeneration (C and D) and severe degeneration (E and F). Arrow heads indicate axons, note how axonal fragmentation is visible proximal to the retinal ganglion cell body where there is severe degeneration. (scale bar = 10µm). Weber *et al.* (1998).

1.1.3 Pharmacotherapy

The primary risk factor for glaucomatous damage in the population at large is age (Broman et *al.* 2008). Age contributes to the risk of developing glaucoma in a number of ways, including alterations in blood flow and extracellular matrices in the optic nerve head (Albon *et al*. 2007, Groh *et al.* 1996, Hernandez *et al*. 1989). As such, rather than attempting to remedy the various age-related factors which may contribute to the development of glaucoma, the primary aim of treatment is to minimise intraocular pressure elevation. The topical administration of anti-hypertensive agents is regarded as an effective method of mitigating the progression of hypertension associated disease. These drugs are divided into three main classes: beta-blockers such as Timolol®, carbonic anhydrase inhibitors such as Brinzolamide® and prostaglandin analogues such as Latanoprost®. The reduction of intraocular pressure with pharmacotherapy has proved to slow reliably, the progression of vision loss in a manner proportional to intraocular pressure reduction. Despite this, in the majority of cases the visual field continues to degenerate and cannot be regained (Caprioli & Coleman 2008).

1.1.4 Surgical therapy.

Similarly to the pharmacological therapies used to treat glaucoma, the primary focus of surgical intervention is to reduce intraocular pressure in the affected eye/eyes. In the case of angle closure glaucoma this can be done surgically with either conventional or laser based treatment such iridotomy or iridectomy in which the iridocorneal block is bypassed by puncture or ablation of the iris, respectively. This restores the outflow of aqueous humour, effectively reducing intraocular pressure and improving the degradation of visual field loss (Robin, 1982; Salmon, 1993).

1.1.5 Treatment outcomes

The advanced glaucoma intervention study (AGIS) (2000) found a direct correlation between post-intervention intraocular pressure and the progression of visual defect up to seven years after intervention. This indicates that although damage reversal is not at present possible and areas of visual field deficit cannot be restored, the management of intraocular pressure is an effective means of controlling vision loss in the long term.

1.2 Animal models of glaucoma

Pharmacological and surgical treatments for glaucoma focus solely on the reduction of intraocular pressure and as such are limited to a post-hoc reduction in the rate of damage. In order to better understand the mechanisms which bring about damage in glaucoma and thus develop a treatment which may either prevent damage in the first instance or repair visual loss, a number of animal models of glaucoma have been developed.

Analysis of human tissue has identified candidates for disease pathways which may be manipulated to mitigate glaucomatous optic neuropathy (Hernandez *et al*., 2002, Tezel *et al*., 2010, Yang *et al*., 2004a). These findings can be based only on post-mortem tissue and non-invasive inspection of glaucomatous retinas restricting the options for manipulating suspected pathways to test novel treatments or gather data in human patients. This has necessitated the development and use of animal models of glaucoma. These models must satisfy a number of factors including; accurate replication of the disease processes present in human glaucoma as near as is possible, facilitate genetic and/or pharmacological manipulation of the ocular tissues and providing this data while keeping animal suffering to a minimum (Russell and Burch 1959). Early work on animal models of glaucoma involved the use of macaques, rhesus monkeys and primates (Hiraoka *et al*. 2012, Allingham *et al*. 2009, Miyahara 2003, Quigley & Anderson 1976). These are large, visual and intelligent animals and as such have associated housing costs which limit numbers of animals which can be in a study as well greater ethical concerns when compared with traditional lab animals which are less reliant on their visual system (Russell and Burch 1959 Chapter 2: The concept of inhumanity - Pain and distress).

Subsequent developments of animal models of glaucoma have utilised smaller, more traditional laboratory animals such as rats and mice. These can be used in larger numbers facilitating the testing of potential treatments with a higher statistical power. Additionally rats and mice rely on their olfactory system as their primary source of information regarding their surroundings rather than their visual system, reducing the impact of progressive visual loss on animal welfare compared to simian or primate models. Murine models have been particularly useful given the comparative malleability of the mouse genome and the similarity of the murine central nervous system to our own (Howell *et al*. 2008).

Although age is the primary risk factor in the development of glaucoma, simply aging laboratory animals would not provide a suitable means of replicating glaucomatous optic neuropathy as the penetrance would be low and housing costs would be high. To replicate glaucomatous neuropathy without resorting to ageing strategies typical animal models of diseases rely upon increasing intraocular pressure by blocking aqueous humour outflow, which is done using a variety of methods.

1.2.1 Ghost red blood cells

Early attempts to physically obstruct the outflow of aqueous humour through the anterior chamber at the iridocorneal angle utilised fixed, endogenous red blood cells (ghost red blood cells) in both the rabbit and primate (Quigley & Addicks 1980). These experiments produced a reliable increase in intraocular pressure from one or two injections over a period of up to 23 days. The requirement to draw and process blood from each animal (as exogenous blood would be more likely to generate an inflammatory response) makes this method unsuitable for a model of inducible

glaucoma in large numbers of small animals. In addition, the same study observed that injected ghost red blood cells settled to form a solid mass at the base of the angle and that in order to produce a reliable pressure increase 75% of the anterior chamber needed to be filled. The ability of this model to deposit such a large number of cells into the anterior chamber is an advantage over models using polystyrene microspheres (Sappington *et al*. 2010; Quigley & Addicks 1980b; Crish *et al*. 2010). These models would be unable to deposit such a large volume of particles in the anterior chamber as it may lead to haemorrhage in the anterior chamber due to the greater mass of the microspheres compared to ghost red blood cells.

1.2.2 Polystyrene microspheres.

Injections of fully synthetic particles into the anterior chamber have been undertaken extensively in the mouse and rat (Sappington *et al*. 2010, Cone *et al*. 2010, Weber & Zelenak 2001). These studies have reported success in producing and sustaining an elevation in intraocular pressure for a period of over two weeks. This model does, however, introduce solid microspheres into the anterior chamber. These microspheres follow gravity and pool at the inferior aspect of the iridocorneal angle. It is possible that deposition of solid microspheres at the base of the angle may interfere with rebound tonometry. This would come about as the probe striking areas of the cornea where beads were resting may encounter more resistance than at other areas which were not in contact with beads. It has also been observed that the efficacy of this model is highly variable between mouse strains (Vecino & Urcola 2006), this is likely to be a result of the degree of genetic variation between in-bred

strains of mouse. This variation effectively limits the number of mouse strains can be used to model glaucoma, potentially limiting the number of genetic knock out models which can be used to model glaucomatous optic neuropathy.

1.2.3 Genetic models

The DBA/2J strain of mouse has mutations in the *TRYP1* and *GPNMB* genes which causes a degenerative phenotype with striking similarity to human exfoliative glaucoma. These animals shed pigment from their iris which becomes trapped in the trabecular meshwork (Anderson *et al*., 2002) leading to an elevation in intraocular pressure. This model has an age-related increase in the susceptibility to intraocular pressure elevation and a corresponding increase in retinal ganglion cell degeneration with 100% of animals developing severe optic nerve degeneration by 12 months of age. The similarity of the disease phenotype to the human disease, in that age, gender and intraocular pressure are both predictive factors for glaucomatous damage, is a distinct advantage to this model.

However, as these mutations arose spontaneously in an in-bred mouse strain they co-exist with a number of other, potentially confounding mutations. In particular, the DBA/2J mouse carries the Hc^0 allele of complement component 5 (Nilsson & Müller-Eberhard, 1967). This allele arises from a 2 base-pair deletion, causing a frame-shift and truncation of the protein. This mutation makes studying the role of the complement cascade in glaucoma in the DBA/2J mouse model impossible, as without C5 the membrane attack complex cannot be formed. The membrane attack complex has been shown to have roles in promoting Wallarian degeneration (Ramaglia *et al*. 2007) and cell survival (Badea *et al*., 2002, Tegla *et al*., 2009,

Weerth *et al*. 2003), as such this mutation may prove to be a confounder in the study of the mechanisms underlying glaucomatous optic neuropathy.

Recently, work has been conducted which re-introduces functional C5 expression in DBA/2J mice (Howell *et al*. 2013). This work has identified that C5 sufficient DBA/2J animals develop more severe glaucoma than those who are C5 deficient. The increased deposition of the terminal complement complex at both the optic nerve head and retinal ganglion cell soma was identified as the causative factor in this C5-mediated worsening of damage. Also of note from this study, however, is the detection of the terminal complement complex on non-glaucomatous retinal ganglion cells. The implications of this will be discussed fully in chapter 7.

Unlike the rat, guinea pig and human, the mouse have no identifiable lamina cribrosa (Morrison *et al*. 1995) and instead possess a network of glial cells providing mechanical support to the optic nerve as it exits the retina. This structure is central to the biomechanical properties of the optic nerve head (Burgoyne 2011). The difference of this structure compared to that of the human in this model may produce significant biomechanical discrepancies. These discrepancies may ultimately limit the use of the mouse as an animal model of glaucoma.

1.2.4 Hypertonic injection of saline into episcleral veins - The Morrison model.

The model of experimental glaucoma developed by Morrison *et al.* (1997) involves unilateral injection of hypertonic (1.75M) saline into the episcleral vein of a rat. This procedure produces a reliable and long-lasting increase in intraocular pressure following as few as two injections and could be considered the gold standard of experimental intraocular pressure elevation. There are, however, numerous

practical considerations which limit the usefulness of this model. The cannulation procedure is technically challenging and the pulled-glass micropipettes used for the injection are extremely fragile making them difficult to use and store. The pipettes must be completed and watertight before the procedure, meaning that a number of cannulae must be manufactured by hand before each procedure to account for breakages. This makes inducing an intraocular pressure elevation in a large number of animals both time-consuming and technically demanding. It was also found that intraocular pressure elevation varied between strains of rat, implying an unidentified resistance to the sclerotic agent which may further affect the usefulness of this model.

1.3 Microglia

Quiescence in retinal ganglion cells has been shown to induce elimination by resident microglia (Tremblay *et al*., 2011, Tremblay, Lowery, & Majewska, 2010). In development this process functions to eliminate aberrant synapses of retinal ganglion cells and other neurones. In both cases this refinement is dependent on the activity of the classical complement cascade (Chu *et al*., 2010, Stevens *et al*., 2007).

Microglia resident in the retina are activated in glaucoma (Bosco *et al.* 2011, Langmann 2007) and components of the classical cascade of complement activation are up-regulated in retinal ganglion cells. This suggests that processes involved in microglia-mediated retinal ganglion cell refinement during development may be responsible for the removal of retinal ganglion cells during glaucoma. Removal of retinal ganglion cells is a critical step in the development of visual deficits in glaucoma as these cells, once lost cannot easily be replaced due to highly specific interactions with other cells within the retina and the vision centres of the brain. Understanding the ultimate role of microglia in retinal ganglion cell atrophy will therefore be important in understanding the progression of glaucoma glaucoma.

1.3.1 Microglia in glaucoma

The production of adenosine triphosphate in the retina is increased in response to an elevation in intraocular pressure (Reigada *et al*. 2009), adenosine triphosphate triggers protection in neurones which are associated closely with microglia. Astrocytes in culture respond to an increase in extracellular adenosine triphosphate by further increasing their own production of extracellular adenosine triphosphate (Anderson *et al*. 2004). In the glaucomatous optic nerve head astrocytes increase

production of adenosine triphosphate synthesis and trafficking proteins (Yang *et al*. 2004b). These data suggest that localised extracellular adenosine triphosphate also mediates the translocation of microglia to the site of injury via secondary adenosine triphosphate production by astrocytes (Davalos *et al*. 2005). This biphasic adenosine triphosphate response may be responsible for the translocation of microglia to the site of damage in glaucoma.

1.3.2 Microglia in the healthy and developing brain

Resting microglia frequently sample the surrounding environment and have been shown to make contacts, lasting approximately five minutes every hour, with synapses and axons under physiological conditions (Wake *et al.* 2009) and have been shown to selectively prune smaller spines from dendrites of the mouse visual cortex (Tremblay *et al.*, 2010), this interaction is depicted in figure 1.2. Recent evidence suggests that this interaction may also play a role in modulation of the synapse, hippocampal microglia secrete adenosine triphosphate in response to lipopolysaccharide which activates purinergic receptors on astrocytes, triggering the release of glutamate and increasing excitatory post-synaptic potentials via α-amino-3-hydroxy-5-methyl-4-isoxazolepropionic acid (AMPA) receptors (Ben-Achour & Pascual 2010), indicating that glial modulation of synaptic activity is dependent on inflammatory state. It may be that the short half-life of adenosine triphosphate, which is rapidly degraded into adenosine in the extracellular space, may be acting to positively reinforce cells which are making close contact with microglia while drawing activated microglia to the site of injury.

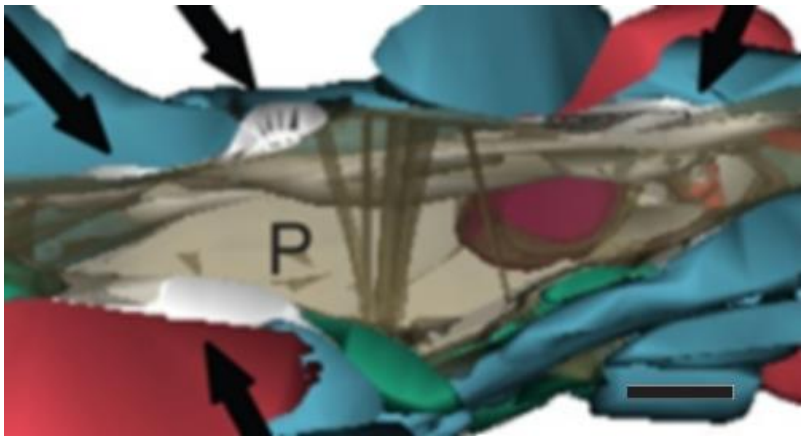

Figure 1.2 Resident microglia in close contact with neuronal tissues. A 3-dimensional, scanning electron micrograph reconstruction of the microglial proximal process. The microglial process (P) is shown in close proximity to axon terminals (blue), dendritic spines (red), and perisynaptic, astrocytic processes (green). Phagocytosed neuronal material is indicated in purple., and are surrounded by pockets of extracellular space varying in size and shape (white; black arrows) Scale bar = 100nm. From Tremblay *et al*. (2011).

As glial-neurone interactions are regulated by activity (Tremblay *et al*., 2010), the potentiation of activity in neuronal processes which are interacting with microglia may be a mechanism for the selective protection of neurones which are structurally sound, over those which are degenerating and retracting away from resident, inactive microglia. In mice between post-natal days 5 and 9, microglia are responsible for phagocytising inactive retinal ganglion cell axons (Stevens 2011), this may be applicable to the clearance of axons and other cellular debris in glaucoma.

The role of microglia in pathogenesis is highly complex, microglia increase phagocytic activity in response to markers of oxidative stress (Bruce-Keller 1999), however ischaemic preconditioning and low-level lipopolysaccharide treatment of microglia have each been shown to be neuroprotective (Franco *et al.* 2008). This may be a consequence of ischaemic preconditioning acting via similar mechanisms

to lipopolysaccharide and stimulating excitatory post-synaptic potentials via AMPA receptors.

Interestingly; extracellular adenosine triphosphate triggers the release of the neuroprotective cytokine, TNF-α by microglia (Hide *et al*. 2000; Dolga *et al*. 2008) by the activity of the $P2x_7$ purinergic receptor. Moreover, the absence of extracellular adenosine triphosphate at $P2X_7$ has been shown to trigger phosphatidyl serine-dependent phagocytosis of non-opsonised beads and microbes by $P2X_7$-transfected human embryonic kidney cells (Gu *et al.* 2011) and of SH-SY5Y neuroblastoma cells by macrophages, whereas in the presence of extracellular adenosine triphosphate, phagocytosis did not occur. Together this suggests a complex role for adenosine triphosphate in neuronal pathogenesis as a housekeeping molecule, attracting and activating microglia while simultaneously providing short-range protection for active neurones.

1.4 Complement

1.4.1 Introduction to complement

The complement system is a network of serum proteins and their soluble and membrane-bound regulators. The activities of this system include opsonisation and lysis of pathogenic bacteria as well as the clearance of immune complexes and apoptotic self-cells. Self-cell apoptosis/necrosis can also occur as a result of unregulated or aberrant complement expression. The complement system is composed of at least three primary pathways and has been implicated in many facets of neurodegeneration, reviewed in Perry & O'Connor (2008a). In particular the classical pathway of complement activation (Summarised in figure 1.3) has been implicated in synaptic pruning and glaucomatous retinopathy (Stevens *et al*. 2007; Chu *et al*. 2010; Howell *et al*. 2011).

The common feature of the complement cascades is the formation of a stable convertase of the fifth component of complement (C5). In the classical complement cascade this convertase consists of the molecules C2a and C4b, C2 is cleaved by the initiator molecule of the classical cascade C1. Upon binding of C1 to a target cell surface by antibodies or proteins on bacterial cell surfaces(Merino *et al*. 1998), C1 undergoes a conformational change allowing it to recruit and cleave C2 (Thielens *et al.* 1999), C2a recruits C4 to the target cell surface where it is cleaved to form C4b and C4a, the former remains bound to C2a (Gagnon 1984). C2a functions as the catalytic site for the cleaving of C3 to C3b and C3a, C3b remains attached to the C3 convertase and catalyses the proteolysis of C5. C5 is converted to C5a – a potent anaphylotoxin (Kacani *et al*. 2001) and C5b which recruits C6, C7, C8 and multiple molecules of C9 (Peitsch & Tschopp 1991), C6 functions to anchor this terminal

complement complex to the cell membrane and interact with host intracellular processes (Badea *et al.* 1998) and C7 recruits C8 which contains a hydrophobic domain that binds to a similar domain on C9 allowing multiple molecules of C9 to be recruited and form a pore in the cell membrane. Via these mechanisms the classical complement cascade is a mediator of destruction of cells by lysis and phagocytosis by cells of the adaptive immune system.

Stevens *et al.* (2007) found that the complement components C1 and to a lesser extent C3 are a requirement for synaptic refinement in mice and that deficiency in either of these proteins can lead to a breakdown in synaptic refinement of ipsilateral projections from the retina (figure 1.4). The role of complement in retinal ganglion cell refinement in glaucoma is of relevance to the study of glaucoma as; similarly to the deterioration of quiescent, superfluous axons in development, glaucomatous neurodegeneration begins with the atrophy of retinal ganglion cell axons *(Weber et al*., 1998b).

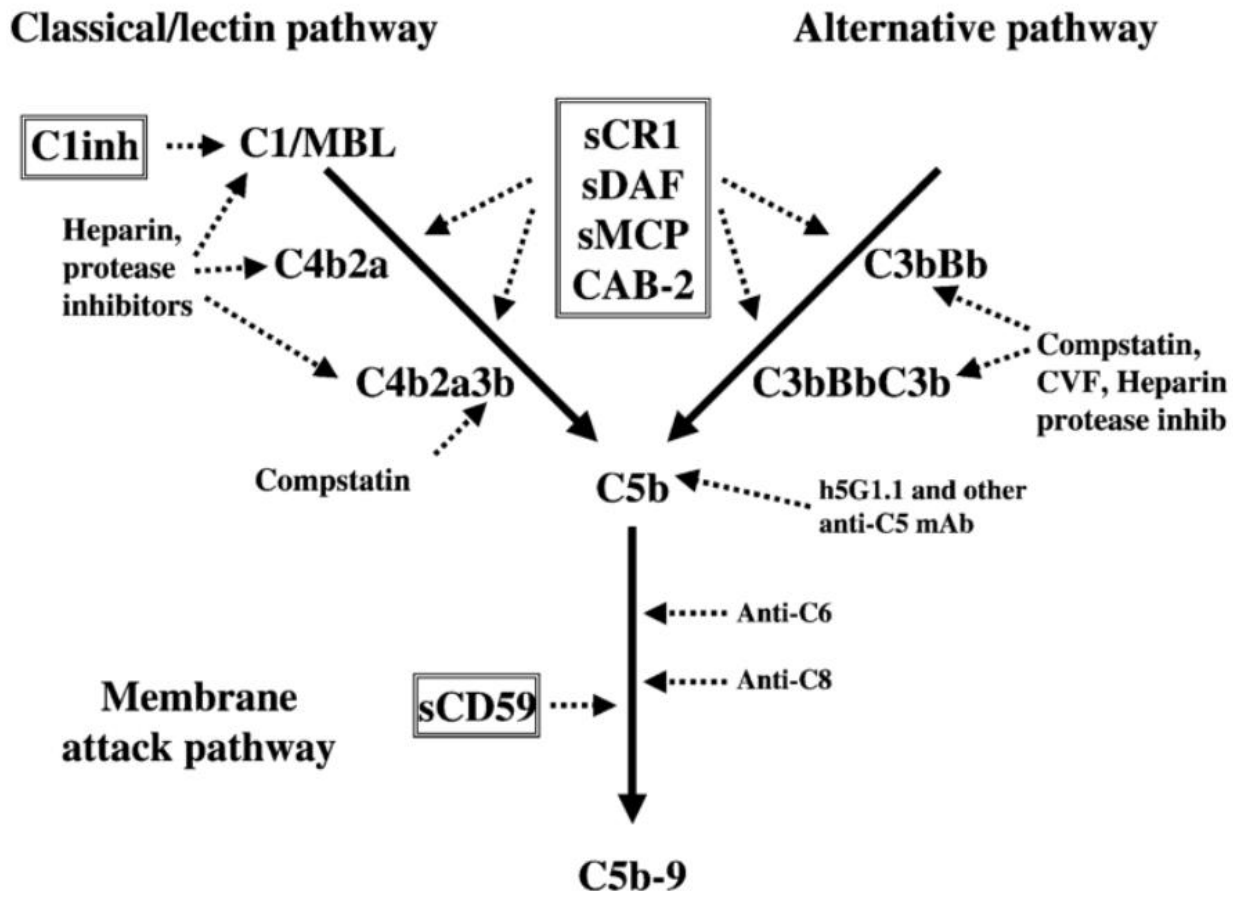

Figure 1.3 Schematic overview of the three main complement cascades. An outline of the three main complement cascades with emphasis on therapeutic complement regulators derived from endogenous agents (boxed). The primary inhibitor of the classical complement cascade is C1-inhibitor (shown here as 'C1inh'). The alternative pathway begins with autohydrolysis of complement component C3 to from C3a and C3b, which forms a stable C3 convertase by recruiting factor B, which in turn is cleaved by factor D to leave a non-catalytic subunit (Ba) and a catalytic subunit (Bb) which remains bound to C3b. This convertase formation is regulated by factor H and factor I (not shown). From Morgan and Harris (2003)

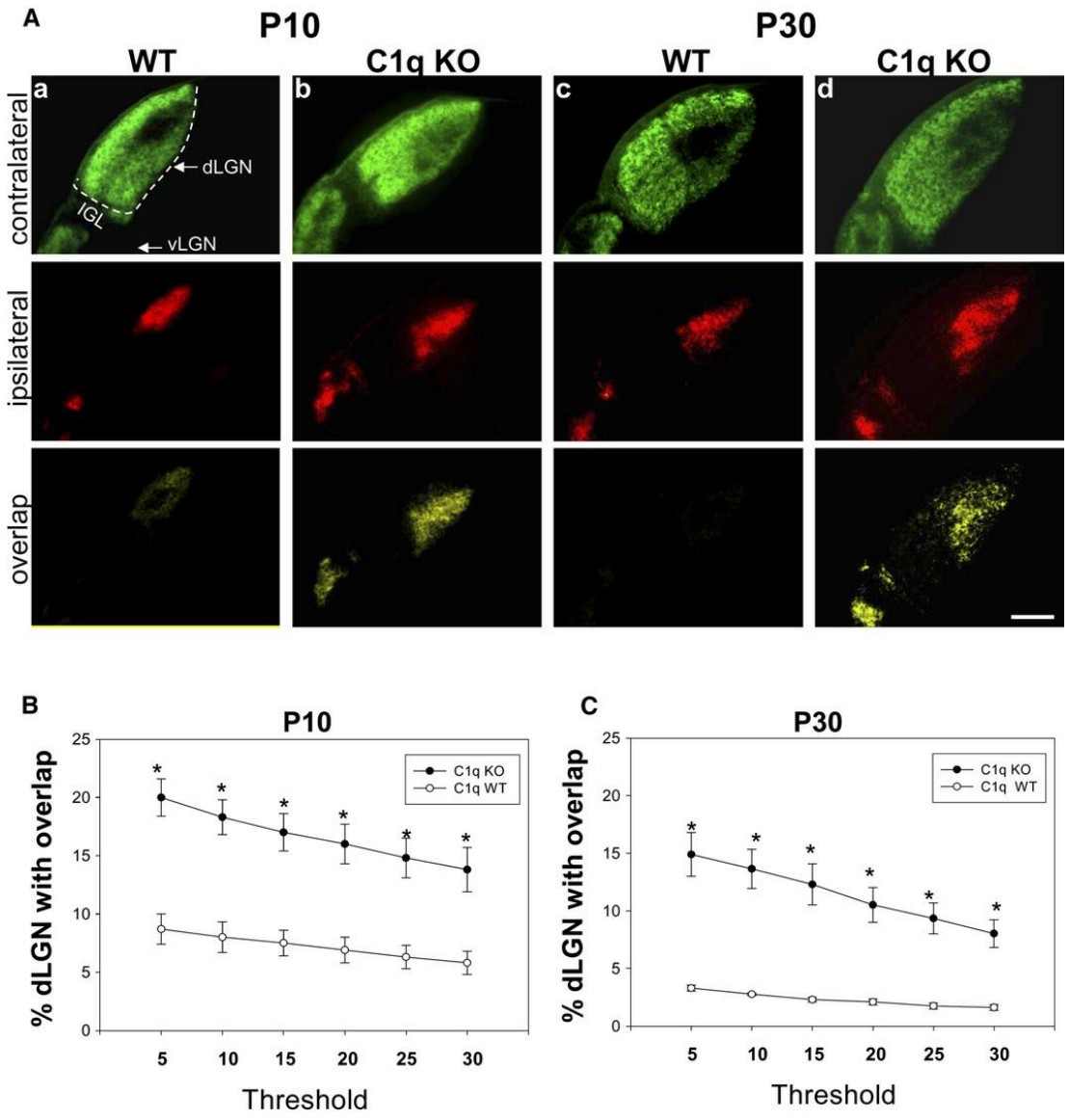

Figure 1.4 Defects in synaptic refinement and eye-specific segregation of C1q deficient mice. Projection patterns of retinal ganglion cell axons at the geniculate nucleus visualised with injection of b-choleratoxin conjugated to AlexaFluor® 594 (red) or AlexaFluor® 488(green) into the right and left eyes respectively of C1q sufficient and knockout mice. C1q knockout mice at postnatal day 10 (A-b) and 30 (A-d) have significant overlap (yellow) between retinal ganglion cell inputs from ipsilateral and contralateral eyes compared to littermate, C1q sufficient controls (Aa and Ac) (scale bar - 200 mm). (B and C) Quantification of the percentage the percentage of the dorsal lateral geniculate nucleus which receives overlapping inputs in C1q knockout versus C1q sufficient, littermate controls at postnatal days 10 (B) and 30 (C). C1q knockout mice exhibit significantly more overlap than C1q sufficient littermates, regardless of threshold. Stevens *et al*. (2007).

1.4.2 Complement in neurodegeneration.

Complement is responsible for the clearance of apoptotic neurons in the central and peripheral nervous systems in both disease and development both *in vitro* and *in vivo* (Ramaglia *et al*. 2007; Stevens *et al*. 2007; Chu *et al*. 2010). The first component of the classical pathway of complement activation; C1, directly enhances the clearance of apoptotic neurons by microglia in a manner that also suppresses the production of pro-inflammatory cytokines IL-1α, IL-1β, Il-6 and TNFα (Fraser *et al*. 2010), indicating a protective element for complement activation in neurodegeneration.

Conversely, complement components have been identified as constituents of central nervous system plaques in both Alzheimer's disease and Huntington's chorea (Goldknopf *et al*., 2006; Singhrao, Morgan, & Gasque, 1999; Webster *et al*., 2000) and have been implicated in the subsequent necrosis and neurodegeneration.

The role of complement in Alzheimer's disease is unclear, however it has been established that both amyloid beta and tau protein, the constituents of senile plaques in Alzheimer's disease each activate the classical complement system *(Webster et al*. 2000; Shen *et al*. 2001; Ying *et al*. 1993). This activation is caused by binding of amyloid beta and tau to both the globular heads and the collagen-like domains of the C1q molecule. However it is unclear if this activation increases plaque clearance, cytotoxicity or indeed both.

Polymorphisms in the receptor of activated C3; complement receptor 1 (CR1) and the regulator of the terminal complement complex – clusterin, have been associated with an increased risk of Alzheimer's disease in numerous genome-wide

association studies (Harold *et al*., 2009; Lambert *et al*., 2009; Brit-Maren *et al*., 2011).

Two isoforms of CR1; CR1-S and CR1-F, of CR1 make up the majority of CR1 expressed in humans and differ in the number of binding sites for C3b with four and three respectively. The CR1-S isoform has been associated with a 30% increase in the risk of developing Alzheimer's disease and it has been conjectured that the additional binding site increases binding affinity for C3b. This increased binding enhances its function as a cofactor for the complement inhibitory molecule; factor I leading to increased inhibitory activity on complement (Brouwers *et al*., 2011). However, as there is no data regarding any functional or binding differences between the risk associated isoform and the low risk isoform, it is not possible to draw any conclusions regarding the exact nature of the role of CR1 in the development of Alzheimer's disease.

The role of complement activation in Alzheimer's disease is debated; C1q (an activator of complement) and clusterin (a complement regulator) deficiencies have each been associated with a reduction in disease severity in mouse models (DeMattos *et al*. 2002; Fonseca *et al.* 2004). This suggests that the initial complement activation triggers microglial activation, worsening pathology and regulation of the terminal complement complex inhibits the clearance of senile plaques.

What is clear from genome-wide association study data is that defects in the regulation of complement activation are intrinsically linked to the development of pathology in Alzheimer's disease. In addition, numerous genome analysis studies have directly implicated the complement receptor 1 (CR1) and the regulator of the

terminal complement complex: clusterin have been implicated in Alzheimer's disease (Harold *et al*., 2009).

It has been observed that the binding of amyloid proteins to C1q increases β-sheet formation and inhibits the re-suspension of the pathogenic amyloid 1-40 peptide (Webster, Barr, & Rogers, 1994). A reduction in re-suspension suggests that the development of amyloid beta plaques may be enhanced by C1. Conversely, Fonseca *et al.* (2004) found that C1q deficiency had no significant effect on the amount of amyloid beta plaques in Alzheimer's disease. However the role of complement in mouse models of Alzheimer's disease has proven to be highly variable between strains (Fonseca *et al*. 2011). This complicates the study of complement as a whole in Alzheimer's disease using mouse models. Blocking the receptor of C5a with the inhibitor PMX205 is neuroprotective in Alzheimer's disease (Fonseca *et al*. 2009) suggesting that the activation and migration of microglia in Alzheimer's disease is destructive and driven by complement.

It should be noted that as an inhibitor of C5a receptor, PMX205 would not reduce the formation of the terminal complement complex. The fact that a C5a receptor reduces damage suggests that complement mediated neurotoxicity in Alzheimer's disease may be the response of sub-lytic activation. Additionally, this inhibitor acts on a point in the complement system after the formation of the C5 convertase, as C5a is produced at this step. Therefore this protective mechanism is independent of both pathway and level of activation, be it lytic or sub-lytic. This minimises the information provided by observations of the action of PMX205 as to the exact role of complement in Alzheimer's disease. This emphasises the scope for the potential influence of complement in neurodegenerative disorders.

Complement has also been implicated in the progression of Parkinson's disease. Parkinson's disease is characterised by the progressive degeneration of neurons in the substantia nigra pars compacta, resulting in a loss of fine motor control which leads to the classical symptoms of Parkinson's disease ; bradykinesia and resting tremor. The presence of Lewy bodies in the brain is a hallmark of Parkinson's disease, activated complement components and activated microglia have been detected in these Lewy bodies (Yamada *et al.* 1992). Complement activation has been implicated in the death of neurons containing lewy bodies(Togo *et al*., 2001). Indeed the complement cascade has been strongly implicated in the destruction of central nervous system xenografts with the apparent preservation of avascular immune privilege. Xenograft destruction under these circumstances indicates that complement produced by cells of the central nervous system has the capacity to destroy neuronal material in Parkinson's disease without influence from the adaptive immune system (Barker *et al*., 2000).

The role of complement in development, maintenance and pathology of the central nervous system is multifactorial and complex and the amount of literature suggesting a role in glaucomatous degeneration is substantial. There is evidence for activation of the adaptive immune response in glaucoma, however there is little evidence that this is a causative agent and much of the evidence for direct cytotoxicity by the adaptive immune response is from *in vitro* experimentation (Huang *et al*. 2009; Perry & O'Connor 2008a; Howell *et al*. 2007). There is also evidence that mitigation of the adaptive immune response by destruction of bone marrow may provide protection against glaucomatous damage (Anderson *et al*. 2005). This evidence is however based on the DBA/2J mouse model of glaucoma which involves the adaptive immune response causing an exfoliative degeneration of

the retinal pigment epithelium. As such, dampening of the adaptive immune response to the exfoliation syndrome as a result of bone marrow destruction may play a role in the mitigation of damage in this case. It would also be difficult to modulate the adaptive immune response without affecting other systems of the body and as such I will be working on modulating the complement system in the retina to mitigate damage in glaucomatous optic neuropathy.

The complement system is a vital part of development, homeostasis and host defence, particularly in the central nervous system where the adaptive immune system is largely absent. For these reasons I will examine the role of complement in retinal ganglion cell loss in glaucoma.

1.5 Outline of work

I will begin by developing a model of glaucoma in the rat utilising paramagnetic microspheres. This model will function to allow me to establish in complement is up-regulated in glaucoma and then test potential treatment methodologies. As this is an inducible model of glaucoma it will be possible for me to administer agents before or during the elevation in intraocular pressure. This will allow me to combat early stage biochemical changes in the retina, such as complement activation (Howell *et al*. 2011) which would not be possible with an age dependent model of glaucoma such as the DBA/2J mouse model.

In developing this model, to overcome the drawbacks and risks associated with the deposition of beads and other technical challenges in existing models of inducible glaucoma we have developed an inducible model of glaucoma utilising polystyrene microspheres with a paramagnetic, iron-oxide core. These

microspheres can be manipulated with a hand-held magnet following injection, which will allow them to be drawn into the trabecular meshwork around the entire circumference of the angle. This will induce a reliable and sustained increase in intraocular pressure.

Using antibodies specific for proteins of the classical complement cascade and those produced by complement activation, C1q and C3b/iC3b respectively, I will establish if the classical complement cascade is producing activated complement components in glaucomatous retinas.

Using retinas from rodents with complement knockout mutations, cultured under elevated hydrostatic pressure and rats with elevated intraocular pressure treated with the classical complement cascade inhibitor C1 inhibitor, I will examine the nature of the relationship between complement and glaucoma at various stages of the complement cascade.

1.6 Hypothesis and aims

The classical cascade of complement activation plays an established role in both the loss of retinal projections during development and neurodegeneration at large. At present, all treatments for glaucoma simply reduce the rate of progression of the disease. This is a consequence of a reactionary mode of treatment, aimed at reducing elevated intraocular pressure after a significant visual field deficit has already developed. Complement activation has been identified as an early molecular event in glaucomatous optic neuropathy. Given the established role of complement in retinal degeneration, it is reasonable to expect a pathological role for this activation in the progression of glaucomatous optic neuropathy. Establishing the role of complement in retinal ganglion cell degeneration in glaucoma may allow the

development of treatments which can overcome the inevitable progression of visual degeneration in glaucoma patients. Treatments for human disease which are based on manipulation of the complement system are already widely used, specifically, the inhibition of the classical complement cascade with C1 inhibitor in hereditary angioedema. The existence of such treatments could drastically speed the development of glaucoma treatments based on complement system manipulation if that proves to be a suitable option.

The aims of this study are: to identify if complement is activated in an animal model of glaucoma, to determine the effects of complement deficiency on retinal ganglion cell survival following hydrostatic pressure elevation and to attempt to prevent retinal ganglion cell degeneration in animal glaucoma with an inhibitor of the classical complement cascade.

Chapter Two: Materials and Methods

2.1 Introduction

Existing animal models of glaucoma have been used to identify the underlying mechanisms of the disease and test potential treatments. In order to examine the role of complement in retinal ganglion cell loss in glaucoma, I will develop a rat model of glaucoma that is robust, inducible and reproducible. With this model I will use specific detection of activated complement and synaptic density to correlate the activation of the complement cascade with retinal neurodegeneration in glaucoma. Using complement deficient animal models and Sholl analysis of retinal ganglion cell dendritic integrity I will attempt to establish what, if any, is the effect of complement deficiency in retinal ganglion cell loss. Finally, I will use the inhibitor of the classical complement cascade – C1 inhibitor – in the model of glaucoma developed here to attempt to treat glaucomatous neurodegeneration and establish if complement inhibition is a viable treatment in glaucoma.

Recently, the cell line which has previously been used to study glaucomatous optic neuropathy, the RGC5 cell line, has been shown to be a less than ideal model of retinal neurons (Van Bergen *et al*. 2009). This requires the use of animal models in the study of glaucoma. The use of animals in this body of work is detailed in table 1.

Table 1: Overview of animal use in experimental chapters.

Chapter	Rats killed	Mice killed	Total animals culled
3 – Microsphere model development	31	0	31
4 – Complement activation in experimental glaucoma	20	0	20
5 - In Vivo and In Vitro Pressure Elevation in Complement Deficient Animals	12	14	26
6 - Inhibition of the classical complement cascade in experimental glaucoma.	28	0	28

2.2 Paraformaldehyde and buffer preparation

Four per cent (weight/volume) paraformaldehyde was prepared by dissolving 40g of anhydrous paraformaldehyde (Sigma-Aldrich, UK) in 500ml of deionised water produced by an Advantage A10 Ultrapure Water Purification System (Merck-Milipore, Germany) and adding 1 molar NaOH (Sigma-Aldrich, UK), dropwise to the solution until it cleared. The resulting solution was then added to a 2X concentrated solution of phosphate buffered saline consisting 9g of NaCl (Sigma-Aldrich, UK) of 10.9g of anhydrous Na_2HPO_4 (Sigma-Aldrich, UK) and 6.4g NaH_2PO_4 (Sigma-Aldrich, UK) in 500ml of deionised water. The pH of the solution was altered to 7.8 using either 1M HCl (Sigma-Aldrich, UK) or 1M NaOH. The pH of solutions was measured with an Orion 420A pH meter (Gemini BV, Netherlands).

Standard (0.1M) phosphate buffer was prepared by dissolving 10.9g of anhydrous Na_2HPO_4 and 6.4g NaH_2PO_4 in 1000ml of deionised water.

Solutions of 1 molar tris buffer were prepared by dissolving 121.136g of Trizma® base (Sigma-Aldrich, UK) in 1 litre of deionised water, the pH was adjusted with the addition of 1M NaOH..

2.3 Animal husbandry

All animal procedures were carried out under the provisions of the Animals in Scientific Procedures Act (1986), project licence 30/2470 and personal licence 30/8485 and the ARVO statement on animal welfare.

Adult, retired breeder, Brown Norwegian rats (*Rattus norvegicus* from Charles River, UK), aged between six and nine months and weighing between 340 and 450g were fed on rodent global diet pellet (Harlan, UK) and given water *ad libitum*. To minimise diurnal fluctuations in intraocular pressure, animals were housed in constant low light (90lux).

Six month old mice from a C57BL/6 background were provided by Dr Timothy Hughes. These animals were housed overnight with food and water *ad libitum* on a twelve hour light/dark cycle. All mice were killed by cervical dislocation, without any regulated procedures being performed.

2.3.1 Animal culling

Animals whose retinas were needed for culture were killed by exposure to a rising concentration of carbon dioxide until loss of consciousness and failure of the corneal reflex, death was confirmed by cervical dislocation.

Animals whose retinas were to be sectioned for immunofluorescence were killed by perfusion fixation. Animals were restrained by the scruff of the neck and a 1ml dose of Euthetal® (200mg sodium pentobarbitone/ml) was administered under the peritoneum with a 26 gauge needle.

Following the termination of the corneal reflex and heartbeat, the animal was transferred to a fume hood, the thoracic cavity was opened, the diaphragm was incised and the rib cage was opened with rib spreaders (Duckworth and Kent, UK), exposing the heart. The heart was cannulated through the wall of the left ventricle with a large-bore needle attached to 8mm tubing (Cole Parmer, UK), the needle was clamped using a surgical clamp (Cole-Parmer, UK). Phosphate buffered saline (Sigma-Aldrich, UK) was then fed through the tubing into the heart using a peristaltic pump (Stoelting, Germany) at a rate of 8ml/minute. A hole was cut quickly in the right atrium to allow the escape of fluid. Once the fluid leaving the heart no longer contained traces of blood 4% paraformaldehyde was fed through the tubing, at the same rate.

Once paraformaldehyde exposure-related muscle twitching had ceased the clamp and cannula were removed and the ocular tissue was removed with micro scissors (Duckworth and Kent, UK).

2.4 Paramagnetic microsphere preparation

2.4.1 Corpuscular microspheres

Five-micron diameter microspheres were obtained from corpuscular (USA). These microspheres were prepared for *in vivo* use by; removing the supernatant by centrifugation in a bench-top centrifuge at 7000rpm for 7 minutes and re-suspending in deionised water. This was repeated three times before the water was replaced with an equal volume of balanced salt solution (Mid Optic, UK) with a pipette.

2.4.2 Invitrogen microspheres.

Four and a half micron-diameter, epoxy-coated microspheres were purchased from Invitrogen UK. These beads were designed for use in immunoprecipitation assays and contained reactive epoxy groups on its surface. To terminate these reactive groups, 1ml of bead solution was added to 50ml of 1M tris buffer solution at pH11 and this solution was mixed on a horizontal roller for 24 hours at 4°C. Beads were removed from the solution by affixing a pair of magnets to the tube and returning to the roller for ~4 hours. The tris buffer was replaced and the procedure was repeated. The tris buffer was then removed and the beads were washed with 1ml deionised water and resuspended in 500µl of balanced salt solution (Mid Optic, UK).

Balanced salt solution was used as the injection fluid rather than normal saline or the original fluid provided by the bead manufacturer (distilled water) to reduce any effect on the corneal endothelium that may influence the reading of intraocular pressure (Edelhauser *et al*. 1975).

2.4.3 Gamma irradiation

The bead solutions were aliquotted into 100µl/200µl amounts and sealed in 600µl Eppendorf tubes (StarLab, UK) which were sealed with parafilm (StarLab, UK). The tubes were then sterilised using a Gammacell (Gammacell, US) gamma irradiator with a dose of 2000cGy and refrigerated until use. Before use, microsphere preparations were vortexed for thirty seconds using a Vortex-genie 2 (Cole-Parmer, UK). This was to ensure an even distribution of microspheres in the solution.

2.5 Induction of experimental glaucoma

2.5.1 Anaesthesia

Anaesthesia was induced in rats by the administration of Isoflurane (Bayern-Bayern, Germany) suspended in medical oxygen (BOC, UK) at a flow rate of 2l/min. Animals were first placed in a custom-designed Plexiglas chamber until light anaesthesia was produced and then transferred to a custom face mask to facilitate examination of the left eye while maintaining deep anaesthesia.

2.5.2 Bead injections

Following anaesthesia, topical 0.5% chloramphenicol (Mid Optic, UK) was administered to the surface of the cornea of the left eye. The sclera of the left eye was grasped with cup-toothed forceps (Duckworth and Kent, UK) and an incision was made with a 32 gauge tri-bevelled needle attached to a 100µl Hamilton syringe (WPI Europe, Germany) containing the volume of bead solution to be injected. The incision was made as described in Langerman (1994), an initial incision was made part-way into the cornea at a right angle. The needle was then partially removed and the angle changed so that it was closer to orthogonal with the cornea and the incision was made into the anterior chamber.

Beads were injected into the anterior chamber using a gentle and constant pressure on the syringe. Beads were then drawn away from the syringe and directed into the iridocorneal angle with the hand-held magnet (figure 2.1) and a small amount of fluid (1-2µl) was withdrawn from the anterior chamber and re-injected, this was done to flush beads from the dead space of the needle. The beads were then manipulated within the anterior chamber with the needle still in

place, beads were drawn around the circumference of the iridocorneal angle before the needle was removed.

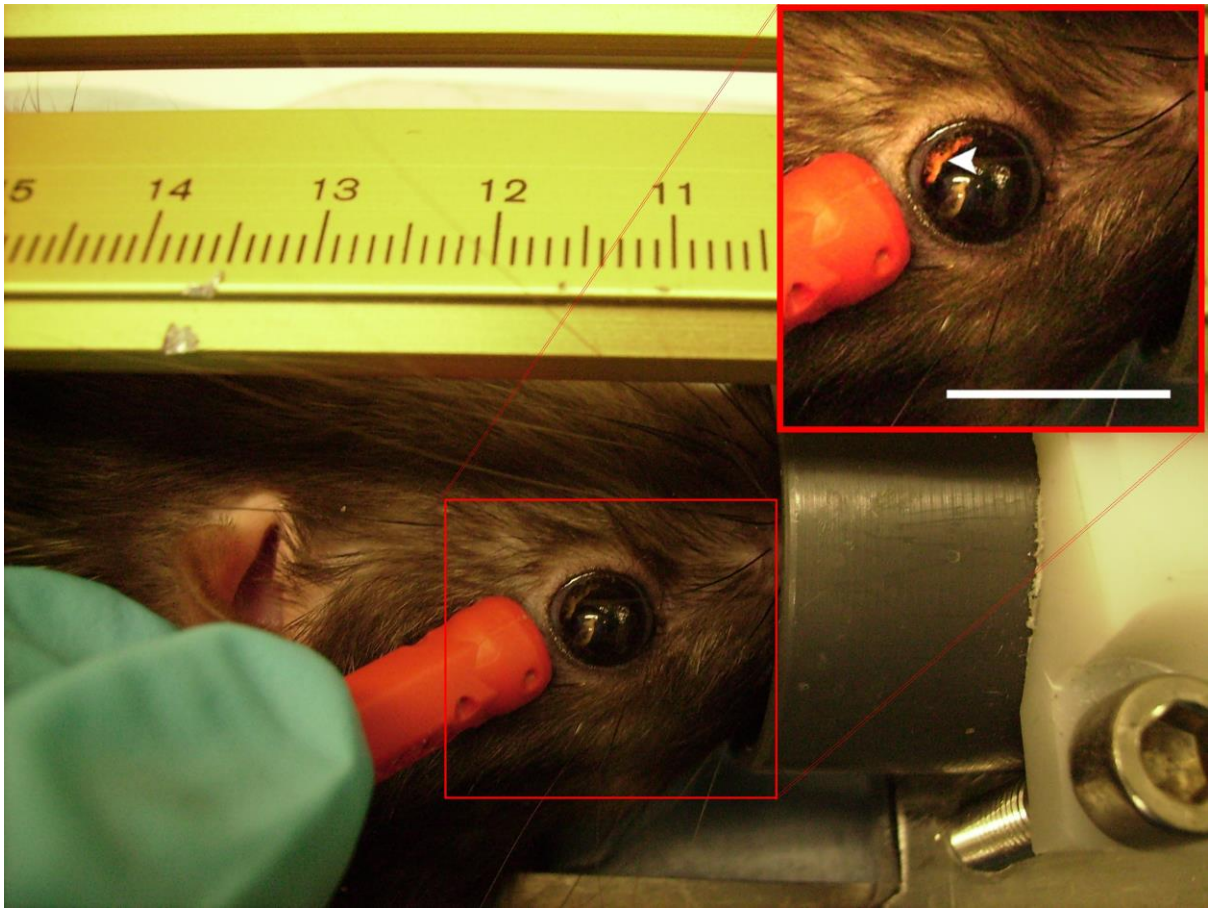

Figure 2.1 Positioning of paramagnetic microspheres within the anterior chamber of the eye with a hand-held magnet. The beads (arrow head) can be observed migrating from their initial deposition site at the inferior angle of the anterior chamber under the influence of the magnet. This migration allows the beads to embed in the nasal, temporal and superior aspects of the iridocorneal angle. This allows a larger portion of the angle to be occluded than would be possible with polystyrene microspheres. Scale bar = 1cm.

2.5.3 Intraocular pressure measurement

Animals were restrained gently and topical oxybuprocaine hydrochloride (mid-optic, UK) was administered to the surfaces of both corneas. A Tonolab® tonometer (Tiolat, Finland) was used to measure the intraocular pressure. Keeping the tonometer as level as possible in the horizontal plane to minimise variation in results due to positional inaccuracy (Prashar *et al,.* 2007). The tonometer is activated by pressing a small button on the grip (Figure 2.2), which activates a small plastic probe, which bounces off the cornea with the returning force being used to calculate the intraocular pressure. The tonometer takes six such measurements, the highest and lowest values are discarded and the remaining four used to calculate a single value which is displayed to the user. Six of these values are averaged to give a measure of intraocular pressure for a single time point. Intraocular pressure measurements were recorded using a database based on the CRITTER design (Lees *et al*. 1993) and developed by Gavin Powell of '+10 technologies'.

Figure 2.2 The Tonolab® tonometer. The trigger (arrow) is pressed to activate probe (arrowhead) which contacts the animal's cornea to take a measurement of the intraocular pressure. (Image from TioLat, Finland). The placement of the activation button on the handle allows for single-handed operation, leaving one hand available for gently restraining the animal which is being measured. The small contace surface of the probe (1mm in diameter) allows for measurements to be taken soley from the centre of the cornea, preventing any confounding effects which may be produced by the probe striking microspheres in the iridocorneal angle.

2.6 Retinal dissection

Fourteen days following the induction of elevated intraocular pressure, animals were killed and eyes were immediately enucleated and placed into iced Hank's balanced salt solution (Sigma-Aldrich, UK) in cell culture dishes (Gibco, UK). A puncture was made in the orbit with a large gauge needle (Cole-Parmer, UK) at the level of the ora serrata and the eye was cut in two at that level using micro-scissors (Cole-Parmer, UK). A cut was made in the eye cup at the superior aspect for the purposes of orientation of the retina. The cup was then turned inside-out to release the retina and two further incisions were made to give a three-leafed retina.

For tissue culture experiments, including diolystic labelling and *in vitro* hydrostatic pressure elevation retinas were then placed onto a cell culture insert (Millipore, UK) which were then rested on suitable culture medium.

For wholemount immunofluorescence, retinas were mounted directly onto slides and excess buffer solution was drawn off with foam buds (Star labs, UK).

2.7 Diolistics and analysis of retinal ganglion cell morphology

Disected retinas were shot placed on a culture medium Cell culture medium adapted from Sun, Li, & He, (2002) which was produced by pipetting 1ml Neurobasal medium, 2mM L-glutamate, 200µl B27 supplement and 100µl N2 supplement (Gibco, UK) into a 1.5ml Eppendorf tube (Starlab, UK). Medium was only produced as needed and was not stored for any length of time to prevent bacterial contamination.

Retinas were labelled with the DiO and DiI carbocyanine bullets using a Helios® gene gun (Bio-rad, UK), in a similar manner to Neely, Stanwood, & Deutch, (2009) and Sun *et al*., (2002).

The bullets were prepared as in Sun *et al*., (2002), 8mg of DiI (Invitrogen UK, UK) and 16mg of DiO (Invitrogen UK, UK) were dissolved in 800µl of trichloromethane (Sigma-Aldrich, UK), the resultant solution was pipetted on to a glass slide with 100mg of fine tungsten particles (Invitrogen UK, UK). The trichloromethane was then allowed to evaporate under a fume hood and the remaining powder was tapped into a 45cm length of 8mm diameter vinyl tubing (Cole Parmer, UK). In order to coat the tubing with the powder, the tube was placed on a rotating platform for a minimum of 24 hours in darkness before being cut into 1cm bullets with a razor blade.

The Helios® gene gun uses a 12 cartridge cassette to hold a single 1cm length of tubing containing the carbocyanine dye in the path of a volume of helium pressurised at 120 pounds/inch^2 (figure 2.3) followed by a second release of helium at 90 pounds/inch^2 to ensure clearance of the cartridge. To prevent dense clumps of DiI/DiO-coated tungsten beads hitting the retina, a 3µm-pore filter (Falcon) was

positioned over the cell culture dish. Retinas were incubated for 30 mins at 37°C in 95% air/5% CO2, the culture medium was discarded prior to fixation in 4% paraformaldehyde and sealed with Parafilm® (BioStar, UK) and stored at 4°C for 25 minutes. Paraformaldehyde was discarded and the membrane of the culture insert was cut in order to remove the retinas, which was subsequently mounted on a Histobond® (Marienfeld, Germany) slide and circled with a hydrophobic pen (Vector Laboratories, UK). ToPro-3® solution was added to the retinae on the slide and incubated for 10 minutes at room temperature in the dark, removed with a three washes of 1ml phosphate buffered saline. The retinas were mounted with ProLong Gold® (Invitrogen, UK) under a glass coverslip which was sealed with clear nail varnish.

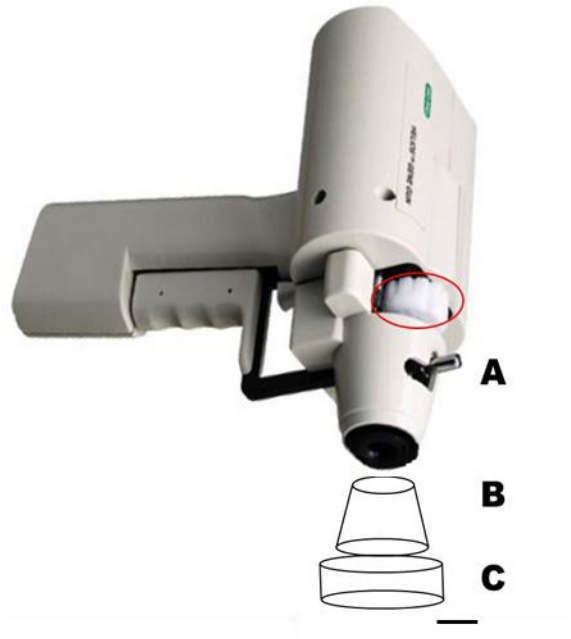

Figure 2.3 Diagram of modified Helios® gene gun. Diagram showing approximate, relative position at the time of use. A – Helio® gene gun with barrel removed to allow for closer proximity to the filter. The red circle shows the barrel containing the DiI/DiO loaded tubing. B – Falcon-filter in position to scatter the fired tungsten particles. This was designed to create a more uniform spread of particles and filter out larger particles to reduce kinetic damage to the tissue. C – Cell culture insert with retina to be labelled mounted on the upper surface. Scale bar = 1cm.

2.7.1 Sholl analysis.

All image processing and data acquisition was carried out masked. This was done using the ‘Masked images’ macro for the ImageJ platform (see appendix). Each file in a specified folder is opened within the memory of the computer without displaying the image to the user, a random number of a length specified by the user is generated and the file is saved in a new directory/folder with that number as the file name. A key file is then generated containing a table of the masked and original file names in the source directory/folder.

Image analysis was carried out using the ImageJ software (NIH, USA), z-stack images were processed using ‘Sholl processing’ macro (see appendix) to automate image processing once aberrant staining caused by bead aggregation and other artefacts had been manually removed. The relevant colour channel pertaining to the dye which had labelled the cell in question was isolated. Images were discarded if the morphological criteria of a retinal ganglion cell (no axon or cell nucleus not residing in the ganglion cell layer as indicated based on ToPro-3® labelling).

The image slices were z-projected using the sum of the slices of the stack to produce a single image which contained as many features of the dendrites as possible. Images were then converted to 8-bit .jpeg files for Sholl analysis. Sholl analysis of confocal images was performed using a custom MatLab® (MathWorks, USA) plugin developed by Professor Alun Davies, detailed in Gutierrez & Davies (2007), briefly, the user delineates the scale bar, identifies the dendritic roots, bifurcations and terminals and the plugin calculates the number of dendritic branches at a specified number of regularly spaced distances from the soma, in this case

calculations were made for 30 distances from the cell soma at 10µm intervals (Illustrated in figure 2.4). This generated a graph referred to as a ‘Sholl plot’, containing two key metric which are relevant in the analysis of dendritic health; the number of intersections at a given distance from the cell and the area under the curve (AUC). The AUC of the Sholl plot represents the total number of intersections in a retinal ganglion cell dendritic field and will be used as a single indicator of dendritic integrity.

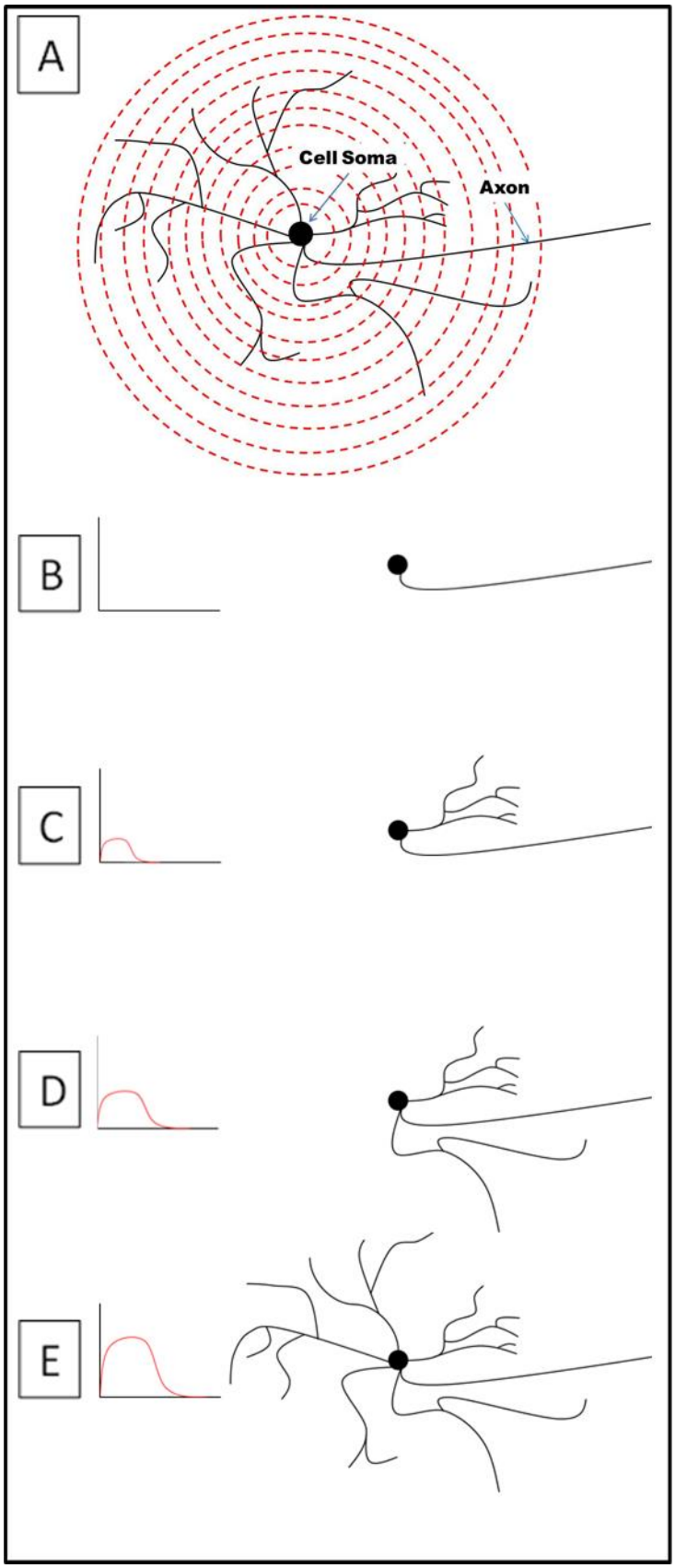

Figure 2.4 Schematic representation of a Sholl analysis. A - Cell soma and axon are indicated, red-dashed lines indicate the positions of the theoretical concentric circles. The intersections of cell dendrites with the circles are calculated to quantify the retinal ganglion cell's dendritic integrity. (B – E) Illustration of changes in Sholl plots as retinal ganglion cell morphology changes, number of intersections are represented on the y-axis and the distance of the intersections is represented on the x-axis.

2.8 Confocal imaging

2.8.1 Diolistically labelled cells

Images were acquired using a confocal microscope (LM510, Zeiss, Germany) using a x20 objective lens, excitation at 543nm for DiI, 488nm for DiO and 633nm for ToPro, scaling at; 0.38432µm/pixel on the x and y axes and 0.19 µm/pixel on the z axis at an image resolution of 1024x1024 pixels (x and y axes, respectively), this produced an image 393.54 µmx393.54 µm, stacks were taken through the thickness of the retinal ganglion cell and inner plexiform layers, resulting in scan depths of between 7.3 µm and 151.4 µm.

2.8.2 Immunofluorescence

Three dyes were used for all immunofluorescence, AlexaFluor® 488, AlexaFluor® 594 and ToPro-3 iodide (Invitrogen UK, UK). These were imaged using a confocal microscope (Zeiss, Germany) with laser excitation at the wavelengths 488nm, 543nm and 633nm and psedo-coloured green, red and blue respectively. Z-stacked images were taken through each retinal section with 20x objective lenses, laser settings were adjusted only between experiments so that comparable results were produced within each experiment.

Grey values corresponding to the detection of each dye were obtained using ImageJ (NIH, USA) by isolating the channel of interest, converting the image to 8-bit and measuring the total antibody detection present in the region of interest. In images of wholemounted retinas the region of interest was obtained by manually segmenting the inner plexiform and ganglion cell layers from a single field of view 393.54x393.54µm at 1.5mm from the optic nerve head.

In images of fluorescently labelled sections this was a 100µm region of the inner plexiform and retinal ganglion cell layers measured from the right edge of the image, this was done to correct for slanting of images. The area measured was then divided by the total value of the pixels counted to give a mean grey scale value. This value is represented in arbitrary units with a theoretical maximum of 9294/µm (with a voxel size of 0.38x.038x0.19µm and the maximum pixel value for an 8-bit image being 255) for wholemount images and 4647/µm (voxel size of 0.38x0.38x0.38µm) for sections.

2.9 Retinal sectioning

Animals were killed at by exposure to a rising concentration of CO_2, confirmed by cervical dislocation. Eyes were enucleated and fixed for 1hour in 4%paraformaldehyde at room temperature , the anterior chamber was then cut away and removed at the limbus and the eye was cryoprotected by submerging in increasing concentrations of sucrose at (10-20-25%) concentrations. These solutions were prepared by dissolving 10, 20 and 30 grams of sucrose powder (Sigma-Aldrich, UK) in 100ml of deionised water.

Eyes were then embedded in optimum cutting temperature medium (Tissue-Tek, UK) and snap-frozen in liquid nitrogen-cooled isopentane (Sigma-Aldrich, UK) and sectioned at 7µm. The frozen tissue block was trimmed until observation of beginning of the structures associated with the optic nerve head before sections were taken to ensure uniformity of the retina in the sections. Eight sections were taken from each eye for each set of stains that were required in addition to eight sections for control stains. Sections were removed from the cryostat by touching the section to the room temperature slides, ensuring that 3-4 evenly spaced sections

were on each slide. Sections were stored at -20°C in sealed slide boxes until required. Slides were defrosted at room temperature for 30 minutes prior to immunofluorescent staining.

2.10 Retinal section immunofluorescence

Blocking solution, consisting of 10% donkey serum in phosphate buffered saline was added to the retinal sections. The blocking solution was made by diluting 1ml of donkey serum with 9ml of phosphate buffered saline. This solution was left on for 1 hour at room temperature before being pipetted off.

For complement and neuronal marker detection: Primary antibody solution (Table 2) consisting of 1 part in 50 monoclonal mouse antibody to rat C3b/iC3b and either 1 part in 400 polyclonal rabbit antibody to rat neuronal marker PSD95 (Cell Signalling, UK) or 1 part in 100 polyclonal rabbit antibody to rat C9 (Courtesy of Dr Claire Harris, Cardiff University) diluted in phosphate buffered saline. 50µl of primary antibody solution was added to each retinal section and incubated at room temperature for 1.5 hours.

For C1 inhibitor or C1q detection: either 1 part in 1000 rabbit anti-human C1 inhibitor (Provided by Dr Svetlana Hakobyan, Cardiff University) or 1 part in 100 rabbit anti-rat C1q antibody (Cell Signalling, UK) was diluted in phosphate buffered saline and 75µl primary antibody solution was added to each slide and incubated overnight (minimum 16 hours) at 4°C (C1q staining was carried out by Dr Claudia Calder, Cardiff University). The primary antibody solution was then washed off by rinsing with phosphate buffered saline three times.

Table 2 Primary antibodies used for immunofluorescence

Target	**Raised in**	**Dilution**	**Other**
PSD95	Rabbit	1:400	Polyclonal
C3b/iC3b	Mouse	1:50	Monoclonal
C1 inhibitor	Rabbit	1:1000	Polyclonal
C9	Rabbit	1:150	Polyclonal
C1q	Rabbit	1:100	Polyclonal

The relevant secondary antibody solution (detailed in table 3) was then added to the sections. The secondary antibody solution was incubated for 1.5 hours at room temperature and then pipetted off. Sections were washed three times in phosphate buffered saline and mounted with prolong gold ® antifade reagent (Invitrogen, UK) prior to imaging.

Table 3 Secondary antibodies used for immunofluorescence.

Target	**Raised in**	**Dilution**	**Flurophore**	**Other**
Rabbit	Donkey	1:400	AF488	
Mouse	Donkey	1:400	AF594	
Rabbit	Donkey	1:400	AF488	ab_2 fragment only
Mouse	Donkey	1:400	AF594	ab_2 fragment only

2.11 Statistical analysis

Statistical analysis was performed using SPSS (IBM, US). For all datasets that were to analysed, the Anderson-Darling test was used to test for normality. The outcome of this test determined what further statistical analysis was carried out.

2.11.1 Intraocular pressure measurements

Baseline intraocular pressure measurements and those from control, uninjected eyes were typically normally distributed, whereas those of microsphere-injected eyes were not. This is a consequence of the large changes in intraocular pressure associated with microsphere injection. In order to compare normally distributed control intraocular pressure values with those of microsphere injected eyes the Mann-Whitney U test was used. This test was used under these circumstances as it compares the ranking of the data sets rather than the means. This quality is advantageous as the intraocular pressure of a microsphere injected eye may be highly variable and as such the mean may not be representative of any values in the dataset.

2.11.2 Sholl analysis

The data points that make a Sholl curve are complex and universally not normally distributed. A typical Sholl plot is a positively skewed dataset, with a large number of dendrites closer to the cell soma compared to a decreasing number at greater distances. Preferential loss of secondary and tertiary dendrites increases the positive skew of the dataset (illustrated in figure 2.5), meaning that changes between data sets are not even (Sun *et al*. 2002). In order to account for these factors a statistical test which accounts for factors other than distribution was needed. To account for these factors a Kolmogorov–Smirnov test was used to compare Sholl

plots as this test also analyses skewness of a dataset (Toutenburg 1975). This test was performed on the means of the measured number of intersections at each distance from the cell soma for each group of cells. The AUC for each dataset is included in the analysis for illustrative purposes as this gives a representative value for the integrity of the dendritic fields.

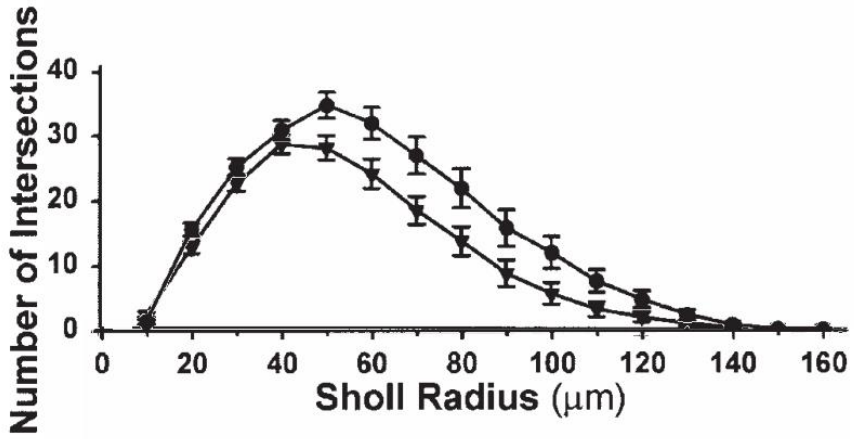

Figure 2.5 An example of normal and glaucomatous Sholl plots. Illustration of the effect of glaucomatous degeneration on a Sholl plot derived from primate retinal ganglion cells. The glaucomatous Sholl plot (Triangles) has preserved denrites up to 40μm radius compared to the normal Sholl plot (Circles), whereas dendrites over this radius are lost. This has the effect of changing the skewness of the Sholl curve, meaning that a statistical test which accounts for changes in skew is usefull in comparing glaucomatous and healthy Sholl plots. Figure modified from Weber & Harman (2005).

Chapter Three: Microsphere Model Development

3.1 Introduction

Existing models of glaucoma in laboratory animals have achieved a great deal in the modelling of disease progression and pathology. This includes: identifying specific details regarding the patterns of axonal loss (Jakobs *et al.* 2005; Quigley & Addicks, 1980; Quigley & Anderson, 1976), isolation of genes involved in retinal ganglion cell apoptosis and clearance (Guo *et al*., 2010; Hernandez, Agapova, & Yang, 2002; Howell *et al*., 2011; Khalyfa et *al.* 2007; Miyahara, 2003; Tezel *et al*., 2010) and the investigation of novel treatments for glaucomatous optic neuropathy (Anderson et *al.* 2005). Despite these advances, each of the currently available models has inherent limitations.

These existing models of glaucomatous optic neuropathy have been shown to be capable of replicating acute or chronic, unilateral or bilateral, and pseudoexfoliative or angle closure glaucoma. However, they each have their own, specific weaknesses. The aim of this section is to develop a model of glaucoma that addresses as many of these concerns as possible.

To demonstrate the efficacy of any treatment and remove any possibly confounding influence of age-related degeneration, the most time-and cost-efficient model for the testing of neuro-protective agents in glaucoma should be one that is inducible rather than inherited. This would also allow glaucoma to be either unilateral or bilateral and allow intervention to begin before or concurrently with the onset of disease. Inducing unilateral glaucoma has the advantage of providing an internal control in the contralateral, normotensive eye. Inducing bilateral glaucoma may allow the testing of two different treatments within the same animal, potentially removing confounding variables that may occur between animals. As there are no

data already available for this model, robust control tissue will be necessary from the outset. With this in mind, it was decided that the model of glaucoma developed here would involve a unilateral intraocular pressure elevation. Existing models of microsphere injection have been demonstrated by other groups to be useful and straightforward. As a result of these factors, it was decided that trabecular meshwork occlusion with microspheres was a suitable starting point for development of a model of glaucoma. Polystyrene microspheres, once injected, follow gravity and sink to the inferior aspect of the anterior chamber. This behaviour creates three problems: (i) only the inferior aspect is effectively occluded, limiting the subsequent intraocular pressure elevation, (ii) the contact of the beads on the cornea may interfere with tonometry measurements and (iii) the number of beads injected is limited by the physical stress on the inferior aspect of the anterior chamber.

The use of paramagnetic microspheres was considered to remedy these issues as they can be externally manipulated post-injection to draw the microspheres into the trabecular meshwork. This would cause the microspheres to become physically trapped around the entire circumference of the iridocorneal angle rather than simply the inferior aspect. This in turn would allow for a greater number of beads to be used with greater trabecular outflow obstruction and minimal effect on the cornea.

In order to establish the optimum protocol for inducing a unilateral elevation in intraocular pressure, different concentrations of paramagnetic microspheres will be used with or without magnetic manipulation.

3.2 Methods

3.2.1 Toxicity assay

To determine whether or not paramagnetic microspheres were inherently toxic to neuronal cells, microspheres were cultured with cells from an SH-SY5Y neuroblastoma cell line. The viability of the cells was assessed using an 3-(4,5-dimethylthiazol-2-yl)-2,5-diphenyltetrazolium (MTT) assay. Paramagnetic microspheres were prepared as in section 2.4.2 Invitrogen microspheres. The SH-SY5Y neuroblastoma cell line was kindly provided by Professor Robert Maclaren (University of Oxford, UK), and cell culture and viability assays were performed by Dr Debbie Tudor. Cells were grown in (1:1) Ham′s F12 (Sigma-Aldrich, UK), Eagle's minimum essential medium (Invitrogen, UK) supplemented with 2 mM L-Glutamine, 1% non-essential amino acids, 15% foetal bovine serum and 100U/ml penicillin and 100µg/ml streptomycin (Invitrogen, UK), maintained at 37°C in air with a constant CO_2 concentration of 5%. Cells were seeded at $3x10^4$ per well in 96 well flat bottom culture plates (Star lab, UK). One hundred microliters of paramagnetic microsphere preparations were then added to each well at concentrations of 2x10, $2x10^2$, $2x10^3$, $2x10^4$, $2x10^5$ and $2x10^6$ per well. Positive controls for cell toxicity were carried out using 0.1% Triton X® and 5mM H_2O_2 (Sigma-Aldrich, UK) in PBS in place of microsphere preparations. Cultures were continued for a further 48 hours prior to MTT assay to determine the toxicity of the paramagnetic microspheres.

The MTT assay was carried out according to the manufacturer's (Millipore, UK) instructions. Ten microliters of MTT solution was added to each well and incubated at 37^oC for four hours, after which, ten microliters of a 0.04M solution of HCl in isopropanol was added to each well. After one additional hour one hour the

absorbance of the wells at a wavelength of 570nm was measured using a Versamax® (Molecular devices, US) plate reader. Absorbance was compared to that of a well containing a fresh culture of $3x10^4$ cells, which allowed me to determine if the beads were an inhibitor of growth or actively toxic to cells. Cultures and toxicity assays were performed in triplicate. The results of cell viability assays were normally distributed and for that reason, viability assays were compared using a two-sample t-test.

3.3 Factors affecting induction of an elevation in intraocular pressure

3.3.1 Microsphere size

Paramagnetic microspheres of 1-3µm diameter induced no significant intraocular pressure elevation in 5 injected animals (Figure 3.1 A) (mean intraocular pressure of 28.71mmHg, SD=4.88mmHg) compared to the uninjected control eye (Mean=27.04mmHg, SD=4.07mmHg, p=0.92 Mann-Whitney U test). A sustained intraocular pressure elevation was produced in 7 animals injected with 5µm diameter beads, with a mean elevation of 21.22mmHg (Figure 3.1 B, n=7 animals, $p<0.05$ Mann-Whitney U test)) and 3 animals requiring a second injection at day 15 to maintain elevation. Beads of 10-12µm diameter could not be injected as they became trapped in the needle during injection. These data suggest that the optimum diameter of beads injected into the anterior chamber for the purpose of increasing intraocular pressure is approximately 5µm.

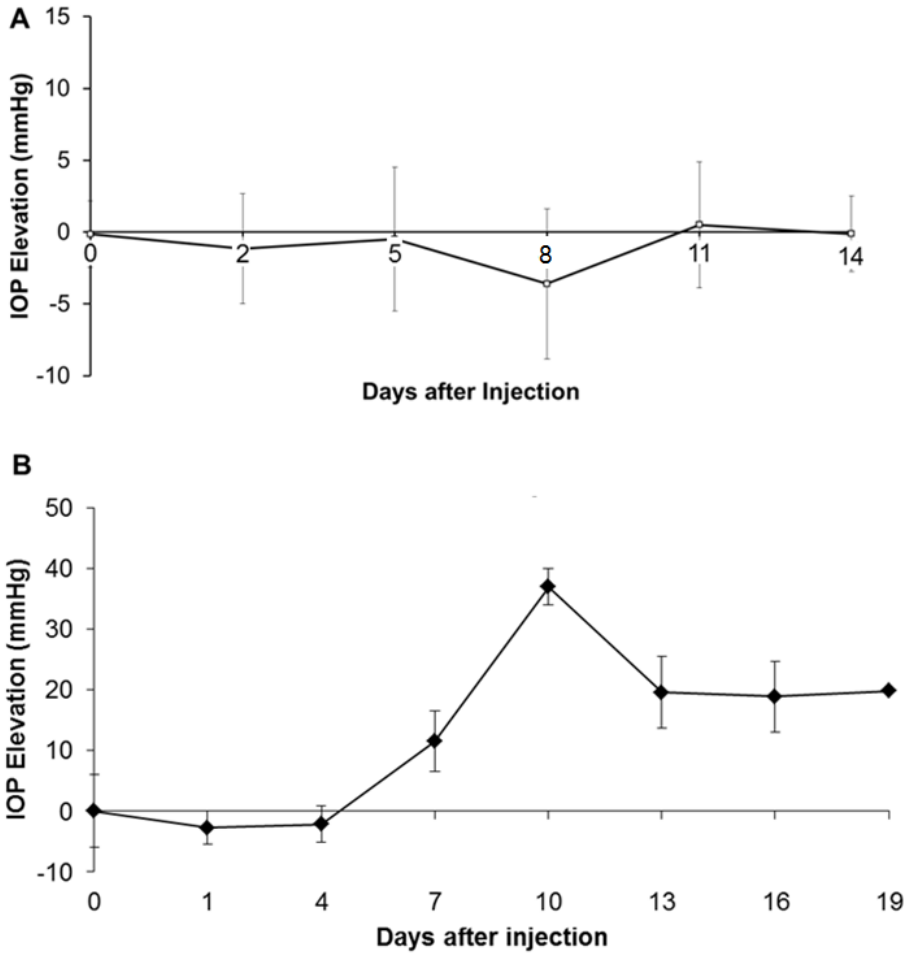

Figure 3.1 Microspheres of a minimum 5µm in diameter are required to generate an increase in intraocular pressure. (A) Intraocular pressure elevation profiles (injected eye pressure – uninjected eye pressure) of five animals injected with 1-3µm beads, showing no intraocular pressure elevation in the injected eye (mean intraocular pressure of 28.71mmHg) compared to the contralateral, control eye (Mean=27.04mmHg, n=5 animals, p=0.92 Mann-Whitney U test). (B) Mean intraocular pressure elevation profiles of seven animals which had a unilateral injection of paramagnetic microspheres (5µm in diameter). The mean intraocular pressure of the injected eyes was elevated by and average of 21.22mmHg (n=7 animals, $p<0.05$ Mann-Whitney U test) over the course of the experiment.

3.3.2 Microsphere concentration and manufacture.

Beads purchased from Corpuscular, Inc (NY, USA)**,** had a higher variance in concentration and size than those purchased from Invitrogen UK. Inspection of corpuscular beads using a transmission electron microscope (Courtesy of Dr Guy Jones, Cardiff University) revealed a variation in size from 5.2-7.5µm (Figure 3.2). In addition, the beads supplied by Invitrogen were more tolerant of use at elevated concentrations and could be injected at a concentration (i.e. $8x10^8$ beads/ml, which is two times the stock concentration or $8x10^6$ beads in a 10µl injection). In future, this property of the Invitrogen supplied beads may prove useful as a means to titrate the bead particle dosing and gain finer control of the induced elevation in intraocular pressure. It was also observed that after repeated injections with a single syringe using the Corpuscular microspheres, even when washing syringes with 10mM ethylenediaminetetracetic acid (Sigma-Aldrich, UK) after use, syringes would block up at unpredictable intervals. This characteristic may be associated with the variation in microsphere size and roughness of the microsphere surface apparent in figure 3.2A. For these reasons, the microspheres produced by Invitrogen were used exclusively in the later work in the project.

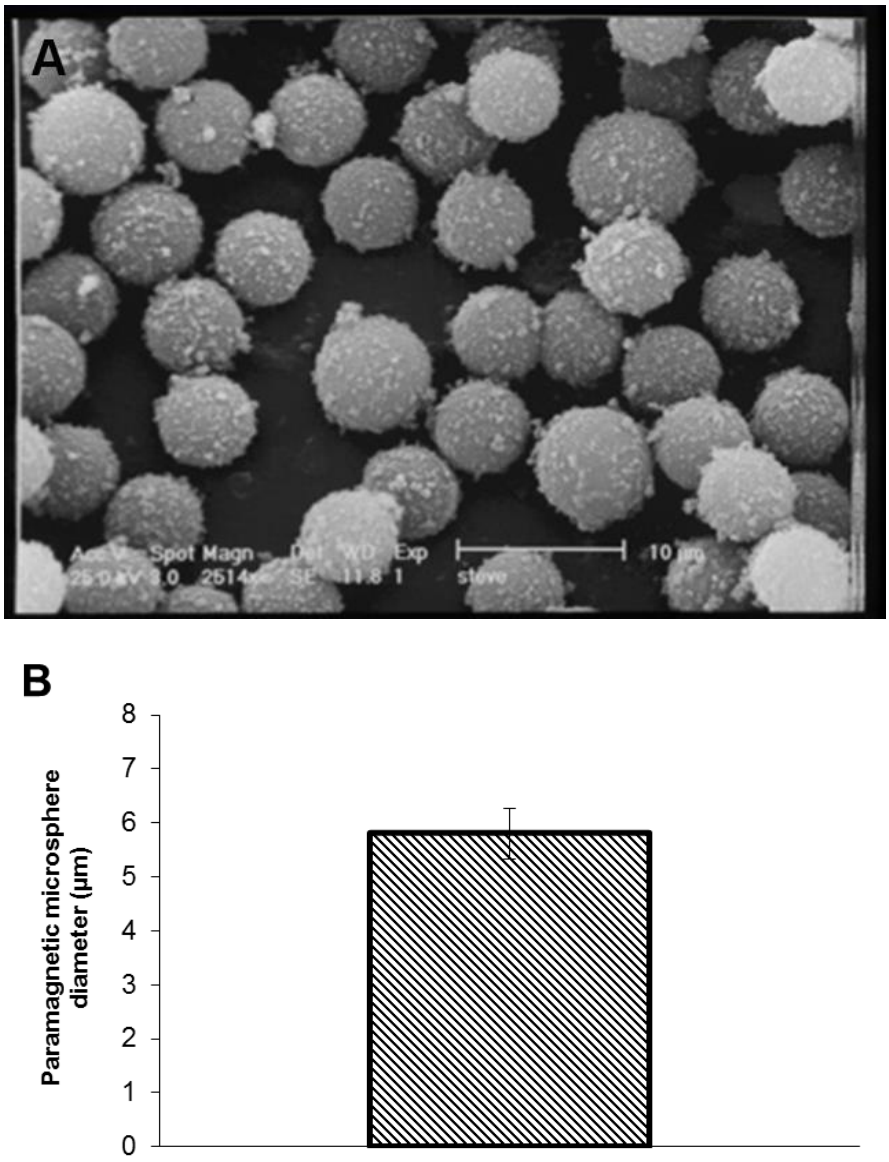

Figure 3.2 There is a large variation in the diameter of Corpuscular-manufactured paramagnetic microspheres. (A) Transmission electron micrograph of magnetic microspheres supplied by Corpuscular, Inc., showing a noticeable variation in bead particle size, scale bar = 10µm. (B) Measurements of 44 paramagnetic microspheres imaged by electron microscopy (mean thickness=5.8µm, minimum diameter=5.2µm, maximum diameter=7.5µm). Error bars indicate standard deviation of 0.46µm. This variation may explain the occasional blocking of the syringe observed during work. Future work may benefit from filtration of the microspheres prior to injection.

3.3.3 Magnetic manipulation

In this experiment, rats received unilateral injections of either 10µl or 20µl of Corpuscular microspheres (2 animals each group) as described in section 2.5, without manipulation with a magnet to determine the effect of bead injection alone on intraocular pressure. Animals were housed for 20 days to monitor the development of any increase in intraocular pressure.

Of the two animals injected with 10µl of microspheres, the mean intraocular pressure elevation over 20 days was 2.11mmHg, although this was not statistically significant (SD=8.9mmHg, *p*=0.09 Mann-Whitney U) (Figure 3.3 A). At day one post-injection, there was a dramatic and very similar increase in intraocular pressure in the injected eyes of both animals (21.2 and 21.6mmHg). However, this elevation immediately disappeared, and the intraocular pressure of the injected eyes was not significantly different from uninjected control eyes until day 20.

Of the two animals in the group injected with 20µl of beads, one developed an initial spike in intraocular pressure of 29.4mmHg over the contralateral eye at day one following injection. This elevation was not sustained, and the intraocular pressure of the injected eye was not significantly different from that of the control at any further time point. In this animal, the mean intraocular pressure in the injected eyes (Figure 3.3 B mean=24.07 mmHg, SD=10.94mmHg) was not significantly different from that of the uninjected, control eye (mean=20.31 mmHg, SD=4.03mmHg, *p*=0.10 Mann-Whitney U).

The other animal in this group showed an intraocular pressure elevation of 40.8mmHg over that of the control, uninjected eye 1 day following microsphere injection. The pressure elevation fluctuated between -0.8 and +26 over the following

five days (Figure 3.3 C). This animal then developed a substantial haemorrhage in the anterior chamber, which caused blood to pool on top of the beads and a noticeable corneal ectasia (see figure 3.4). As a result of the intraocular haemorrhaging, the animal in question was culled early to prevent unnecessary suffering. Post-mortem, the microspheres in the eyes of all animals that did not undergo post-injection magnetic manipulation were still visibly motile within the anterior chamber.

In light of the increased damage caused by microspheres without magnetic manipulation, it was decided that closer monitoring of animals was necessary. With that in mind the experiment was redesigned and 5 animals were injected with 20µl of standard Corpuscular bead solution without magnetic manipulation over the standard time period. The eyes of the animals were inspected twice daily to monitor for anterior chamber haemorrhage and corneal ectasia. Beads remained motile in the anterior chamber (Figure 3.5), and no significant intraocular pressure elevation was observed in the injected eyes compared to the contralateral controls (Figure 3.6 n=5 animals, mean= 28.9mmHg, SD=3.2mmHg and mean=27.08mmHg, SD=3.3mmHg respectively, p=0.35).

When paramagnetic microspheres were manipulated with a hand-held magnet after injection into the anterior chamber, they remained evenly distributed around the entire iridocorneal angle. The manipulated microspheres remained static upon movement of the animal, did not adhere to the iris and did not remain in the visual axis (Figure 3.7). The paramagnetic microspheres, which were manipulated with a hand-held magnet, were also not associated with any cases of intraocular haemorrhaging.

These observations indicate that post-injection manipulation of the paramagnetic microspheres is required for the safe and reliable induction of an elevation in intraocular pressure. This is a crucial observation as it validates the hypothesis underlying the mechanism of the model – that the distribution of microspheres around the iridocorneal angle is an important element of a stable intraocular pressure elevation.

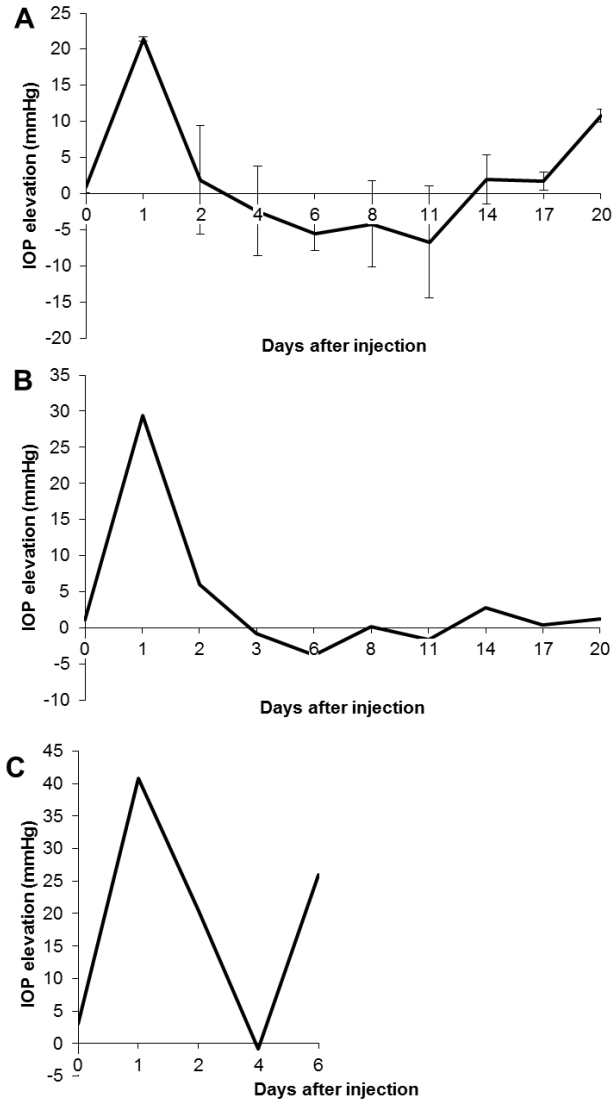

Figure 3.3 Paramagnetic microsphere injection without magnetic manipulation produces erratic or minimal elevation in intraocular pressure. (A) Mean intraocular pressure elevation profile of two animals injected with 10µl of Corpuscular microsphere solution; error bars are standard deviations. Both animals developed an elevation of intraocular pressure one day after injection (mean=21.4mmHg, n=2 animals). By day two there was no significant difference between the uninjected, control eye and the injected eye until day twenty where there was a mean pressure elevation of 10.8mmHg (11.4mmHg and 10.2mmHg). Over the twenty days, the mean intraocular pressure of the injected eyes (Mean=28.48mmHg, SD=10.01mmHg) was not significantly different from that of the uninjected, control eyes (Mean=26.37mmHg, SD=4.2mmHg, *p*=0.09 Mann-Whitney U). (B – C) Individual intraocular pressure elevation profiles for 2 animals injected with 20µl of microspheres without magnetic manipulation. One animal (B) developed an elevation in intraocular pressure of 29.4mmHg at day one following injection. This elevation dropped to 6mmHg at day two and no further elevation was observed. The mean intraocular pressure over the twenty day time period for the microsphere-injected eye (mean=24.07 – mmHg, SD=10.94mmHg) was not significantly different from that of the uninjected, control eye (mean 20.31=mmHg, SD=4.03mmHg, *p*=0.10 Mann-Whitney U). The other animal in this group developed an increase in intraocular pressure, varying from -0.8mmHg to +40.8mmHg over the first 6 days following injection. However, the animal also manifested a number of health problems associated with the injection (See figure 3.4).

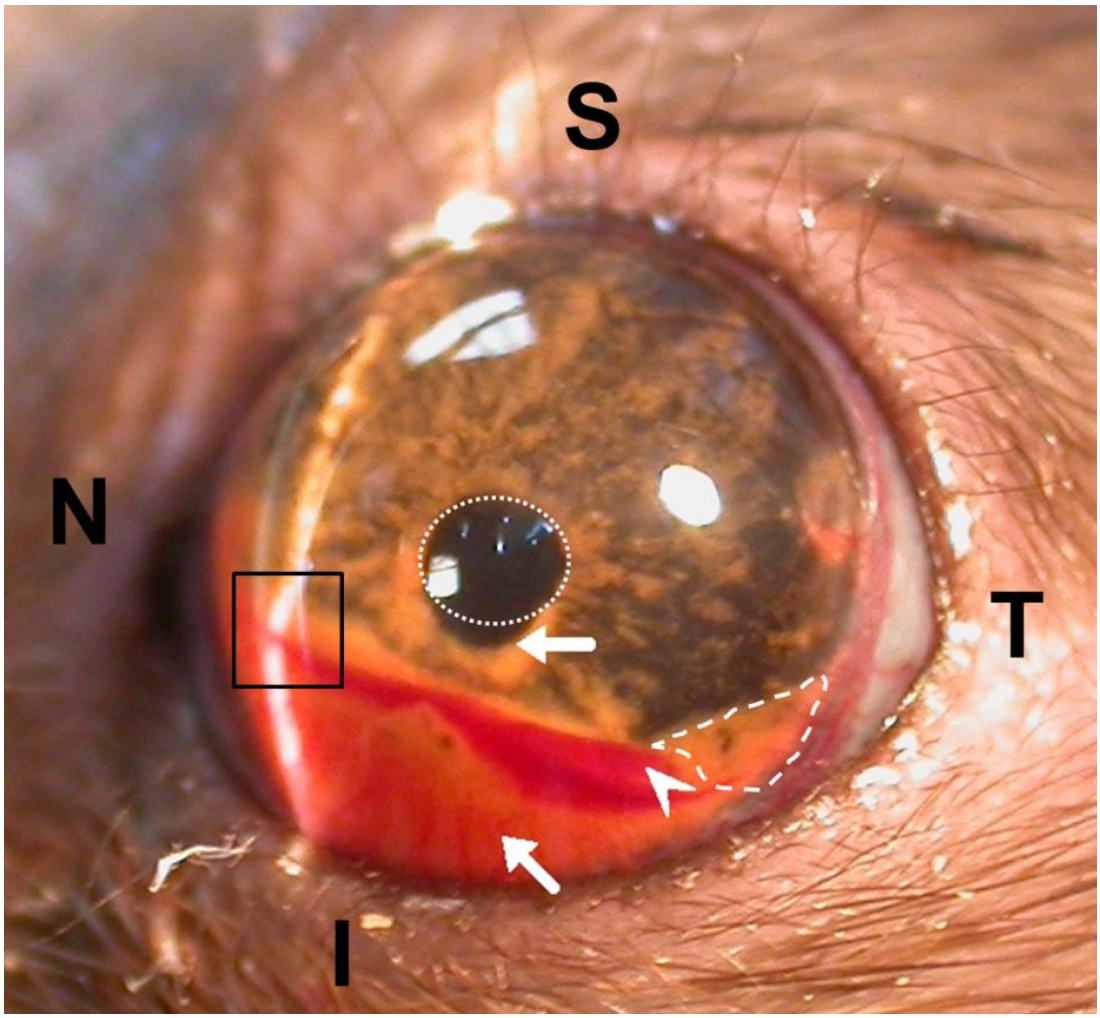

Figure 3.4 Magnetic manipulation is required for the safe administration of paramagnetic microspheres into the anterior chamber of the eye. Arrows indicate the position of the injected beads, with marked neovascularization present in the inferior aspect of the cornea. Arrow head shows a pool of blood resting on the beads. The dotted line indicates the 'Tide mark' left by the beads as they moved around in the eye of the animal. The starred line indicates the position of the pupil, note the deformation of the pupil; at the inferior aspect, which may result from the adherence of beads to the iris. There is a noticeable corneal ectasia at the level of the beads indicated by the shift in light reflection, highlighted by the black box. Markings indicate nasal (N), superior (S), temporal (T) and inferior (I) aspects of the eye.

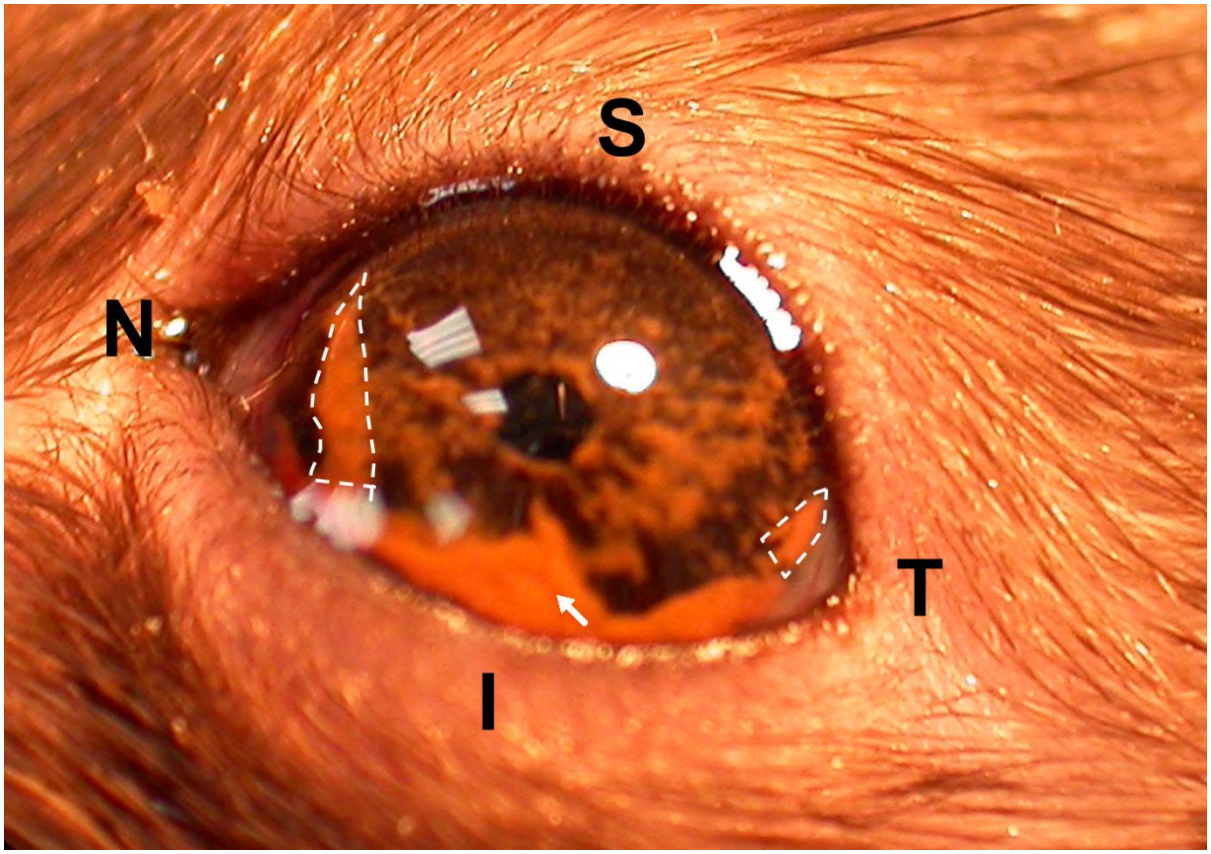

Figure 3.5 Bead injection without magnetic manipulation causes pooling of free beads in the inferior aspect of the iridiocorneal angle. Arrow indicates beads resting at the inferior aspect of the anterior chamber, and dotted lines delineate the motile beads that roll around the eye during normal animal movement. Markings indicate nasal (N), superior (S), temporal (T) and inferior (I) aspects of the eye.

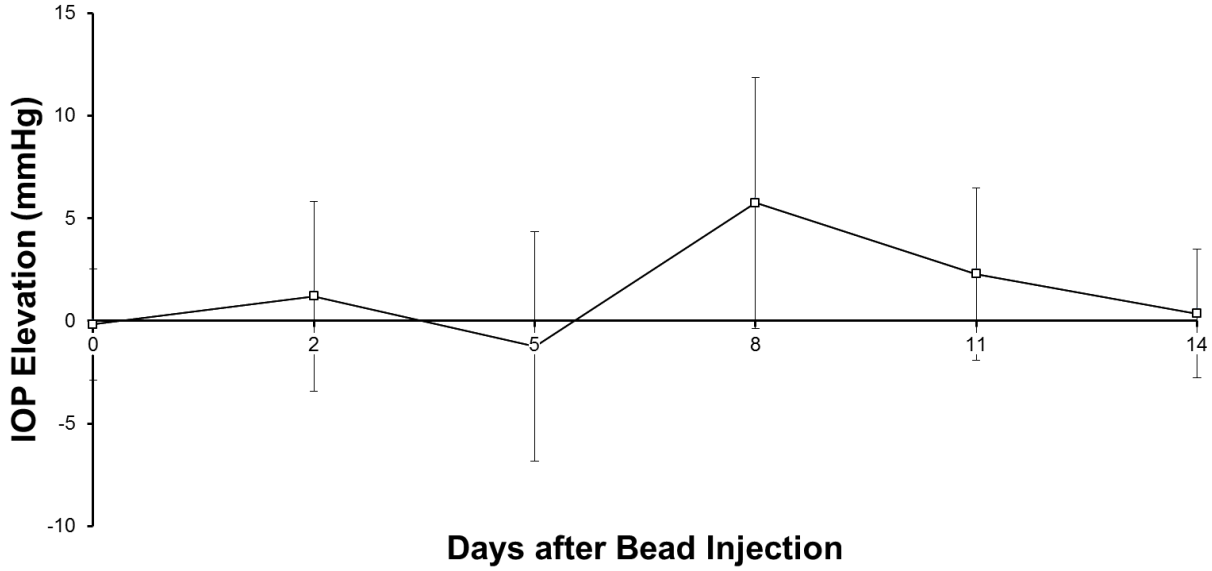

Figure 3.6 Magnetic manipulation of paramagnetic magnetic microspheres is required to induce an elevation in intraocular pressure. Mean intraocular pressure elevation over fourteen days of 5 animals injected with paramagnetic microspheres and not manipulated with a magnet. Un-injected, contralateral eyes had a mean pressure of 27.08mmHg (SD=3.3mmHg, n=5 animals). The intraocular pressure of eyes which received injections of paramagnetic microspheres without magnetic manipulation were not significantly elevated with a mean intraocular pressure of 28.9mmHg (SD=3.2mmHg, p>0.05 by Mann-Whitney U test, error bars are standard deviations).

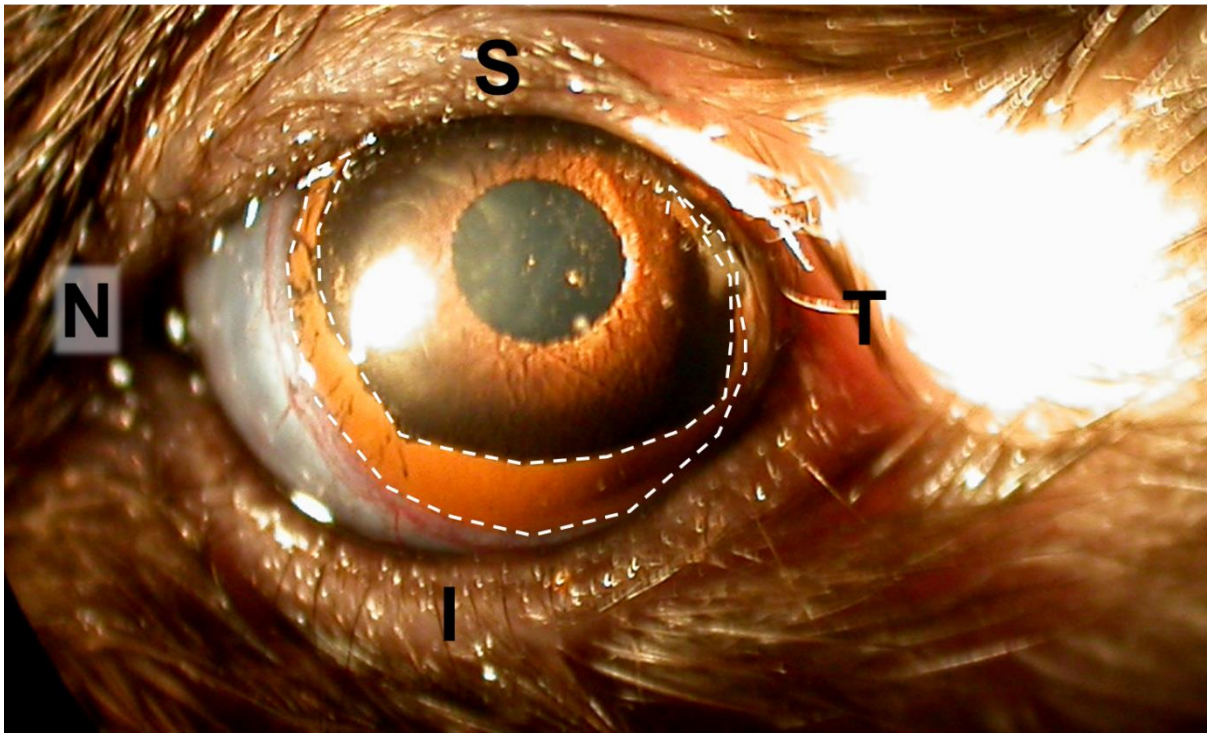

Figure 3.7 Bead injection with magnetic manipulation results in an even distribution of beads around the iridocorneal angle. Following the manipulation of paramagnetic microspheres with a hand-held magnet, beads were trapped in the trabecular meshwork, preventing pooling of beads at the inferior angle. Moreover his was associated with an absence of ocular haemorrhage and corneal ectasia. There is no apparent vascularisation of the cornea or deformation of the pupil, and the beads are uniformly distributed around the circumference of the irirdocorneal angle as indicated by the dotted lines. The absence of motile beads in the anterior chamber following magnetic manipulation is indicative of a more efficient distributio,n which helps to explain the greater elevation of intraocular pressure produced.

3.3.4 Microsphere injection

It was necessary to ascertain whether injection of balanced salt solution in conjunction with exposure to a magnetic field could illicit an increase of intraocular pressure to confirm that it was the paramagnetic microspheres that were responsible for any observed increase. To that end, five animals were injected with 20µl of balanced salt solution (Alcon, US) into the anterior chamber, and the eye was treated with the hand-held magnet similarly to the standard protocol. The mean intraocular pressure of the injected eyes over a fourteen day period was 30.0mmHg compared to a mean control pressure of 26.1mmHg (Figure 3.8), which indicated an elevation of 3.9mmHg that was not statistically significant when compared with a Mann-Whitney U test (p>0.05). These results indicate that balanced salt solution vehicle and exposure to a localised magnetic field are not sufficient to induce an elevation in intraocular pressure. This is an important determination in the use of this model as it eliminates the vehicle and procedures involved in the method as potential confounders in the proposed mechanism of paramagnetic microsphere induced intraocular pressure.

Figure 3.8 Vehicle injection and magnetic manipulation are not sufficient for a significant elevation in intraocular pressure. Graph showing the mean intraocular pressure elevation in five animals that underwent unilateral, balanced salt solution injections. The mean intraocular pressure of eyes injected with balanced salt solution was 30.0mmHg with a standard deviation of 3.2mmHg. This compares to a mean intraocular pressure in the contralateral, uninjected eyes of 26.1mmHg with a standard deviation of 2.9mmHg. There was no significant difference between eyes which underwent balanced salt solution and exposure to a magnetic field and contralateral, untreated eyes over a fourteen day period when pressures were compared with a Mann-Whitney U test(n=5, error bars are standard deviations).

3.4 Microsphere toxicity

To determine whether the paramagnetic polystyrene microspheres are toxic to neuronal cells, SH-SY5Y neuroblastoma cells were incubated with the microspheres for 48 hours and cell viability was measured by an MTT viability assay. With a microsphere concentration of $2x10^6$/ml, at a ratio of 66.67 microspheres to SH-SY5Y cells, the beads induced 20.1% (SD=3.898, $p<0.05$, t-test, figure 3.9, n=3) cell death, whilst the positive controls for cell death, H_2O_2 and 0.1% Triton-X, induced 34.7% (SD=1.784, $p<0.01$) and 90% (SD=0.714, $p<0.005$) cell death, respectively. The greatest number of microspheres injected into a single eye was $8x10^6$ (10µl injection of $8x10^8$ Invitrogen microspheres/ml). Assuming that 10% of all injected microspheres leak from the anterior chamber of the eye into the vitreous chamber, there would be up to $8x10^5$ microspheres in the vitreous chamber. Assuming that there are, on average 86,282 (Fileta *et al*. 2008) retinal ganglion cells in the retina of a brown Norwegian rat, this would produce a ratio of 9.27 microspheres per retinal ganglion cell.

This is a worst-case scenario for estimating the level of microsphere toxicity, as it assumes a very high level of microsphere efflux that has not been observed during these experiments (See figure 3.7). This scenario also assumes that all microspheres entering the vitreous chamber associate with retinal ganglion cells. This is unlikely as retinal ganglion cells constitute only a minority of the cells in the retina. In addition, there is no reason to suspect that microspheres would be able to migrate through the dense vitreous humour. Even in this worst-case scenario, the ratio of microspheres to retinal ganglion cells is below that at which microspheres are observed to cause toxicity. This is an important observation for the use of

paramagnetic microspheres in a model of glaucoma as it establishes that the microspheres themselves are not responsible for any toxicity observed in the model.

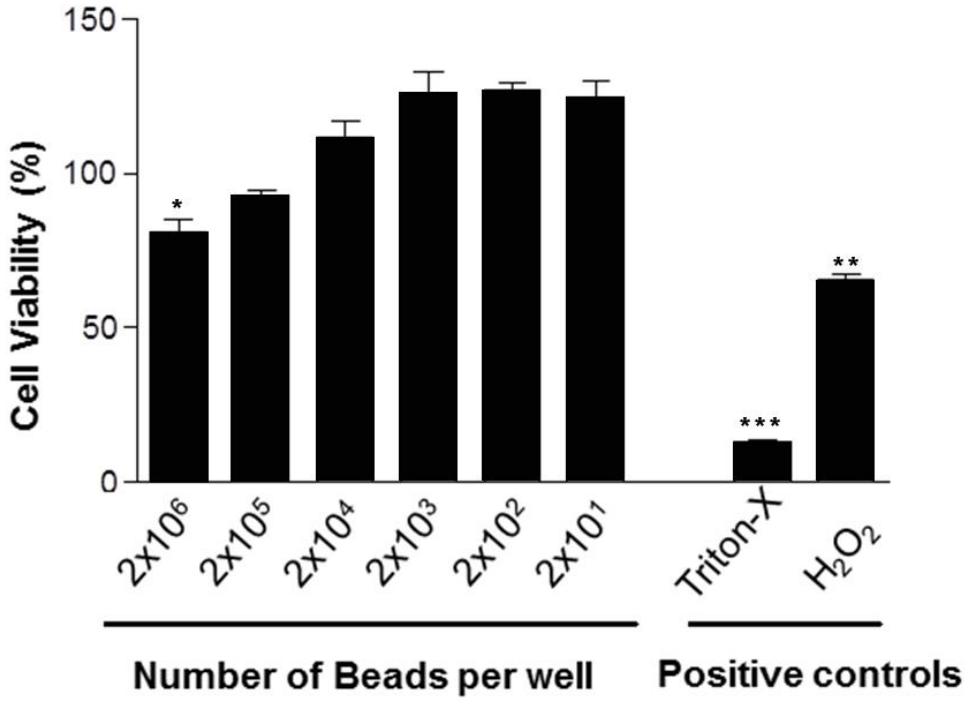

Figure 3.9. At elevated concentrations, paramagnetic microspheres exhibit minimal toxicity. SH-SY5Y cell viability was not significantly reduced compared to the freshly seeded wells (100% viabilty) when cultured with Invitrogen microspheres at concentrations lower than $2x10^6$ microspheres per well. At $2x10^6$ microspheres per well, there was a 20.1% (SD=3.89%, two sample t-test, $p<0.05$, n=3) reduction in cell viability. This compares with reductions of 34.7% (SD=1.78%, $p<0.01$) and 90% (SD=0.71%, $p<0.001$) in cells cultured with H_2O_2 and Triton-X®, respectively. These data show that at microsphere to cell ratios of lower than 66.67:1, there is no observable toxicity associated with paramagnetic microspheres.

3.5 Discussion

In this chapter, I have detailed how injection and manipulation of paramagnetic microspheres can induce a sustained elevation in intraocular pressure. I have controlled for each factor of the procedure: the act of injecting carrier solution, injection of paramagnetic microspheres and magnetic manipulation. None of these factors is sufficient to induce an elevation in intraocular pressure on its own, However, the entire procedure induces a sustained and significant elevation in intraocular pressure. The results of these control experiments were included in the initial publication of this model by Samsel *et al*. (2011). It should be noted that the use of paramagnetic microspheres does not interfere with rebound tonometry. The rebound tonometer uses a metal probe, which is propelled towards the eye by a magnetic field, to determine the intraocular pressure. The magnetic field used to propel the probe is contained within the hand-held device, which does not come into direct contact with the eye. The paramagnetic nature of the microspheres means they do not generate a magnetic field. These facts indicate that there is no direct interaction between the probe (or it's associated magnetic field) and the paramagnetic microspheres injected into the eye.

When discussing existing models of glaucoma that utilise microsphere injection, it should be noted that in several studies using polystyrene microspheres the intraocular pressure was measured with a Tonopen XL ®. This device has a contact surface of $1cm^3$. This is exceedingly large compared to the cornea of a rodent eye and would result in the surface of the probe contacting cornea which has microspheres resting on it, this would undoubtedly have influenced the measured intraocular pressure. For this reason, during model development, I used the TonoLab ® (Tiolat, Finland) tonometer, which uses much smaller probes (1mm

diameter). A previous study carried out in this lab (Prashar *et al.* 2007) showed that positional inaccuracies when using the TonoLab® have no significant impact on the measurement of intraocular pressure. However, this study identified that the first measurement obtained with the TonoLab was significantly different from following measurements. For this reason, a total of six measurements were taken and the first was discarded to leave five comparable measurements for each time point.

One potential drawback of the model may be the presence of a spike in intraocular pressure following injection. Although this did not cause a noticeable increase in retinal ganglion cell death, which continued over time, it is possible that this initial elevation triggers both chronic and acute stressors within the retina.

Beyond the formation of a self-sealing corneal incision, the injection of paramagnetic microspheres is a relatively simple procedure. As I had no prior surgical experience and was able to become proficient in the implementation of the model, it is reasonable to surmise that there is little technical challenge to the implementation. With this in mind, it is reasonable to suggest that a titration of beads, where repeated and progressively smaller injections are used, induces a more gradual rise in intraocular pressure. The only likely confounder observed during the use of this model thus far, is that animals have typically adapter to the increase in intraocular pressure, which has typically fallen over a period of approximately fourteen days. The ease of use of this model has other benefits such as reducing the potential for mistakes which may lead to unnecessary animal culling or confounding factors resulting from damaged blood vessels, which may occur in episcleral vein injection or laser cautery models.

The data presented in this chapter establish that the injection of paramagnetic microspheres into the anterior chamber can reliably induce an elevation in intraocular pressure. It is also established that paramagnetic microspheres are not directly toxic to neuronal cells and therefore the retinal ganglion cell toxicity observed can be attributed to the increase in intraocular pressure.

Injecting the paramagnetic microspheres without magnetic manipulation established that the beads themselves were insufficient to sustain an elevation in intraocular pressure. This experiment also demonstrated that, without manipulation post-injection, microspheres follow gravity and sink to the inferior aspect of the anterior chamber. This replicates observations made in other models that are based on polystyrene microspheres. The effect of magnetic manipulation is to greatly increase the efficiency of the microsphere distribution at the iridocorneal angle, improving the induced intraocular pressure. This is achieved while reducing damaging and potentially confounding side-effects to the front of the eye. Further control experiments established that the elevation in intraocular pressure shown in this model is caused specifically by by the paramagnetic microspheres. This was achieved by showing that injection of vehicle solution and magnetic manipulation alone are insufficient for the induction of an elevation in intraocular pressure.

The proposed method of action for this model is that, upon injection of vehicle solution, the anterior chamber of the eye increases in volume temporarily. This has the effect of increasing the iridocorneal angle. The injected paramagnetic microspheres are then drawn into the angle with the hand-held magnet. As the vehicle solution drains from the eye, the angle returns to normal, trapping the microspheres in place; this effect is illustrated in figure 3.7. The use of a self-sealing incision prevents excess fluid leaving the eye through the injection site. This may

lead to some microspheres coming free from the angle in the time it takes the excess fluid to drain via the trabecular meshwork. These beads would then sink to the inferior aspect of the eye. This may be responsible for the slightly greater amount of beads in the inferior aspect observable in figure 3.7. The self-sealing incision is necessary, however, to prevent collapse of the anterior chamber. This would lead to an efflux of beads through the injection site and a drop in intraocular pressure. The drawbacks to the use of the self-sealing incision are, however, minimal. Beads are present at all aspects of the iridocorneal angle and beads at the inferior aspect are not motile and are effectively trapped in the trabecular meshwork.

This model represents a reliable, reproducible and technically straightforward way of elevating intraocular pressure in the laboratory rat. It was crucial to establish this and properly control for all aspects of the surgical procedure in order to be able to examine the role of complement in glaucomatous retinal ganglion cell loss. Using this model, I will examine the activation of the complement cascade in the glaucomatous retina. The use of an inducible model of hypertonic glaucoma will also allow me to pre-treat diseased retinas with an inhibitor of the classical complement cascade and allow me to test the hypothesis that activation of the classical complement cascade is a mediator of damage in glaucomatous optic neuropathy.

Chapter Four: Complement Activation in Experimental Glaucoma

4.1 Introduction

The early components of the classical cascade of complement activation, up to the point of the formation of a stable C3 convertase enzyme have been identified in human and animal glaucoma (Howell *et al*., 2011; Tezel *et al*., 2010). To establish if comparable processes are activated in our model of glaucoma, I will carry out Immunofluorescent labelling using an antibody which specifically binds to the activated fragments of C3 – C3b and iC3b. This will allow me to detect not only an increase in the native protein, as has been found by others, but an increase in proteolytic activity indicative of opsonisation and cell clearance by the complement system.

It is important to establish that there is cell loss and neuronal degeneration in this model as these as these are hallmark features of glaucoma. In order to detect changes in the neuronal integrity of retinal ganglion cells in glaucoma, I will use antibodies for marker of post-synaptic density (PSD95). This will be accompanied by retinal ganglion cell counting, facilitated by nuclear counterstaining with ToPro-3-iodide® (Invitrogen UK, UK) labelling. Changes in the relative amounts of activated complement components and dendritic synapses, as measured by PSD95, will help to establish if there is a relationship between complement activation and dendritic pruning in glaucoma.

These experiments will help me to identify the extent of complement activation in glaucoma and determine if that activation is associated with a loss of neural connectivity and apoptosis.

4.2 Methods

4.2.1 Immunofluorescent staining of wholemounted retina

Retinas were fixed with 4% paraformaldehyde for 1 hour at room temperature, submerged in rising concentrations of sucrose from 10, 20 and 30% in order to add rigidity to the retina to ensure it survived immunofluorescence intact. Each retina was placed on a slide and circled with a hydrophobic pen (Sigma-Aldrich, UK) which was allowed to dry before immunofluorescent staining.

Prior to staining a drop of 1% solution of Triton X detergent (Sigma-Aldrich) in phosphate buffered saline was placed on the retinas for 24 hours at 4°C. This solution was pipetted off and a blocking solution consisting of 10% donkey serum in phosphate buffered saline was added to the slide. The blocking solution was made by diluting 1ml of donkey serum with 9ml of phosphate buffered saline. This solution was left on for 1 hour at room temperature before being pipetted off.

Primary antibody solution (summarised in table 2) consisted of 1 part in 50 monoclonal mouse antibody to rat C3b/iC3b and 1 part in 100 polyclonal rabbit antibody to rat neuronal marker PSD95, diluted in phosphate buffered saline. One-hundred and twenty-five microlitres of primary antibody solution was added to each retina and incubated at room temperature for 24 hours in a humidity chamber. The primary antibody solution was then washed off by rinsing with phosphate buffered saline three times.

Secondary antibody solution (summarised in table 3) was then added consisting of 1 part in 100 each of donkey anti-mouse antibody ab_2 fragment conjugated to AlexaFluor®-594 (Invitrogen UK, UK) and donkey anti-rabbit antibody ab_2 fragment conjugated to AlexaFluor®-488 (Invitrogen, UK). The secondary

antibody solution was incubated for 24 hours at room temperature and then pipetted off. Wholemounts were washed three times in phosphate buffered saline for two minutes at room temperature and mounted with ProLong Gold ® anti-fade reagent (Invitrogen, UK) prior to imaging.

For the wholemounted retinal immunofluorescence, ab_2 fragments were used as the secondary antibodies in order to minimise non-specific binding of the fragment-c region of the secondary antibodies to glycose amino glycans in the retina.

Fluorescent images were acquired and measurements of secondary antibody detection were acquired as described in section 2.8.2 Immunofluorescence.

4.2.2 Cell counting

To give an indication of cell loss in the experimental retinas labelled with wholemount immunofluorescence, cell counts were taken from the retinal ganglion cell layer of each retina. To ensure a homogenous distribution of retinal tissue, 6 regions of interest (ROI) were taken from approximately 1.5mm from the optic nerve head, three from the superior aspect of the retina and three from the inferior aspect, approximately sixty degrees apart. The colour channel representing the ToPro-3-iodide® (Invitrogen UK, UK) nuclear counterstain was then isolated and the number of cell nuclei present in each region of interest were counted manually.

4.2.3 Statistical analysis

Intraocular pressure measurements were analysed as described in section 2.11.1. Retinal ganglion cell counts and grey value measurements were normally distributed. These values were therefore compared using a paired 2-tailed student t-test.

4.3 Immunofluorescence and cell counts in sections of glaucomatous and control retinas

4.3.1 Intraocular pressure elevation

Of ten animals injected, five developed a significant increase in intraocular pressure following the first microsphere injection at day zero, these animals were culled at day 16. The remaining five animals were given a second injection at day 21. Of the five animals that received two injections, three maintained an intraocular pressure elevation for sixteen days and were killed on day thirty-seven. The eight animals with an intraocular pressure elevation were included in the study, and the elevation for each animal was calculated from the date of the injection preceding the elevation. In those eight animals, the mean intraocular pressure of the injected eyes was 31.60mmHg (SD=4.5mmHg) compared to a mean intraocular pressure of 21.33mmHg (SD=3.75mmHg) in the contralateral, uninjected eye. This corresponds to a mean intraocular pressure elevation of 10.27mmHg. The eight animals were then culled and retinal sections were prepared as described in section 2.5.

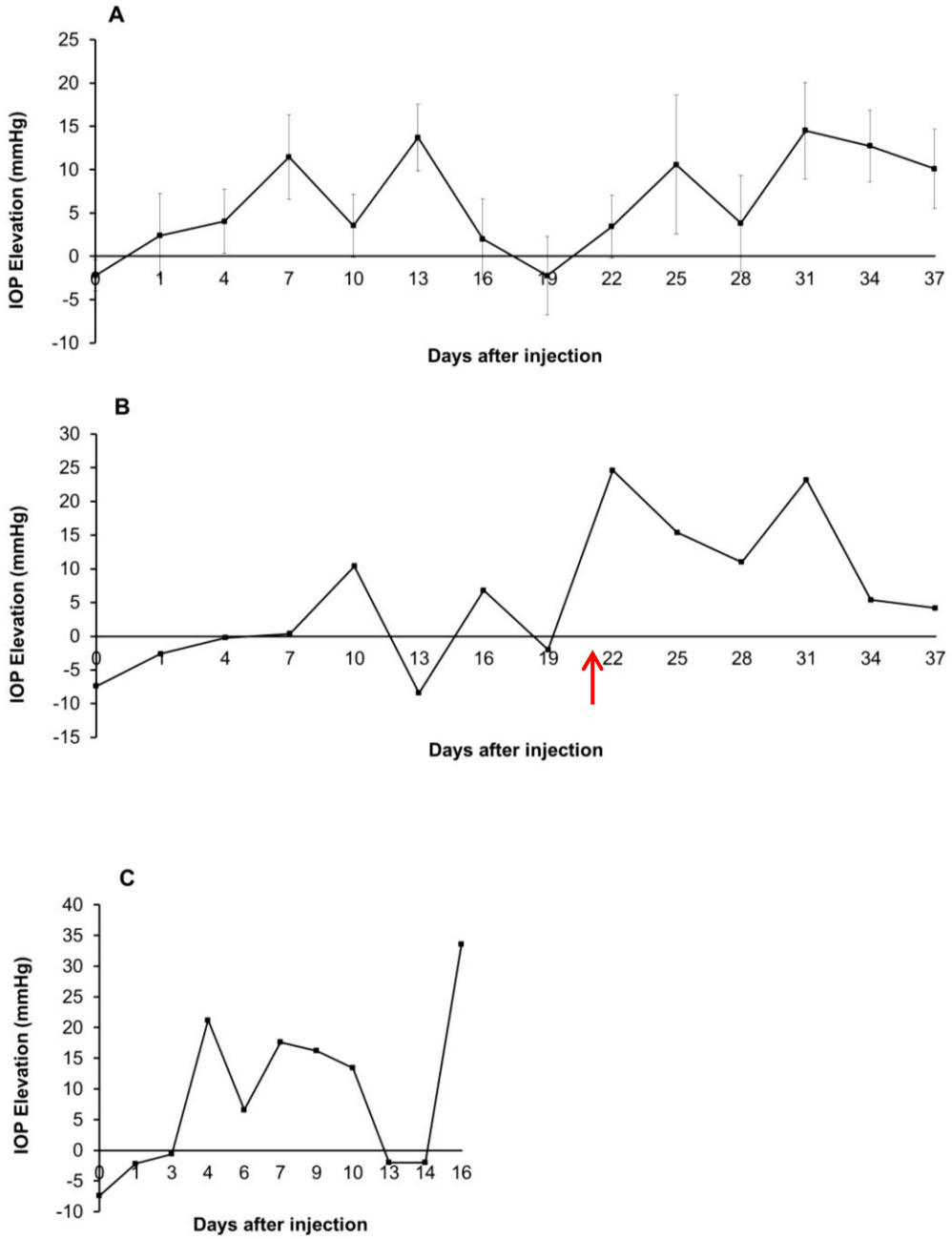

Figure 4.1 – The difference in intraocular pressure between the microsphere-injected and un-injected control eyes of the eight animals used for frozen section immunofluorecence. (A) Mean intraocular pressure elevation of all eight animals used in the study. The mean intraocular pressure of the eight microsphere injected eyes was 31.60mmHg (SD=4.5mmHg) compared to a mean intraocular pressure of 21.33mmHg (SD=3.75mmHg) in the contralateral, uninjected eye over the thirty-seven days of the study. (B) A representative intraocular pressure elevation profile for a single animal which required reinjection at day 21 (arrow). (C) An example elevation profile for a single animal which developed a sustained intraocular pressure elevation from a single injection. Error bars = standard deviation.

4.3.2 Retinal ganglion cell counts were reduced and complement component detection was increased in glaucomatous retinal sections

Retinal ganglion cell counts (taken as described in section 2.8.2) were reduced by 38% in sections of glaucomatous retinas compared to sections of control retinas (Mean=10.88 SD=1.9 and Mean=17.58 SD=1.2 retinal ganglion cells per 100µm of retinal ganglion cell layer, $p<0.01$ n=8 animals). Immunofluorescence was detected in the inner plexiform layer and retinal ganglion cell layer of all sections at varying levels by measuring the grey values of the colour channel corresponding to the relevant fluorophore. Although levels of detected C3b/iC3b (in the red channel) and C9 (green channel) were higher in glaucomatous retina than in control retina (Mean=9.96AU, SD=1.5AU and Mean=4.33AU, SD=2.2AU compared to Mean=6.32AU, SD=1.6AU and Mean=2.66AU, SD=1.4 respectively) these differences were not statistically significant (Figure 4.2). Sections stained with antibodies to C1q (1 part in 100 rabbit anti-rat C1q primary antibody, labelled with donkey anti-rabbit antibody conjugated to AlexaFluor®-488), alone showed that the molecule could only be detected in glaucomatous tissue (Figure 4.3 – Staining courtesy of Dr Claudia Calder).

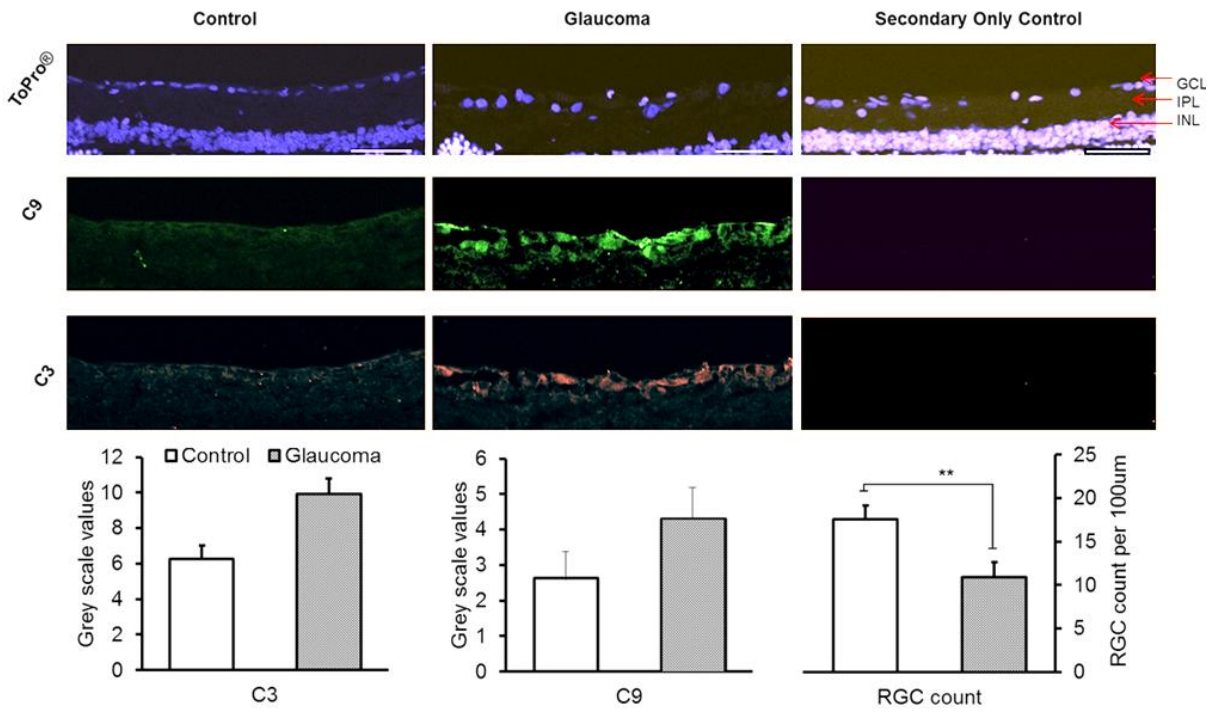

Figure 4.2 – Levels of C3b/iC3b and C9 in the inner plexiform and ganglion cell layers are elevated in glaucoma, accompanying a reduction in ganglion cell number. Counts of retinal ganglion cell counts, labelled using ToPro®-3-iodide, were reduced by 38% in sections of glaucomatous retinas (Mean=10.88 cells per 100µm SD=1.9, n=8 animals) compared to sections of control retinas (Mean=17.58 cells per 100µm, SD=1.2, p<0.01). Although levels of C3b/iC3b (red, Mean=9.96AU SD=1.5AU and Mean=6.32AU SD=1.6, n=8 retinas) and C9 (green, Mean=4.33AU SD=2.2AU and Mean=2.66AU SD=1.4, n=8 retinas) were elevated in glaucomatous retinas compared to controls, these results were not statistically significant. The ganglion cell, inner plexiform and inner nuclear layers are labelled (GCL, IPL and INL respectively) scale bar = 50µm.

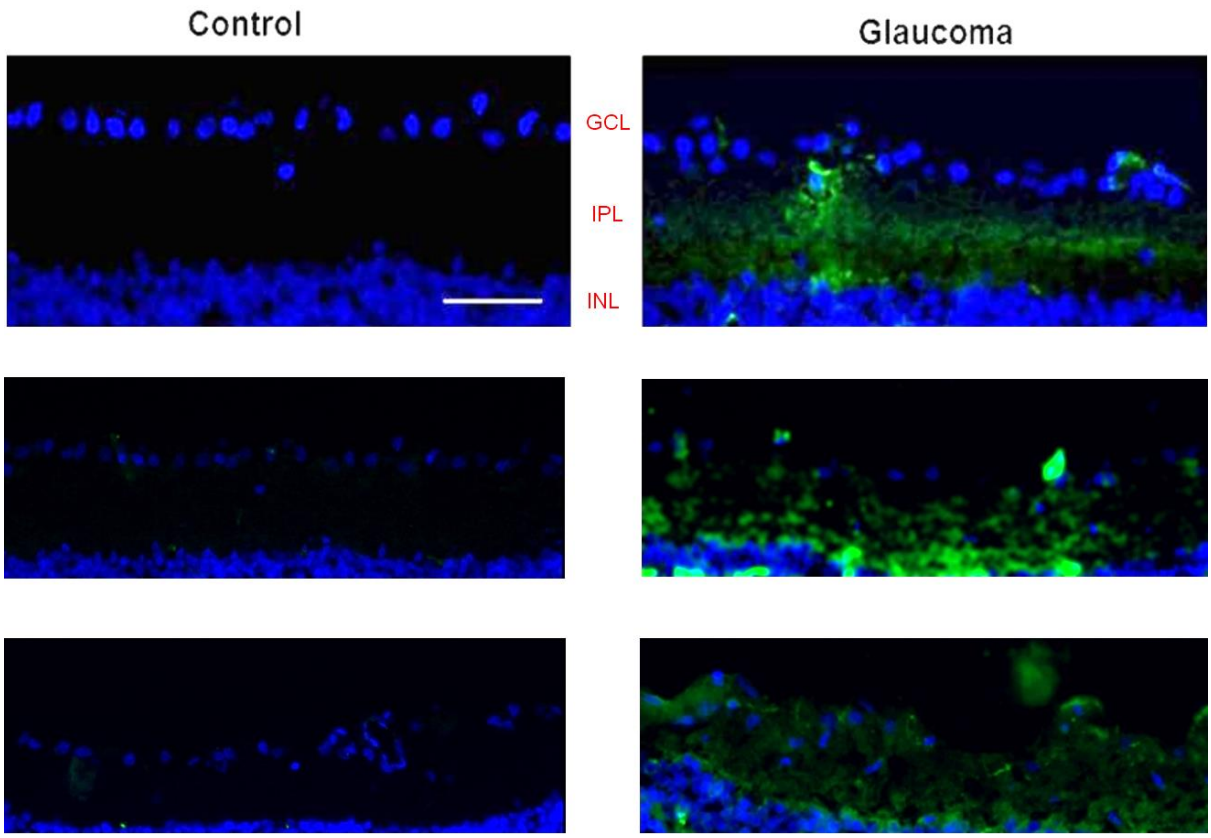

Figure 4.3 C1q immune reactivity is specific to glaucomatous retinas. C1q was detected in all eight glaucomatous retinas whereas no reactivity was observed in retinas from contralateral, normotensive eyes. Staining was detected throughout the ganglion cell layer (GCL), inner plexiform layer (IPL) and inner nuclear layer (INL), scale bar = 50µm.

4.4 Detection of activated complement components in wholemounted retinas is elevated in glaucoma

4.4.1 Intraocular pressure elevation

Of the ten animals injected, nine developed a significant increase in intraocular pressure, with a mean contralateral, uninjected intraocular pressure of 28.18mmHg (SD: 4.65mmHg). This compares to a mean intraocular pressure in the microsphere injected eyes of 44.22mmHg and a mean elevation of 16.03 mmHg (SD=3.16, n=9, survival time 14 days, $p<0.05$ as measured by Mann-Whitney U test figure 4.4). The nine animals which developed an elevated intraocular pressure were culled, and retinas were prepared as described in section 2.6 Retinal dissection. Retinas were then immune-labelled for activated fragments of complement component 3 and PSD95 as described in section 4.2.1 Immunofluorescent staining of wholemounted retina.

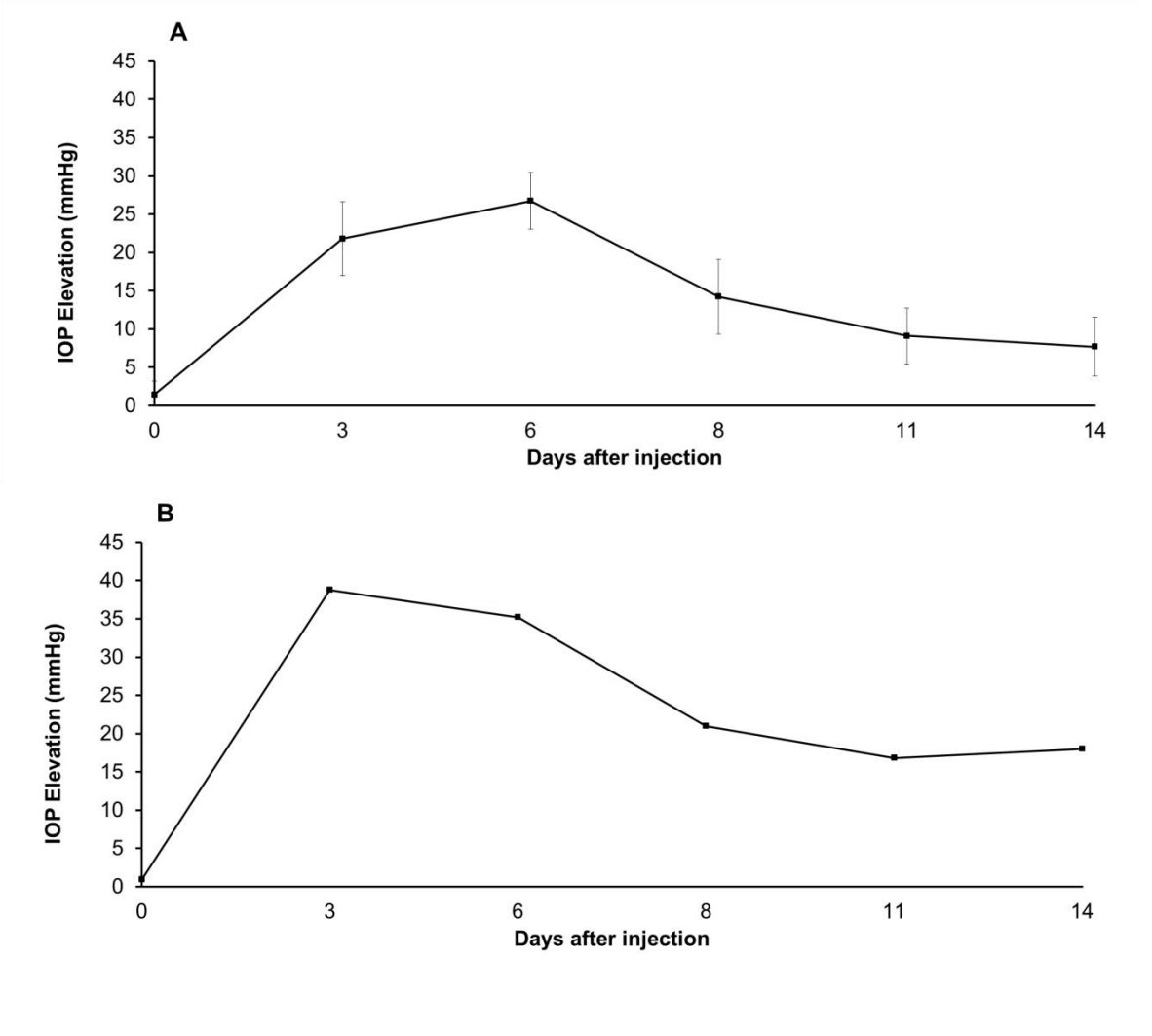

Figure 4.4 Intraocular pressure was elevated in nine animals injected with paramagentic microspheres. (A) Mean intraocular pressure elevation profile of the nine animals used for immunofluorescent labelling C3b/iC3b and PSD95. The mean elevation in the microsphere-injected eyes of the nine animals, across the fourteen days was 16.03mmHg (SD=3.16mmHg, $p<0.05$ as measured by Mann-Whitney U test) over a mean contralateral, uninjected pressure of 28.18mmHg (SD=4.65mmHg) across the fourteen day time period. Error bars are standard deviation. (B) Representative intraocular pressure elevation profile from a single animal with a mean intraocular pressure elevation of 25mmHg (SD=5.25mmHg) across the fourteen day time period. Elevation is calculated by subtracting the mean intraocular pressure of the control, uninjected eye from that of the mean pressure of the microsphee injected eye at each time point. As such, there is no measurement of deviation for a single animal at a single time point.

4.4.2 Retinal ganglion cell counts and grey scale values

Retinal ganglion cell loss in glaucomatous retinas was 30.58% compared to controls with a mean of 327cells/ROI (SD=11.2) in controls compared to a mean of 227cells/ROI (SD=19.86) in glaucomatous retinas (p<0.01, n=9 animals). This was measured at 1.5mm from the optic nerve head in a 393.54µm^2 field of view. Grey scale values associated with detection of C3b/iC3b deposition in the inner plexiform layer indicated a significant increase in glaucomatous eyes (mean=185AU, SD=11.19AU) compared with the control eyes (mean=154AU, SD=10.72AU) (p<0.05). A corresponding reduction in PSD95 detection (mean=1170 SD=76.05AU) in the inner plexiform layers of glaucomatous retinas compared to control retinas (mean=1682AU SD=97.2AU, p<0.001) was observed (figure 4.5). To explore the relationship between synaptic integrity, as measured by PSD95 labelling in the inner plexiform layer and complement activation, a Spearman's rank correlation coefficient was calculated using Microsoft (US) Excel software. PSD95 and C3b/iC3b immuno-reactivity showed a significant negative correlation (r^2=-0.7857, p<0.05).

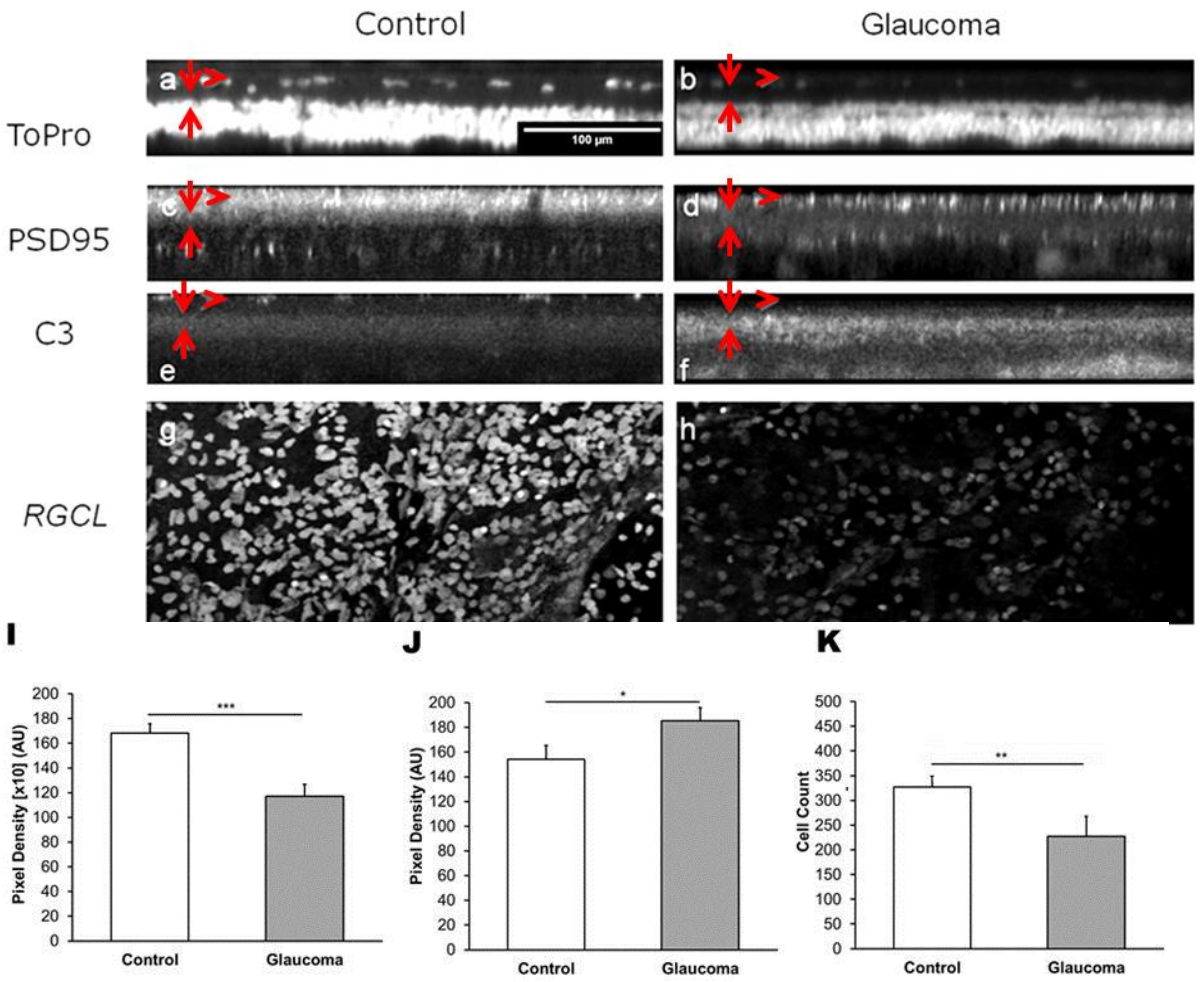

Figure 4.5 Immunoflourescent detection of C3b/iC3b is increased and detection of PSD95 is deceased in glaucomatous retinas. (A-F) Virtual cross-sections from wholemounted retinas showing mean pixel intensity through the x-axis of the 3-dimensional confocal image, revealing retinal histology. Arrow heads show the retinal ganglion cell layer and arrows show the inner plexiform layer. (A-B) Nuclear counterstain showing approximate position of the retinal layers throughout the wholemount.. (C-D) Detection of PSD95 in control and galucomatous retinas. (E-F) Detection of C3b/iC3b fragments. (G-H) View of the retinal ganglion cell layer through the y axis illustrating the reduced density of the retinal ganglion cell population in the glaucomatous retina compared to the control retina. (I) Decrease in detection of PSD95 from a mean of 1682AU (SD=97.2AU, n=9 animals) in control retinas to 1170AU (SD=76.05) in glaucomatous retinas (p<0.001). Increase in detection of C3b/iC3b from a mean of 154AU (SD=10.72) in control retinas to 185AU (SD=11.19) in glaucomatous retinas (J) (p<0.05). Decrease in retinal ganglion cell counts (K) from a mean of 327 cells/ROI (SD=11.2) to 227 cells/ROI (SD=19.86) in glaucaomtous retinas (p<0.01). Grey values and retinal ganglion cell counts were normally distributed and compared with a paired two-tailed t-test.

4.5 Discussion

Up-regulation and activation of classical complement cascade components has been reported in glaucomatous human (Tezel *et al*. 2010) and animal (Kuehn *et al*. 2006; Stasi *et al*. 2006; Howell *et al*. 2011) retinas as well as neuronal cell lines under conditions similar to glaucoma *(*Khalyfa *et al*, 2007). Establishing whether or not complement is activated in this model of glaucoma was essential if the model was to be useful in modelling the role of complement in retinal ganglion cell loss in glaucoma.

An increase in the level of activated complement fragments deposited in the glaucomatous retina, as measured from Immunofluorescent staining of 7µm thick frozen retina sections was not statistically significant regarding. However, the trend observed is in agreement with both the literature and the data from immune-labelled wholemounts. The apparent reduced power of the results from thin, frozen sections may be a result of the high loss of retinal ganglion cells in those retinas. The results here showed a 38% reduction in retinal ganglion cell counts. This is high compared to other models, which have a cell loss of between 10-20% (Libby *et al*., 2005; Morrison *et al*,. 1997; Quigley & Anderson, 1976). The nuclear counterstain used here – ToPro®-3-iodide – binds to double stranded DNA and as such will stain all cells with a viable nucleus. As glaucomatous retinal ganglion cells undergo a prolonged period of atrophy prior to apoptosis (Weber & Zelenak 2001), it is reasonable to expect that a large proportion of surviving cells had degenerated to varying degrees.

Apoptotic retinal ganglion cells are taken up by microglia (Tremblay *et al*., 2010). This may have the effect of masking the epitopes on the retinal ganglion

cell's surface from detection by immunofluorescence. Complement activation is reported to be an early event in glaucomatous optic neuropathy (Howell *et al*. 2011), and components of the complement cascade readily bind microglia (Collier *et al*., 2011; Stevens, 2011). It is therefore reasonable to expect that retinal ganglion cells which express complement components will be cleared before those which do not. The removal of retinal ganglion cells by microglia and the atrophy of remaining cells may have the effect of reducing the complement epitopes that can be detected by immunofluorescence.

As such, it was decided that in subsequent experiments the time course should be more closely regulated and, where possible, thicker tissue sections should be used. It was with this in mind that immunofluorescence on wholemounted retinas was undertaken. Direct complement-mediated lysis was not expected to be a major contributory factor to retinal ganglion cell loss. In order to determine if retinal ganglion cell atrophy observed in other models could be replicated by this model, anti-C9 antibodies were replaced with antibodies to PSD95. This is a marker of postsynaptic density and will illustrate the extent of retinal atrophy occurring in this model. The results revealed a significant increase in C3b/iC3b fragments in glaucomatous retinas and a corresponding decrease in the detection of post synaptic density marker 95. Glaucoma-specific C1q reactivity in the retina indicates that the complement activation observed is a result of classical pathway activation and that the low-level C3b/iC3b detection in the control retina was a result of alternative pathway activation. The significance of this will be discussed later.

Some expansion of the eye could be observed, and it is possible that this could contribute to the apparent loss of retinal ganglion cell density in the retina. Treating the eye as a sphere and assuming that the surface area of the retina is

correlated to the surface area of the eye, the relationship of the size of the retina and the size of the eye should be $\frac{4}{3}\pi r^3$, where r is the radius of the eye. This would make the percentage increase of the surface area of the retina twice that of any increase in eye radius. Given the cell loss of 38% observed here this would require an increase in eye size of 15.365%. The typical length of the rat eye is 6.29mm (Hughes 1979), meaning a global increase of 0.966mm could account for the entire decrease in retinal ganglion cell density observed. However, a uniform and global increase is highly unlikely, given the structure of the eye, is more to expand most at its thinnest point, the centre of the cornea (Levin et *al.* 2011). This would minimise the effect of retinal expansion at the posterior aspect of the eye. Retinal ganglion cells are surrounded by a substantial network of proteoglycans and structural proteins, referred to as the perineuronal net (reviewed in Rhodes & Fawcett (2004)), which would act against the dispersion of retinal ganglion cells as a result of retinal expansion.

With this in mind, however, future work that uses retinal ganglion cell loss observed in a given area should be accompanied by an alternative measurement of retinal ganglion cell atrophy. This may include diolystic or similar labelling and may be accompanied by accurate measurements of the eye before and after the induction of hypertension.

Here I establish that complement activation occurs in this model of experimental glaucoma by the detection of components specific for complement activation. I also present evidence that this complement activation is mediated by the classical complement cascade as identified by the detection of glaucoma-specific C1 – the initiator molecule of the classical complement cascade. To establish the

role this activation has in the pathophysiology of glaucoma, I will go on to examine the effects of complement deficiency on glaucomatous neurodegeneration. In order to confirm that this complement activation is mediated by the classical complement cascade, I will use C1-inhibitor to specifically block that cascade. This will also allow me to examine the possibility that glaucomatous neurodegeneration may be mitigated by complement inhibition.

Chapter Five: *In Vivo* and *In Vitro* Pressure Elevation in Complement Deficient Animals

5.1 Introduction

In vitro hydrostatic pressure elevation on retinal explants and cell lines has been (Garcia-feijoo *et al.,* 2009; Tezel & Wax, 2000; Yang *et al*., 2004) used to study the changes induced during glaucomatous damage extensively. Models of C3 deficient mouse and C6 deficient rats were available to me. These were utilised to elucidate the role of the various stages of the complement cascade in the progression of glaucomatous optic neuropathy.

The aim of this chapter was to induce glaucoma in a C6 deficient rat strain and use *in vitro* hydrostatic pressure elevation in a C3 deficient mouse strain to determine the effects of complement deficiency on glaucomatous damage. {This strain, which is bred in-house from Jackson Laboratory (stock number 003641) is on a C57BL/6 background and was compared to C3 sufficient C57BL/6 mice.}

The purpose of using both C3 and C6 deficient animals was to identify which if any stages of the complement activation after C1 have a role in retinal ganglion cell degeneration in glaucoma. As the paramagnetic microsphere model of glaucoma is yet to be established in the mouse, I decided to use an *in vitro* model of hydrostatic pressure elevation. This would mimic some of the changes induced by intraocular pressure in a manner similar to that used by other researchers (Ishikawa *et al*. 2010; Agar *et al*. 2006; Hernandez *et al*. 2000).

C3 is involved in cell opsonisation and is essential for the formation of the membrane-bound terminal complement complex. The opsonisation of cells by C3 is distinct from that by C1. C3 functions via its degradation products C3b and iC3b to recruit macrophages at complement receptor 1 (Gonzalez *et al*. 2010), whereas C1 binds antibodies (Roos & Daha 2002) and a putative receptor molecule, which is as

yet unidentified (Perry & O'Connor 2008b). The sole effect of C6 is the formation of the active terminal complement complex (Peitsch & Tschopp 1991). This means that any effects of the two genes on retinal ganglion cell fate in hypertensive glaucoma can be attributed to their respective functions in the classical complement cascade. In order to examine the role of complement in retinal ganglion cell degeneration in hypertensive glaucoma I used animal models of C3 and C6 deficiencies in the mouse and rat respectively. This will give an indication as to the effects of these complement components in retinal ganglion cell degeneration.

5.2 Methods

5.2.1 *In vitro* hydrostatic pressure elevation

5.2.1.1 Pressure transducer calibration

A glass burette was elevated using a metal clamp stand (Cole-Parmer, UK) and attached to 4mm diameter nylon tubing, which was connected to a pressure transducer (OmegaPX800-002GV,OmegaCorp, USA). The output of the transducer was read by a USB analogue to digital converter (Futek, USA) with a refresh rate of 20Hz and an accuracy of 0.001mV. Fluid was introduced into the system using a 50ml syringe attached to a two-way luer valve (Cole Parmer, UK).

To produce a calibration curve, the burette was filled to the desired height, allowed to settle for 1 hour and adjusted if necessary. The output voltage of the transducer was then measured over a period of 8 hours (Figure 5.1).

5.2.1.2 Pressure elevation and culture

Ames' medium was prepared by dissolving a vial of dehydrated Ames' medium (Invitrogen UK, UK) in 1 litre of deionised water. The resultant medium was then autoclaved and allowed to cool before use.

The pressure chambers shown in figure 5.2 were washed in 100% ethanol and air dried in a category 2 biosafety cabinet before being assembled by attaching the two segments of polymethylmethacrylate together using 80mmx5mm diameter screws (Maplins, UK). The chamber was left open so that sufficient space was left in the centre to pipette 1.5ml of Ames' medium (Invitrogen, UK) and place the culture dishes into the base of the culture dish chambers.

Six C3 deficient and eight C3 sufficient mice were culled by cervical dislocation. Retinas were dissected from the eye cup, as described in section 2.6 and flattened on to the culture dishes. Culture dishes were rested on top of the Ames' medium in the lower culture dish chamber (Figure 5.2A). A 35mm diameter rubber O-ring (Maplin electronics, UK) was placed around the culture dish to create a seal around it. The chambers were closed by tightening screws in the screw holes and fastening with a bolt and washer. Luer stop cocks (Cole-Parmer, UK) were inserted into the fluid channels of the chamber and attached to the burette with 4mm diameter nylon tubing (Cole-Parmer, UK). The burette was filled with Hank's balanced salt solution to a height of 136cm. Once the output of the transducer had stabilized (±10mV), the stop cock was closed and the chamber incubated at 37°C for 48 hours with the pressure reset and the culture medium changed every 12 hours.

5.3 Transducer output voltage consistently corresponds to burette fluid height

A calibration curve was produced for the hydrostatic pressure apparatus (Figure 5.1). This curve shows a mean output of 5809mV (SD=0.01mV) at 1.5 metres of fluid height over eight hours (approximately 576,000 measurements), 5806.87mV (SD=0.01mV) at a fluid height of 1.36 metres (equivalent to 100mmHg) and 5801mV (SD=0.01mV) at 1 metre. With no fluid in the system the voltage output of the transducer was 5780mV (SD=0.2mV). The relatively small standard deviation of the output voltage of the transducer over 8 hours indicates that the system is suitably pressure-tight. This indicates that the pressure within the system is consistent and that deliberate variation of the fluid height in the system can be accurately monitored.

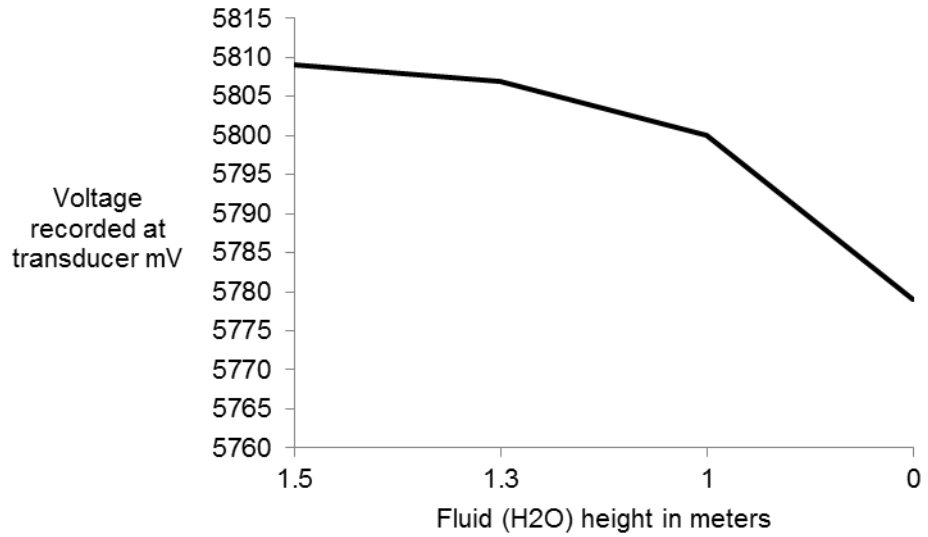

Figure 5.1 The system used for inducing an *in vitro* increase in hydrostatic pressure produces stable measurements between fluid heights of 1.5 and 1 metres. Graph showing the mean output voltage of the pressure transducer at fluid heights of 1.5 down to 1 metres and in an empty system (zero metres). The mean voltage of this 5809mV (SD=0.01mV – not visible on graph) at 1.5 metres, 5806.87mV (SD=0.01mV) at (equivalent to 100mmHg), 5801mV (SD=0.01mV) at 1 metre and 5780mV (SD=0.2mV) in an empty system.

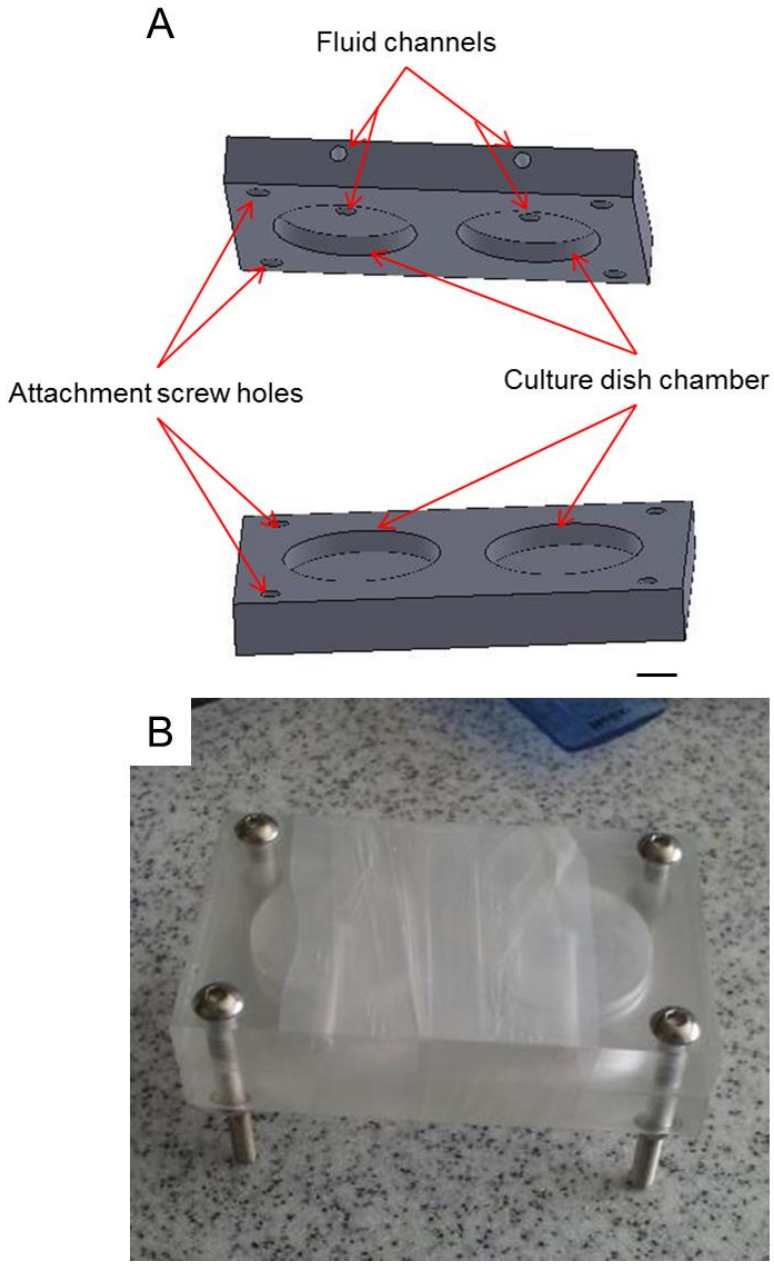

Figure 5.2 The chamber used for *in vitro* hydrostatic pressure elevation in mouse retinas. (A) A diagram of the chamber used to house mouse retinas under elevated hydrostatic pressure. The lower culture dish chamber housed the Ames' medium while the upper section of the chamber housed the retinal culture dish. The attachment screw holes were used to keep the two halves of the chamber in contact. The fluid channels were attached to the burette containing Hank's balanced salt solution, this produced the elevation in hydrostatic pressure. Scale bar = 1cm. (B) A photograph of the assembled chamber sealed with parafilm.

5.4 Glaucomatous C3-/- dendritic trees are significantly reduced compared to those of wild types

There was no significant difference in the mean retinal ganglion cell Sholl plots from retinal ganglion cells from eight wild type and six C3 deficient control groups when compared using a two-sample Kolmogorov-Smirnov test . As such, both groups were treated as a single control group consisting of 42 cells. Compared to the mean Sholl plots of retinal ganglion cells from these normotensive retinas (AUC=142.59, n=42 cells, figure 5.3), retinal ganglion cells from eight wild type retinas cultured at elevated intraocular pressure had significantly reduced Sholl plots (AUC=99.384, n=42 cells, $p<0.01$). The dendritic trees of retinal ganglion cells from six hypertensive C3 deficient retinas were significantly degraded compared to both hypertensive wild-type and normotensive C3-/- retinas and, in fact, few cells could be identified (AUC=35.2, n=12 cells, $p<0.01$). This suggests that C3 expression may be protective against retinal ganglion cell degeneration associated with an elevation in hydrostatic pressure.

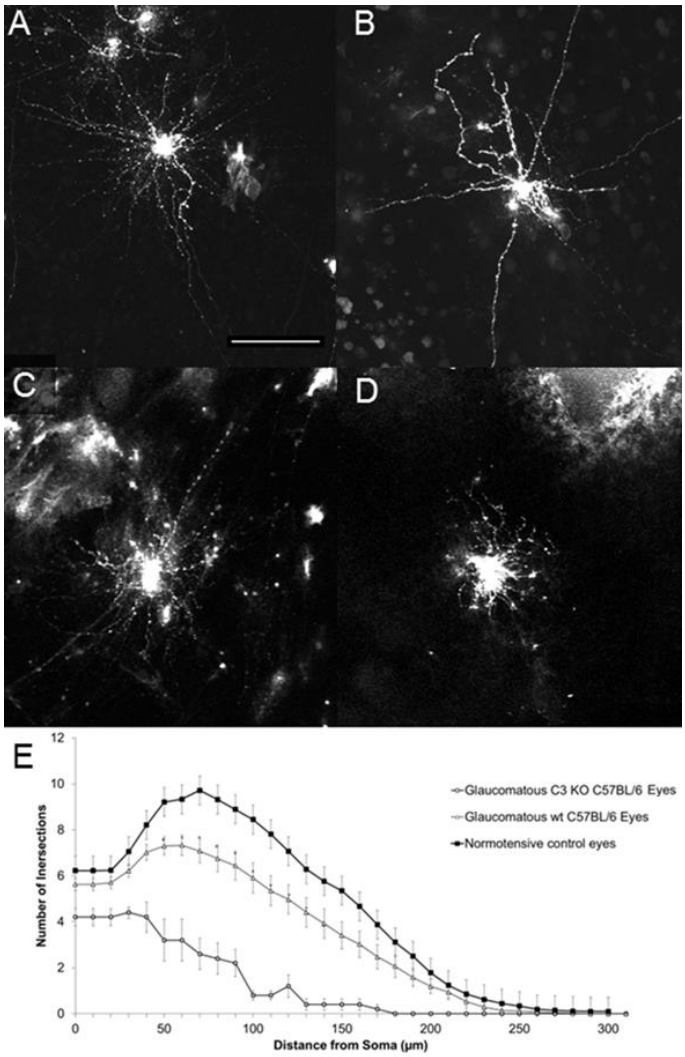

Figure 5.3 Retinal ganglion cell degeneration was exacerbated by C3 deficiency. Representitive retinal ganglion cells from wild-type C57BL/6 (A-B) and C3 deficient (C-D) retinas cultured at atmospheric pressure (A, C) and elevated (to 100mmHg) pressure (B,D) showing a noticable degeneration in retinal ganglion cells from retinas cultured at an elevated pressure, scale bar=100µm. Mean Sholl plots for each group (E) show a degeneration in retinal ganglion cells from eight wild-type cultured at 100mmHg (AUC=99.38, n=42 cells) compared to those from eight retinas cultured at atmospheric pressure (AUC=142.59, n=42 cells, $p<0.01$) using the two-sample Kolmogorov-Smirnov test. Retinal ganglion cells from six C3 deficient mice cultured at 100mmHg had a significantly increased degeneration (AUC= 35.2, n=12 cells, $p<0.01$).

5.5 Intraocular pressure elevation in C6 deficient and wild-type Lewis rats

Six animals from each group of C6 deficient and wild type Lewis rats received a unilateral injection of paramagnetic microspheres as described in section 2.5. All animals required a second injection of microspheres at day five to sustain an intraocular pressure elevation. Following the second injection, a mean intraocular pressure elevation of 10.2mmHg (SD=3.25mmHg, $p<0.01$, Mann-Whitney U test) developed in the wild type animals and an elevation of 12.5mmHg (SD=4.54mmHg, $p<0.01$) developed in the C6 deficient animals (Figure 5.4). The intraocular pressure elevations of the two groups was not significantly different ($p=0.31$, Mann-Whitney U). This indicates that both groups had an equal probability of developing retinal ganglion cell degeneration associated with hypertensive glaucoma.

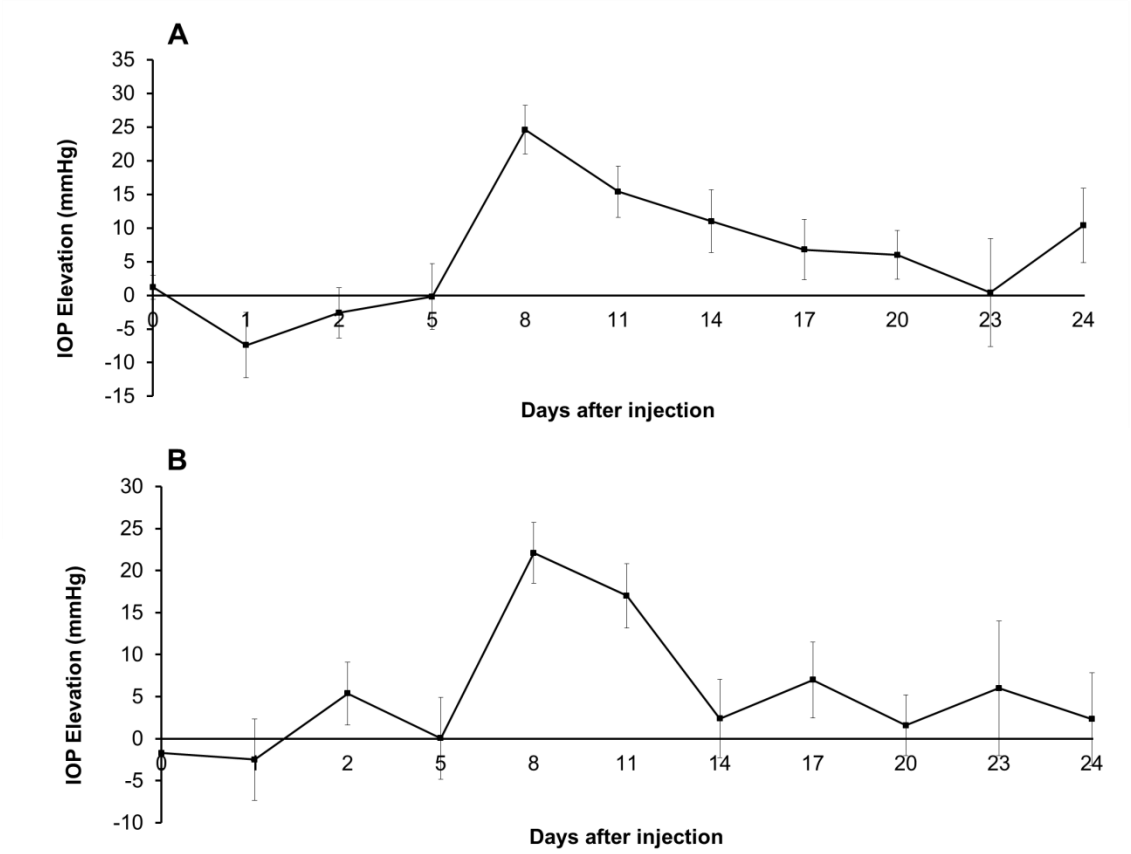

Figure 5.4 Wild-type and C6 deficient rats develop an equivalent elevation in intraocular pressure. Neither group of six animals developed an increase in intraocular pressure following the first injection of paramagnetic microspheres. At day five, following the second injection of microspheres, an elevation of intraocular pressure occurred in both groups. An elevation of 10.2mmHg (SD=3.25mmHg, $p<0.01$) was observed in wild type animals compared to an elevation of 12.5mmHg (SD=4.54mmHg, $p<0.01$) in C6 deficient animals. The elevation in intraocular pressure was significant in each group and was not significantly different between groups when compared by Mann-Whitney U test (p=0.31).

5.6 Glaucomatous C6-/- dendritic trees are significantly reduced compared to those of wild types

There was no significant difference in the Sholl plots of retinal ganglion cells from the normotensive eyes of wild type Lewis and C6 deficient rats and both groups were treated as a single control group of 35 cells. Retinal ganglion cells from six wild type animals with elevated intraocular pressure had significantly reduced Sholl plots (AUC=90.1, n=36 cells from 6 animals, $p<0.01$, two-sample Kolmogorov-Smirnov test) when compared to control cells (AUC=140.2, n=35 cells from 12 animals, figure 5.5). Similarly to C3 deficient retinal ganglion cells, those from C6 deficient retinas were significantly degraded compared to both control cells and complement sufficient hypertensive cells (AUC=56.5, n=12 cells from 6 animals, $p<0.01$). These data show that C6 expression is protective against retinal ganglion cell degeneration associated with an elevation in intraocular pressure.

Existing evidence (Miyahara 2003; Tezel *et al*. 2010) identifies an increase in the early components of the classical complement cascade (C1, C2 and C4), however no corresponding increase in the latter components is observed. These observations, taken together, suggest that complement activation in the healthy retina proceeds by the alternative pathway, which turns over C3 in a way that is regulated by factor H. In glaucoma, however, the classical complement cascade is initiated by the increase in levels of C1, C2 and C4 and the formation of the classical pathway C3 convertase C2aC4b. C2aC4b is not regulated by factor H, but the formation of the molecule is regulated by the molecule C1 inhibitor, which has not been identified as being up-regulated in glaucoma. It may be, therefore, that the complement mediated pathology associated with glaucoma is caused by the shifting of complement activation from the alternative to the classical pathway. This may

explain why an increase in the total expression of C3 is not detected in glaucomatous retinas (Miyahara 2003). It may that the same amount of native C3 is simply processed in a pathological and unregulated manner in the glaucomatous retina. The data presented here raises the possibility that the terminal complement complex may, at low levels, be responsible for the prevention of retinal ganglion cell apoptosis.

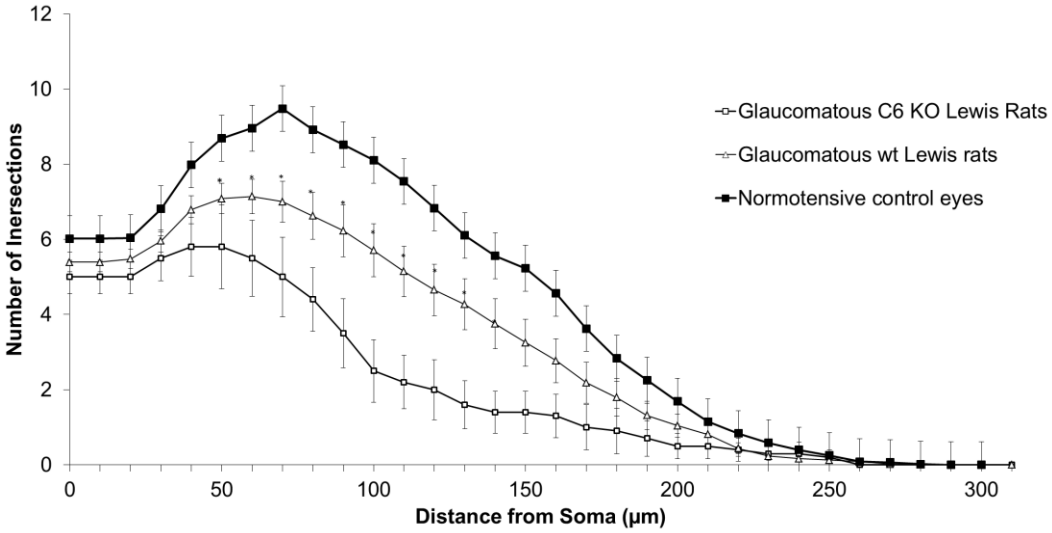

Figure 5.5 Retinal ganglion cell degeneration was exacerbated by C6 deficiency. Mean Sholl plots of retinal ganglion cells from six wild-type and six C6 deficient rats from eyes with elevated intraocular pressure and normotensive contralateral eyes from the same animals. Retinal ganglion cells from eyes with elevated intraocular pressure were significantly degraded (AUC: 90.1, n: 36 cells) compared to control eyes (AUC: 140.2, n: 35 cells, $p<0.01$) using the two-sample Kolmogorov-Smirnov test. This degeneration was significantly worse in animals with C6 deficiency (AUC: 56.5, n= 12 cells, $p<0.01$).

5.7 Discussion

The lack of an available mouse model for *in* vivo induction of hypertensive glaucoma necessitated the use of an *in vitro* model of hydrostatic pressure elevation. This model does have drawbacks as it necessitates the severing of the optic nerve head behind the retina, which would trigger uniform degeneration across the entire retinal ganglion cell layer in a manner not necessarily comparable to glaucomatous damage. The use of cultured retinas is also not ideal as the retina will be under oxidative stress during the time it takes to excise the retina and place it in medium. To minimise the impact of using an *in vitro* system to monitor retinal degeneration, retinal dissections were performed as quickly as possible (2-3 minutes per retina) and both medium and perfusion gases were changed every 12 hours. As both complement sufficient and deficient animals were treated identically, it is possible to draw conclusions regarding the role of complement in retinal degeneration by comparing data from these experiments. With the addition of retinal axonal disruption and hydrostatic pressure elevation, qualified conclusions can be drawn from these data regarding the role of complement in retinal ganglion cell loss in glaucoma.

The C6 deficient animals used in this study were based on an albino strain of rat. Albino animals have abnormal visual system development (Creel & Giolli 1976) and reduced protection from retinal light-induced toxicity (Wenzel *et al*. 2005). Any impact albinism has on glaucomatous optic neuropathy has not been studied thoroughly. There are case reports of individuals with both conditions, where glaucoma was secondary to a structural anomaly not related to albinism (Fivgas & Beck 1997), and a study on albino glaucomatous quails suggests an increase in retinal ganglion cell loss (Takatsuji *et al*. 1988). If albinism does increase glaucomatous optic neuropathy, then it may be via mechanisms distinct from those

that bring about glaucomatous optic neuropathy. Although this is a potential confounder, the animals used in this study were housed in low light (90lux) for the duration of the experiment, which should have helped mitigate phototoxicity during the experiment.

Data presented here suggest that both C3 and C6 are neuroprotective in glaucomatous optic neuropathy. This agrees with a growing body of evidence in the literature showing a neuroprotective role for the terminal complement complex in the central nervous system in response to insult (Monge *et al*., 1995; Rus *et al.* 2006; Soane, Cho, Niculescu, Shin, & Alerts, 2010; Tegla *et al*., 2009; Zwaka *et al*., 2002).

The terminal complement complex activates the protein, response gene to complement 32 (RGC32) (Badea *et al*. 1998). This has been shown to increase progression through the cell cycle by activation of the phosphatidylinositol 3-kinase/akt pathway (Hila *et al*. 2001; Badea *et al*. 2002). Melanopsin-containing retinal ganglion cells are resistant to glaucomatous optic neuropathy and other forms of injury (La Morgia *et al*. 2010). This resistance is reportedly due to the activity of the phosphatidylinositol 3-kinase/akt pathway (Li *et al*. 2008). Similarly, the neurotrophic activity of brain-derived neurotrophic factor in the central nervous system is also reported to be mediated by the phosphatidylinositol 3-kinase/akt pathway (Almeida *et al*. 2005). Disruption in the transport of this molecule has been implicated as a mechanism underlying retinal ganglion cell death in glaucoma (Quigley *et al*. 2000; Ko *et al*. 2001). Inhibition of this pathway has also been shown to be detrimental in rat models of acute ocular hypertension (Y Huang *et al*. 2008; Yao Huang *et al*. 2008).

This evidence in the literature suggests a strong link between the phosphatidylinositol 3-kinase/akt pathway and neuroprotection in glaucoma. The present results suggest that inhibition of the later stages of the complement cascades worsens retinal ganglion cell loss in retinas subjected to elevated hydrostatic pressure. This supports the assertion that RGC32 is a mediator of neuroprotection in retinal ganglion cells in glaucomatous optic neuropathy.

The work presented in this chapter indicates that downstream components common to all complement cascades are involved in retinal ganglion cell degeneration in glaucoma. As the classical complement cascade has been specifically implicated in the literature as an early event in glaucoma, it is important to understand the role of this cascade. To determine the specific role of the classical complement cascade, I will utilise the model of glaucomatous retinal degeneration developed in chapter 3. In chapter 4, I established that complement activation was occurring in this model and was associated with a loss of retinal ganglion cells. To determine whether or not classical complement activation is a causative factor in retinal ganglion cell degeneration in this model, I will inhibit the classical complement cascade in presence of ocular hypertension *in vivo*.

Chapter Six: Inhibition of the classical complement cascade in experimental glaucoma.

6.1 Introduction

The classical pathway of complement activation has been implicated as a potential causative agent in glaucomatous optic neuropathy (Howell *et al*. 2011; Stevens *et al*. 2007; Tezel *et al*. 2010; Kuehn *et al*. 2008). Further to this, this classical complement cascade has been shown to be essential for synaptic refinement in the central nervous system (Stevens *et al*., 2007, Stevens *et al.,* 2011). This is only of functional use with regards to the treatment of glaucoma if manipulation of the complement system can bring about neuroprotection *in vivo*.

Complement inhibition has been used extensively in a therapeutic setting and experimental models of disease (Copland *et al*. 2010; Morgan & Harris 2003). One of these agents, C1 inhibitor (Bork & Barnstedt 2001), regulates the classical complement cascade by blocking the formation of an complete and active C1 molecule. The aim of these experiments was to determine if the administration of C1-inhibitor reduces axonal and or dendritic degeneration of retinal ganglion cells in our animal model of hypertensive glaucoma. It has been established in the literature that up-regulation of the components of C1 is an early event in glaucomatous damage in the human disease and in animal models (Howell *et al*. 2011; Tezel *et al*. 2010) however there is currently no direct evidence that the classical pathway of complement activation is a causative factor in retinal degeneration.

Human C1 inhibitor has been shown to effectively inhibit the classical complement pathway in the rat (Ramaglia *et al*. 2007), as such is suitable for use as an inhibitor of the classical complement cascade in our rat model of glaucoma. In this experiment I aimed to determine if the classical complement pathway is a mediator of glaucomatous optic neuropathy and if C1 inhibitor is a realistic treatment

option for neuroprotection in glaucoma. To that end, animals were given intravitreal injections of the C1-inhibitor protein. These animals were then culled at different time points and, the retinas were immunolabelled for the protein to determine if it could permeate the neural retina. Following this, animals were pre-treated with intravitreal injections of human C1-inhibitor prior to the induction of hypertensive glaucoma. These injections were repeated at regular intervals throughout the course of the experiment to sustain the levels of the C1-inhibitor protein in the retina.

6.2 Chapter methods

6.2.1 Intravitreal injections

In total, twenty-eight animals underwent intravitreal injection. Sixteen animals were injected with human C1-inhibitor and four of these animals were culled to determine the permeation of C1-inhibitor into the neural retina. The remaining fourteen animals in this group were used to study the effect of C1-inhibitor on dendritic atrophy in hypertensive glaucoma. Twelve animals underwent intravitreal injection with phosphate buffer vehicle. These animals served as a vehicle-only control group to the twelve animals injected with C1-inhibitor. This was done to ascertain whether any effect observed in the C1-inhibitor-treated group was attributable to the C1inhibitor or the procedure itself.

6.2.1.1 Preparation for intravitreal injection

Twenty minutes prior to anaesthesia, animals were treated with 1% Tropicamide drops (Mid-Optic, UK) in the left eye to dilate the pupil and facilitate observation of the retina. Anaesthesia was induced with Isoflurane (Bayern, Germany) in oxygen at 2L/min, after ascertaining animals were anaesthetised deeply, by testing for response to eternal stimuli, the animal was transferred to a face mask and the level of Isoflurane was adjusted to the minimum level required to maintain anaesthesia for the remainder of the procedure. The procedure time was typically less than five minutes following the establishment of deep anaesthesia.

6.2.1.2 Intravitreal injection

A drop each of 0.5% oxybuprocaine hydrochloride local anaesthetic and antibiotic chloramphenicol (Mid-Optic, UK) was administered to the surface of the cornea and

the pupil was inspected to ensure sufficient dilation for observation of the needle in the posterior chamber. Clinitas hydrate (Mid-optic UK) viscose fluid was applied to the surface of the cornea to support a glass cover slip to facilitate visual observation of the posterior chamber through the visual axis of the animal during the procedure by neutralising the refractive power of the cornea. The sclera was grasped using cup-toothed forceps (Duckworth and Kent, UK), and an incision was made into the posterior chamber using a 35 gauge, tri-bevelled needle (WPI Europe, Germany) attached to a 100µl Hamilton syringe (WPI Europe, Germany). The tip of the needle was positioned above the optic nerve head and five microlitres of either C1 inhibitor in phosphate-buffered saline or phosphate-buffered saline (vehicle) only was injected at this position and the needle was left in place for approximately 20 seconds to allow diffusion of the fluid before removal of the needle. Following injection, the glass coverslip was removed, any remaining Clinitas hydrate was wiped away using a cotton bud and a further drop of chloramphenicol was applied to the surface of the cornea.

Four animals were injected with C1 inhibitor to evaluate the permeation of C1 inhibitor through the retina. For these animals, a single injection was administered. Twenty-four hours following injection, two animals were culled and the remaining two animals were killed ninety-six hours after injection. Sections were prepared as described in section 2.9 and immune-labelled as in section 2.10 with anti-human C1-inhibitor. Sections were then imaged by confocal microscopy as in chapter 2.8.2.

For the twenty-four animals in this experiment, twelve animals had a unilateral, intravitreal injection of phosphate buffered saline, and twelve animals were injected with human C1-inhibitor. For all animals, intravitreal injections were repeated every 4 days following the first injection for the duration of the procedure.

In each animal, intraocular pressure was elevated by microsphere injection 24 hours following the first intravitreal injection of C1 inhibitor.

6.2.2 Induction of intraocular pressure elevation

In the twenty-four animals where intravitreal injections were used to study the effects of C1 inhibitor on glaucomatous degeneration, the intraocular pressure of the same eye was elevated by microsphere injection. This procedure was carried out using 4.5 µm (Dynal, Norway) microspheres at 2x stock concentration ($8x10^8$ beads/ml) as described in chapter 2.5, 24 hours after intravitreal injection. Microsphere injections were repeated in animals which did not develop and/or maintain an intraocular pressure increase of ≥10mmHg by day 5 following the initial injection.

6.2.3 Optic nerve analysis

Retinal ganglion cell death in glaucoma is preceded by a prolonged period of axonal degeneration. In order to establish if C1-inhibitor injections protected the axons of retinal ganglion cells from degeneration, axon counts of retinal ganglion cells were taken from the optic nerves of experimental and control animals.

Both optic nerves were taken from each of the twenty-four animals which underwent intravitreal injection, yielding forty-eight optic nerves. Twenty-four of these optic nerves were from un-injected eyes, twelve were from eyes injected with C1-inhibitor and twelve were from eyes injected with phosphate buffer. A single optic nerve from the group of animals injected with C1-inhibitor was damaged during retrieval and was discounted from the analysis, leaving eleven optic nerves in that group. For optic nerve analysis, optic nerves were removed from the cranium of animals and fixed in 4% paraformaldehyde for a minimum of 24 hours in a bijou before being transferred to phosphate buffered saline. Retinal ganglion cell axon

counts were kindly carried out under masked conditions by Dr Gareth Howell at Jackson Laboratories (USA) using methods described in Anderson *et al*. (2005). Briefly; semi-thin (1µm) sections were cut from the central portion of the optic nerve and para-phenylene diamine staining was used to differentially stain the axons of healthy or diseased retinal ganglion cells for manual counting by a masked investigator. Twenty evenly-spaced images of the optic nerve were captured and manual counts were taken of the numbers of degenerating and healthy axons. Where degenerating axons made up less than or equal to 2% of the total number of axons, the optic nerve was classified as having 'no or early glaucoma'. Where degenerating axons were greater than 2% but less than 50%, the nerve was classified as 'moderately glaucomatous'. Where degenerating axons made up more than 50% of the optic nerve, it was classified as 'severely glaucomatous'.

6.3 Permeation of human C1-inhibitor into the rat retina following intravitreal administration

Four animals were injected with human C1-inhibitor, two animals were culled 24 hours after injection and two were culled 96 hours after injection. Immunofluorescent detection of human C1-inhibitor was performed as described in section 2.10 using the 'C1 inhibitor' antibody detailed in table 2. Figure 6.1 shows immune detection of human C1-inhibitor at 24 and 96 hours post-intravitreal injection for a single rat at each time point . The use of human protein allows detection to be specific for the human protein by using a primary antibody which is specific for that protein. The human protein also has the advantage of being readily available at a high concentration and purity as it is used as a treatment for hereditary angioedema. The exogenous protein is detected into and beyond the inner plexiform layer of the neural retina at both time points. The positive staining indicates that human C1inhibitor persists in the rat retina for 96 hours following intravitreal administration (Figure 6.1). Unlike the neural retina, there is limited detection of human C1 inhibitor in the optic nerve head, which rapidly drops off further in to the optic nerve (Figure 6.1). This indicates that the C1 inhibitor molecule diffuses throughout the retina but is not able to pass through the structures of the optic nerve head.

.

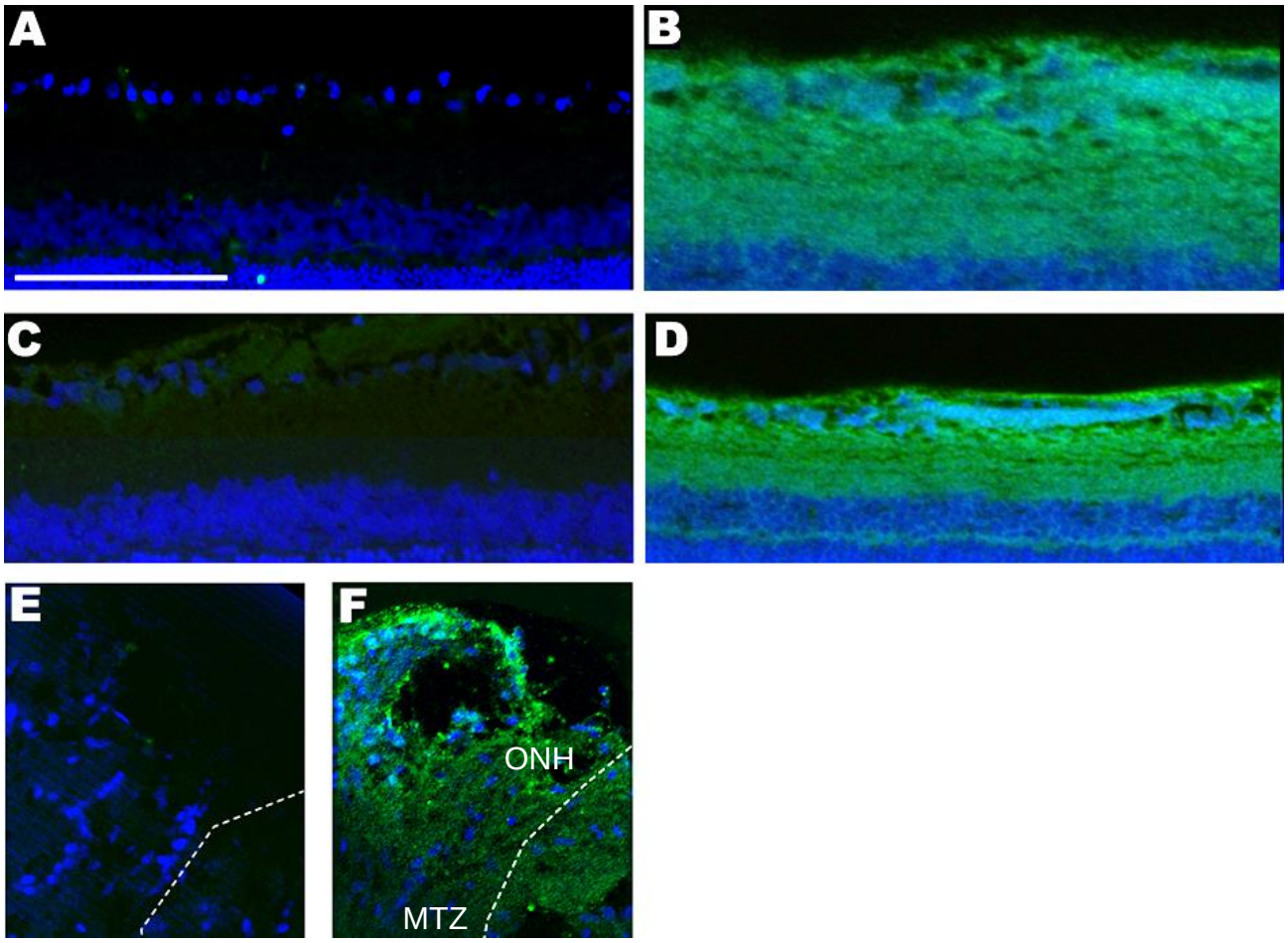

Figure 6.1 Immunfluorescent detection of human serum derived C1-inhibitor in rat retinas 24 and 96 hours after injection of 36µg of C1 inhibitor into the vitreous chamber. Example images from two animals killed 24 hours post-C1-inhibitor injection and two animals killed 96 hours post-injection. Nuclear counterstaining (blue) and anti- C1-inhibitor antibody staining, detected with Alexafluor488® (Invitrogen UK, UK) (green) in the retinas of sham (A) and C1-inhibitor-injected (B) eyes at 24 and 96 (C-D) hours after injection shows the detection of exogenous C1-inhibitor throughout the neural retina at both time points. Sections showing nuclear counterstaining (blue) and anti-C1-inhibitor (green) detection in sham-injected (E) and C1inh-injected (F), eyes at the optic nerve head. Detection of C1-inhibitor is observed at the surface of the optic nerve head (ONH) but is diminished towards the myelin transition zone (MTZ) Scale bar = 100µm

6.4 C1-inhibitor has no effect on contralateral intraocular pressure or Sholl plot

The generated datasets were analysed as described in section 2.11.2. There was no significant difference in the dendritic profiles of contralateral, normotensive eyes from C1-inhibitor treated (AUC=136.3 n=29 cells) or sham-treated animals (AUC=139.6, n=42 cells) (Figure 6.2). As observed in figure 6.1, there is no detectable diffusion of injected C1-inhibitor through optic nerve head. This minimises the possibility of cross-contamination between C1-inhibitor treated glaucomatous eyes and contralateral controls. Animals treated with phosphate buffered saline vehicle control injections underwent the same surgical procedures as the C1-inhibitor injected animals. These facts taken together suggest that there is no biochemical difference between the contralateral and uninjected eyes of C1-inhibitor injected or phosphate buffer injected groups and that data from these eyes can be treated as a single, normotensive control group of 71 cells.

Twelve of the twenty-four animals required a second injection to produce a sustained elevation in intraocular pressure. The mean elevation of all animals was 12.4mmHg (SD: 2.23mmHg) (Figure 6.3) and all animals showed an intraocular pressure elevation of at least 5mmHg for a period of ten days or more.

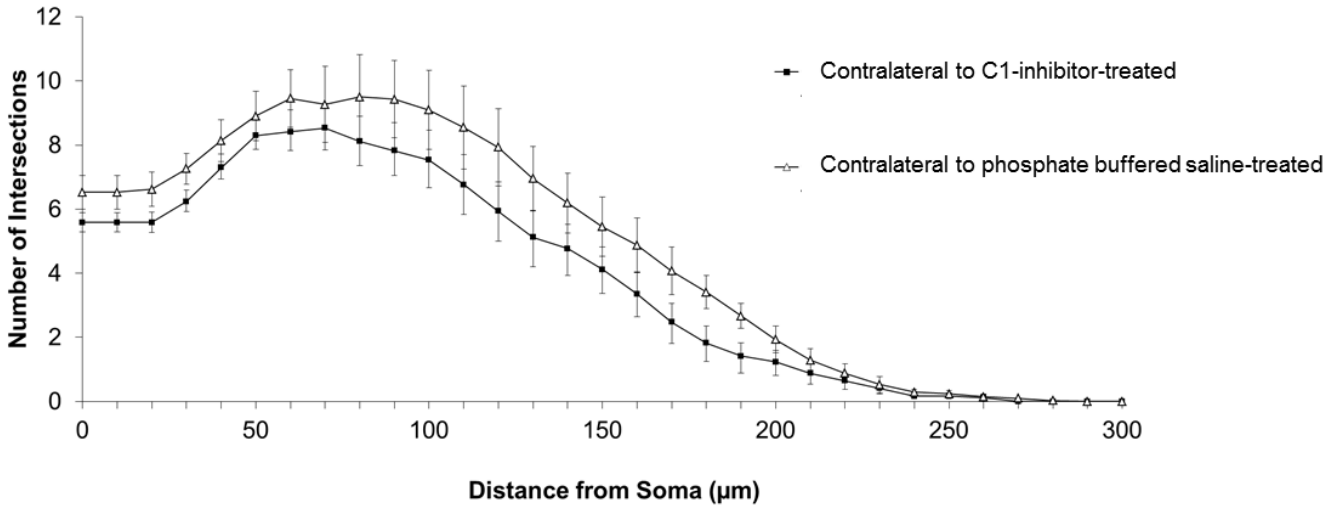

Figure 6.2 C1-inhibitor has no effect on the Sholl plots of retinal ganglion cells from contralateral, uninjected eyes. As analysed by a two-sample Kolmogorov-Smirnov test, there is no statistically significant difference between the mean Sholl plots of C1- inhibitor treated (AUC: 136.3 n=29 cells from 12 animals) or sham-treated animals (AUC: 139.6 n: 42 cells from 12 animals, $p>0.05$) This indicates that retinal ganglion cells from both sets of contralateral, uninjected eyes may be treated as a single population of 71 cells for comparison with glaucomatous retinal ganglion cells.

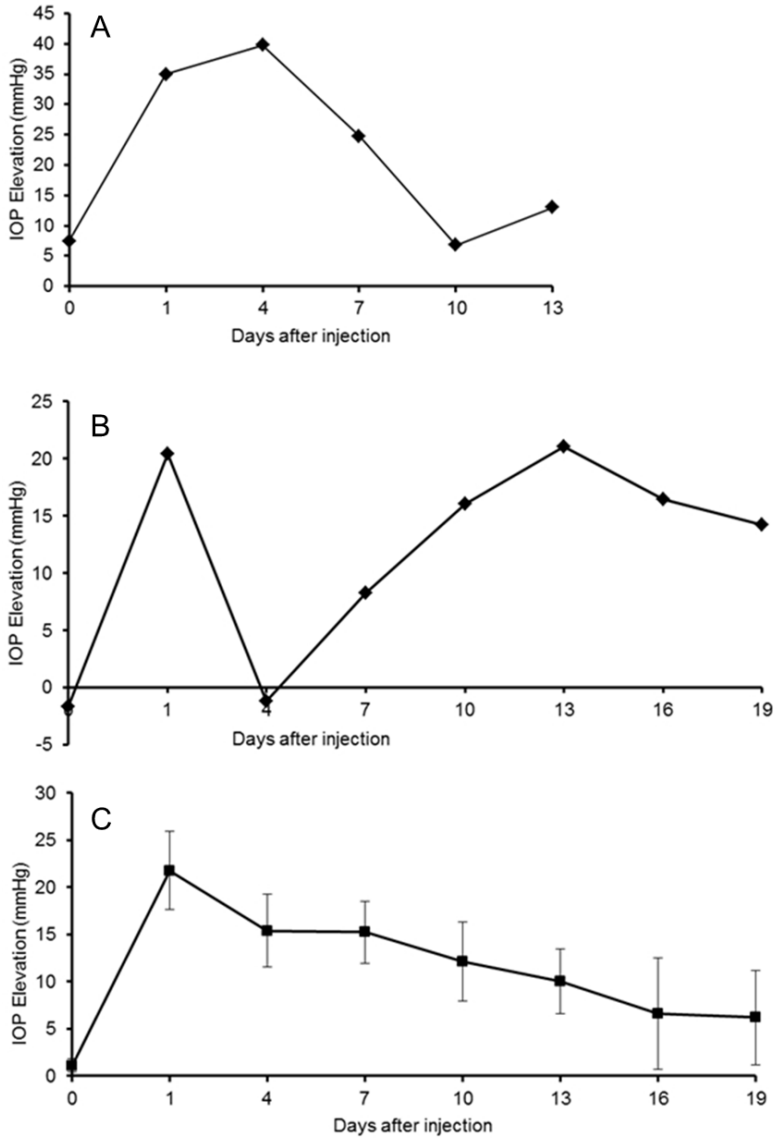

Figure 6.3 Injection of paramagnetic microspheres causes a sustained and significant increase in intraocular pressure. (A) Example elevation profile of a single animal which maintained an intraocular pressure elevation after a single injection with a mean intraocular pressure elevation of 22.45mmHg (SD: 1.25mmHg). (B) Example intraocular pressure elevation profile of an animal which required a second injection at day 5 developing a mean pressure elevation of 12.36mmHg (SD: 3.65mmHg). (C) The mean pressure elevation of all was 12.4mmHg over all days (SD: 2.23mmHg, n=24 animals at days 0-13 and n=12 animals at days16-19).

6.4.1 Dendritic atrophy in hypertensive retinal ganglion cells

Dendritic morphology as measured by Sholl analysis was significantly reduced in retinal ganglion cells from eyes of twelve phosphate buffer-injected animals with elevated intraocular pressure compared to contralateral, normotensive controls (AUC: 115.1 SEM: 8.24 n=67 cells and AUC: 138.3 SEM: 9.2 n=71 cells, respectively $p<0.05$; Figure 6.4). This establishes that there is a relationship in this model between an elevation of intraocular pressure and degeneration of retinal ganglion cell dendritic integrity.

6.4.2 Dendritic protection by C1-inhibitor in hypertensive retinal ganglion cells

The dendritic morphology of retinal ganglion cells from eyes with elevated intraocular pressure and treated with C1 inhibitor was not significantly different from control, normotensive eyes and was therefore (AUC: 148.2 n=74 cells from 12 animals $p<0.05$; Figure 6.4) preserved compared to cells from sham-treated eyes. This indicates that C1 inhibitor effectively protects the dendrites of retinal ganglion cells from neuropathy associated with hypertonic glaucoma. Dendritic degeneration is an early event in glaucomatous optic neuropathy (Weber *et al*. 1998a), and it is possible that protecting the retinal ganglion cell dendrites prevents associated axonal degeneration. To determine if this is the case, I examined the level of degeneration in the accompanying optic nerves.

.

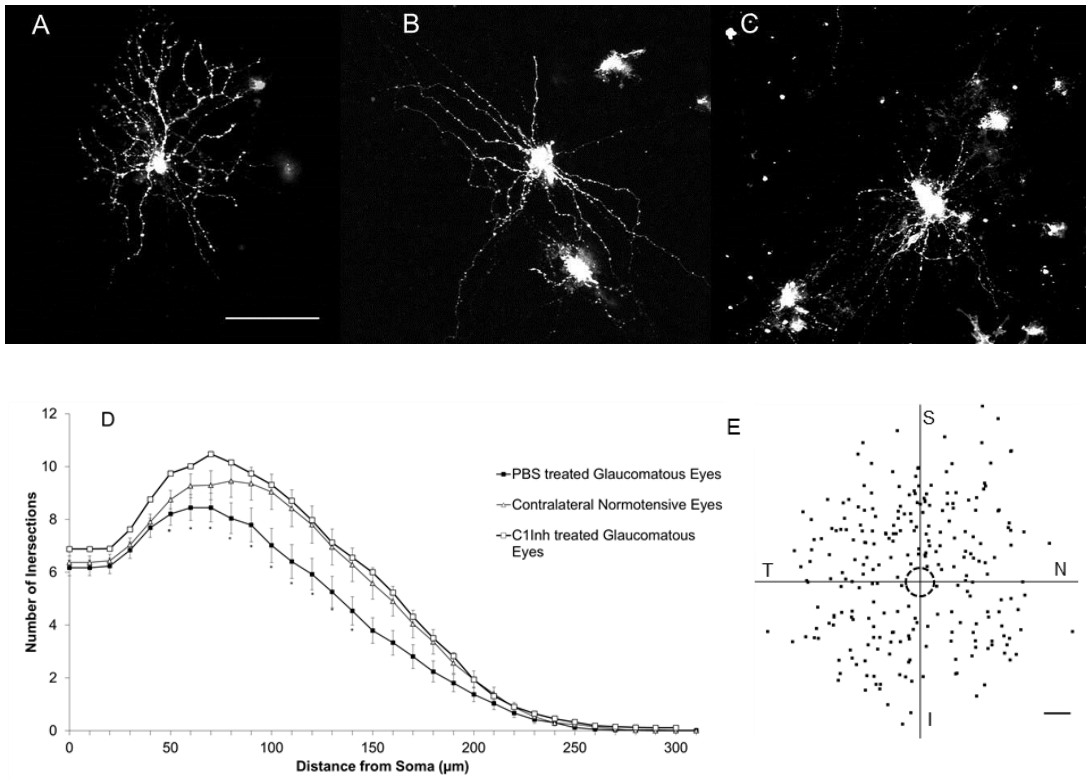

Figure 6.4 Preservation of dendritic morphology in retinal ganglion cells treated with C1-inhibitor. Representative DiOlysitc images of retinal ganglion cells from normotensive control (A), C1-inhibitor treated (B) and phosphate buffered saline -injected (C) glaucomatous retinas, scale bar = 100µm. (D) Mean Sholl plots of all measured cells, showing: (i) degeneration of ganglion cells from phosphate buffered saline-treated, glaucomatous retinas (AUC: 115.1 n=67 cells from 12 animals) compared to those from normotensive control retinas (AUC: 138.3 n=71 cells from 24 animals) and (ii) preservation of ganglion cells of C1-inhibitor treated retinas (AUC: 148.2 n=74 cells from 12 animals) – error bars show standard deviation. (E) Co-ordinates of all measured cells; dotted arrow corresponds roughly to the optic nerve head, scale bar = 1cm.

6.4.3 C1-inhibitor does not protect the optic nerves of hypertensive retinas

A single optic nerve was lost during harvesting from the C1-inhibitor treated group. Of the optic nerves from the C1-inhibitor-treated and phosphate buffer-treated groups (11 and 12, respectively), nine of each group were classified as moderately to severely glaucomatous compared to the optic nerves from control retinas, of which 23 out of 24 were classified as non-glaucomatous (Figure 6.5). This indicates that intravitreal C1-inhibitor administration does not provide protection to the degenerating axons of retinal ganglion cells. Therefore, although axonal degeneration follows degeneration of dendrites, it is not a direct cause, and alleviating dendritic degeneration is not sufficient to preserve vision in glaucomatous optic neuropathy.

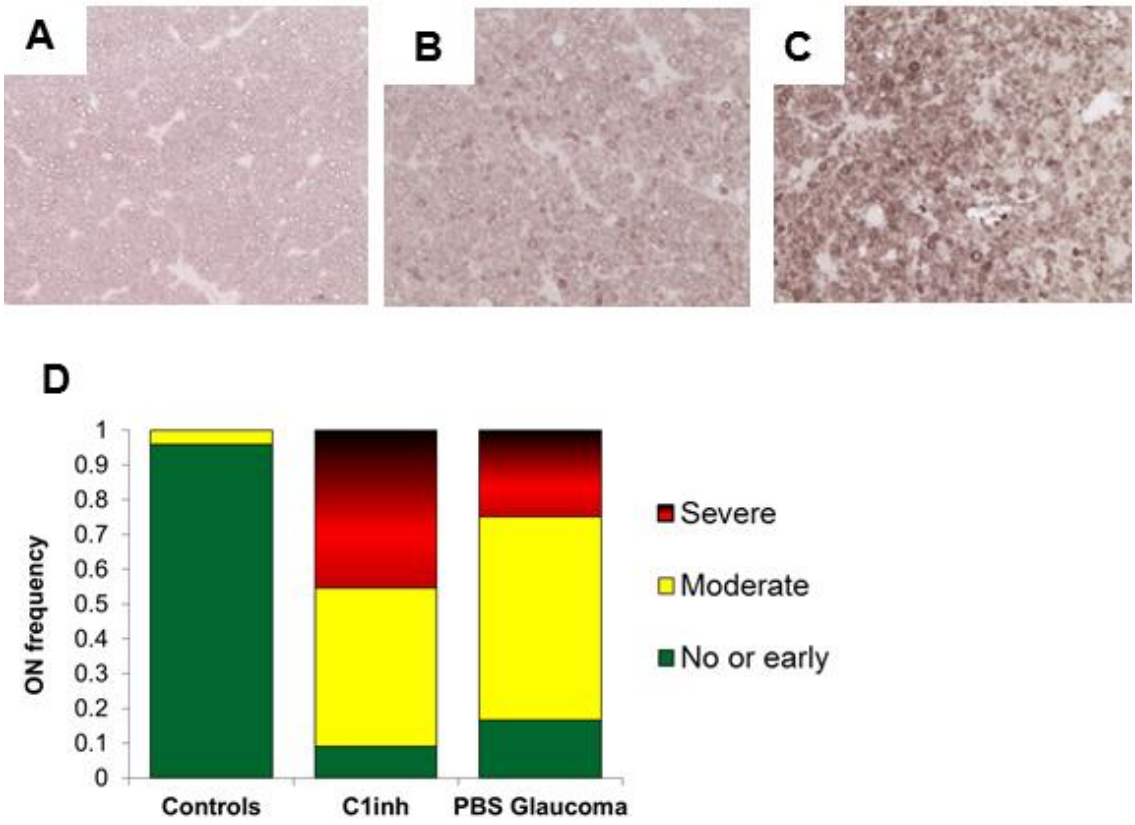

Figure 6.5 C1-inhibitor does not protect the optic nerve (ON) from degeneration. Examples of para-phenylene diamine stained sections of optic nerve, in which damaged axons are differentially stained black, showing the three grades of optic nerve damage: early to no glaucoma (A), moderate glaucoma (B) and severe glaucoma (C). (D) Relative frequency of grades between groups showing no difference between C1-inhibitor (n=11 nerves) and phosphate buffered saline (n=12 nerves) injected glaucoma groups, in which each group comprised having nine severely or moderately affected optic nerves. Only a single optic nerve from the control, uninjected eyes (n=24 nerve) was found to have moderate glaucoma.

6.5 Discussion

The presence of concurrent retinal ganglion cell dendritic atrophy (as measured by Sholl analysis) and optic nerve degeneration (as measured by grading of para-phenylenediamine stained nerves) in animals with elevated intraocular pressure further validates the paramagnetic microsphere model of glaucoma by establishing that dendrites and axons of retinal ganglion cells degenerate in a manner similar to that which has been reported previously (Weber *et al*. 1998b; Quigley & Addicks 1980a).

The classical complement cascade has been implicated in human and experimental glaucoma and this reveals a potential new target for glaucoma therapy in the manipulation of that system. Human C1 inhibitor has been used to effectively inhibit complement activation in the rat (Ramaglia *et al*. 2007), and the relative immune privilege of the eye ensures that there is no immune response to the exogenous protein. Administration of the drug before the induction of the disease state was intended to create a 'best case' scenario and combat the early damage at the optic nerve head in glaucoma. The progression of glaucomatous damage to retinal ganglion cells includes the axonal and dendritic structures of the cell. For this reason, dendritic arborisation and axonal integrity were assessed with masked Sholl analysis and optic nerve grading respectively.

Clearly, C1-inhibitor, when injected in to the vitreous chamber, was able to penetrate all layers of the neural retina (Figure 6.2). C1-inhibitor was not, however, able to penetrate to the same extent at the optic nerve, possibly due to the binding of the globular heads of C1 inhibitor molecules to abundant collagen molecules therein.

The presence of C1-inhibitor in the neural retina was associated with a complete protection of retinal ganglion cell dendritic structure, as measured by Sholl analysis, with the dendritic profiles of C1-inhibitor-treated retinal ganglion cells not being significantly different from those of normotensive controls (Figure 6.4). By contrast, there was no diffusion of C1-inhibitor through the optic nerve head (Figure 6.1), and retinal ganglion cell axons present in this region are not protected from glaucomatous degeneration (Figure 6.5).

The results shown here indicate that although the retinal ganglion cell's dendritic tree remains intact, the loss of optic nerve fibres is unchanged.

The increased production of complement components in glaucoma is specific to retinal ganglion cells (Tezel *et al*. 2010). This may explain why retinal ganglion cells are targeted specifically in glaucoma if complement functions as a mediator of microglial clearance of retinal ganglion cells. Further, the chemotactic effect of the product of the complement cascade, C5a, is responsible for the motility of microglia in the rodent (Nolte *et al*. 1996). As a chemo-attractant C5a will form a concentration gradient outwards from its source attracting microglia to the retinal ganglion cells that produce C5a it and inhibition of complement activation will prevent microglia from migrating towards retinal ganglion cells.

Astrocyte and microglial activation are increased and self-promoting under glaucomatous conditions. The role of microglia in glaucomatous optic neuropathy is expected to be one that could be described as 'housekeeping', where retinal ganglion cell structures tagged with C1 or C3b are phagocytosed by microglia that bind to putative C1 receptors or complement receptor 1, respectively. C1-inhibitor will prevent this action, however it will not prevent the activation of microglia in

response to hydrostatic stress or astrocytic adenosine triphosphate release. If C1 inhibitor can prevent the removal of retinal ganglion cell structures, then the activation of microglia in response to glaucomatous stress may be irrelevant. However, this will be contingent on the presence of the C1 inhibitor molecule. C1 inhibitor has a molecular mass of ~140kDa and a very strong collagen binding motif, which is essential for its function. This may be responsible for the reduced permeation of the molecule through the optic nerve head observed by immunofluorescence.

Based on the data presented here, the effect of the intravitreal administration of C1 inhibitor is that dendritic structures of the retinal ganglion cell are protected whereas the optic nerve is afforded no protection, presumably due to the reduced permeation of the C1 inhibitor molecule. This protection may be the result of blocking the activity of C1 at the putative C1-receptor or by the reduction of complement mediated chemo-attraction of microglia to damaged retinal ganglion cells.

Chapter Seven: General Discussion

7.1 Principle findings

I have identified that complement activation takes place in a microsphere-induced, hypertensive rat model of glaucoma. Building on this I have established that intravitreal administration of the anti-complement agent C1 inhibitor can effectively inhibit retinal ganglion cell dendrite and cell body degeneration. This supports evidence in literature that suggests a causal link between complement activation and retinal ganglion cell degeneration. The persistence of axonal degeneration in retinas with otherwise healthy retinal ganglion cells suggests a compartmentalised progression of retinal ganglion cell degeneration in glaucoma, wherein degeneration of axons is not sufficient to trigger retinal ganglion cell apoptosis. I have also established that mutations affecting the expression of proteins further down the complement cascade, C3 and C6, are not protective as may be expected based on the effect of inhibiting the first component of the complement cascade. This supports evidence from numerous studies conducted by Rus *et al,.* which indicate the terminal complement complex is a neuroprotective agent which essential for neuronal survival following insult. Together these findings support evidence presented by Stevens *et al.,* (2007, 2010 and 2011) indicating that complement component C1 directly mediates retinal ganglion cell destruction in response to quiescence and suggest that this mechanism is responsible for retinal ganglion cell loss in glaucoma.

7.2 Model of hypertensive Glaucoma

Each existing models of glaucoma has drawbacks which limits its implementation such as a high degree of required surgical dexterity, as is the case with the hypertonic saline injection model (also known as the Morrison model) or a limitation on the amount of beads which can be injected (Calkins *et al,.* 2007). The development of this model ultimately led to a model which could reliably increase intraocular pressure in rat eyes from at most two injections, whilst leaving the visual axis clear and facilitating both visual inspection of the eye and measurement of intraocular pressure. Visual inspection of the eye was essential for the experiments that were carried out as repeated injections of C1 inhibitor into the posterior chamber required the positioning of a needle within the vitreous over the optic nerve head. This would not have been possible had the large number of beads injected not been adequately distributed throughout the iridocorneal angle or if they had caused an immune response which would have clouded the cornea.

I have validated the paramagnetic microsphere model of glaucoma by establishing that dendrites, axons and cell bodies of retinal ganglion cells are lost following the elevation of intraocular pressure.

7.2 Complement activation in glaucoma

The role of complement activation in neurodegenerative disease is complex and multifactorial with early complement components being essential for damage in some cases and clearance in others. Later components of the complement cascade are essential for rapid Wallerian degeneration (Ramaglia *et al*,. 2007) and yet, the terminal complement complex is actively involved in cell cycle progression and the maintenance of neuronal integrity via activation of complement response genes such as complement response gene 32, which promotes cell survival though Akt/PKB activation (Rus *et al,*2006 and 2008*)*.

C1 has been shown to be an active component of neuronal degradation in disease and development by facilitating clearance of inactive or stressed neuronal processes and cells. Results shown here indicate that inhibiting the formation of active C1 from C1q, C1r and C1s molecules using human C1 inhibitor, significantly reduces the damage done to retinal ganglion cells in glaucomatous optic neuropathy. However this protection only affects the dendrites of the retinal ganglion cells and does not reduce the degradation of the optic nerve axons.

The initial site of damage in glaucoma has been identified as the optic nerve head, specifically, the myeloid transition zone. The C1 inhibitor administered to the posterior chamber of the eye in chapter 6 did not permeate beyond the neural retina as such it was ineffective at preventing the insult at the optic nerve head. A possible reason for the reduced permeation of C1-inhibitor at the optic nerve head is that this region is rich in collagen which binds C1-inhibitor with high affinity. This collagen binding ability of C1 inhibitor is required for its binding to the collagen-like domain of C1q and hence, its function. This means that it may not be possible to modify C1

inhibitor in such a way that would allow it to pass through the optic nerve head and retain the function needed to prevent clearance of the retinal ganglion cell axons.

It may be possible that axonal degeneration proceeds via a distinct mechanism from dendrite and cell body loss. It has been suggested that compartmentalised Ca^{2+} release and caspase activation may be responsible for the death of retinal ganglion cell dendrites before axons (Whitmore *et al*. 2005; Crish *et al*. 2010). If this is the case it may be that C1-inhibitor failed to prevent axonal degeneration as this occurs via different mechanisms from dendritic degeneration. This is supported by evidence from Beirowski *et al*., (2005 and 2008) who identified the gene Wld, which is responsible for Wallerian degeneration and observed that a mutation in this gene which mitigates axonal degeneration in glaucoma without affecting dendritic atrophy or apoptosis. Data presented here cannot identify whether protection is not afforded to axons due to differences in the underlying apoptotic mechanisms or due to limitations of the administration method for the complement inhibitor. It may be the case that although axonal atrophy is triggered by intracellular processes which are distinct from other compartments within the retinal ganglion cell, complement mediation is still required for clearance of the axon and complement inhibition may be an effective method of preventing this.

Retinal ganglion cell axon terminals are removed during developmental refinement in a C1-dependent manner (Stevens *et al,.* 2007), an up-regulation of C1 in glaucoma and the data presented here suggests that similar mechanisms are involved in glaucomatous retinal ganglion cell removal. In this case, preventative treatment of glaucoma with a complement inhibitor may need to administer that inhibitor to the length of the axon, up-to and including the axon terminal. This poses a challenge as axonal transport is disrupted in the early stages of glaucoma (Quigley

et al,. 2000 and Chidwell *et al,.* 20011) and direct administration to the axon terminals would require brain surgery, which is unlikely to be seen as an acceptable prophylactic treatment for glaucoma.

The increased degeneration of the retinal ganglion cells of C3 and C6 deficient animals compared to complement sufficient animals of the same strain may indicate that neuroprotective mechanisms of low-level formation of the terminal complement complex are crucial to retinal ganglion cell survival in glaucomatous optic neuropathy. This is supported by evidence from other neuronal cell types (Rus *et al,.* 2008) and the expression patterns of glaucomatous retinal ganglion cells (Tezel *et al,.* 2010) which indicate a relatively minor change in the expression of components of the terminal complement complex in glaucomatous retinal ganglion cells.

Although it may appear to be counter intuitive that blocking the complement cascade at C1 prevents damage whereas blocking steps further along the cascade exacerbates damage, this can be explained by the spontaneous activation of complement through the alternative pathway. It is therefore quite possible for inhibition of the classical complement will block damage caused by C1 activity without inhibiting independent activation of the alternative pathway.

In chapter 5.7 I raised the possibility that the pathological changes associated with complement activation are a result of a shift in complement activation from the alternative complement cascade, which is natively regulated in the retina, to the classical complement cascade which is less well regulated. Howell *et al*. (2013) observed that the terminal complement complex could be detected in the retinas of healthy animals as well as those suffering from glaucomatous degeneration. This

supports the idea that low-level and regulated complement activation is present in the healthy retina. This study also identifies a protective role for C5 deficiency in the DBA/2J mouse model of glaucoma. This is in direct contrast to the results shown in chapter 5 where a deficiency in C6 significantly worsened degeneration of retinal ganglion cells. It is of note, however that the models used in these studies are fundamentally different. The DBA/2J mouse model relies on an immune-mediated exfoliation of the iris to induce and elevation in intraocular pressure and as such the effect of restoring C5 may impact on the elevation in intraocular pressure elevation. This differential intraocular pressure elevation is something the authors of Howell *et al*. (2013) acknowledge in their study.

7.3 Conclusions

This project has refined and validated the paramagnetic microsphere model of glaucoma in the rat. Control experiments have established that the magnetic manipulation of microspheres enhances intraocular pressure elevation and alleviates potential side-effects of bead injection such as obstruction of the visual axis and beads resting on the inferior aspect of the iridocorneal angle.

This work adds to the growing body of evidence that complement activation is a mediator of neuronal degeneration in glaucoma. The reduction of damage by inhibiting the early stages of complement activation with C1 inhibitor and the contrary worsening of degeneration in animal models deficient in later stages of the cascade indicates that this role is as a chronic, sub-lytic facilitator of cellular clearance.

The protection of retinal ganglion cells from glaucomatous damage in the rat by C1 inhibitor is mediated by inhibition of microglial binding to C1q and/or the formation of the chemo-attractants C3a and C5a. Similar protection is not afforded by knockout mutations of C3 and C6 which suggest a protective role for the terminal complement complex produced by the constitutively active and C1 inhibitor independent alternative pathway.

7.4 Future work

A possible complement-mediated prophylaxis for glaucoma does suggest itself however, it is possible that knocking out any of the genes involved in C1 assembly may prove protective if it can be done reliably in those at risk of developing glaucomatous optic neuropathy.

It is also possible that inhibiting the activity of microglia in the retina may cause beneficial protection of retinal ganglion cells in glaucoma, particularly of note are anti-purinergic molecules which have been shown to block microglial migration to and clearance of damaged central nervous system neurones (Davalos *et al*., 2005; Reigada, Lu, Zhang, & Mitchell, 2009; Sperlágh & Illes, 2007; Wu, Vadakkan, & Zhuo, 2007). These molecules have the advantage of being significantly smaller than the 150kDa C1-inhibitor which would allow better penetration into the optic nerve head and protection of the retinal ganglion cell axons.

A potentially interesting approach to further characterise the effects of the complement cascade in retinal ganglion cell loss in glaucoma would be the use of the membrane bound inhibitor of the opsonising action of C3b/iC3b APT070 (Souza *et al.* 2005). This inhibitor was initially identified as a potent inhibitor of the alternative and classical complement cascades (Mossakowska *et al.* 1999). The use of APT070 in glaucoma should be investigated by titrating the inhibitor to achieve a level which can block pathogenic complement activation while allowing constitutively active, neuroprotective complement deposition to continue. Inhibition of later proteins in the classical complement cascade may also be considered, however this would not mitigate the opsonising activity of C3b/iC3b.

Extensive evidence in the literature suggests a role for the phosphatidylinositol 3-kinase/akt pathway in the survival of central nervous system cells, and specifically retinal ganglion cells after insult. The use of rapamycin to inhibit the phosphatidylinositol 3-kinase/akt pathway in experimental glaucoma would clarify the role of the pathway in retinal ganglion cell survival in glaucoma.

The use of complement inhibitors with transgenic, glaucomatous mice or rats which have a fluorophore coupled to gene specific to retinal ganglion cells such as beta oestrogen receptor or gamma synuclein (Surgucheva *et al*. 2008; Munaut *et al*. 2001) would allow the phagocytosis of retinal ganglion cell debris by microglia in glaucoma to be quantified. This would demonstrate which specific complement component or components are responsible for the clearance of atrophic retinal ganglion cells in glaucoma.

A useful step in modelling the progress of glaucoma would be the accurate mapping of microglial dynamics in response to an elevation in hydrostatic pressure in a model system. Models exist for the observation of microglia in thin-skull preparations (Tremblay *et al*., 2011; Wake *et al*., 2009) and manometric pressure elevation has been used to simulate the effects of glaucoma (Fortune *et al*. 2011; Pease *et al*. 2006). As visual examination of the optic nerve head is straightforward, it should be possible to observe microglial activity following manometric pressure elevation directly using confocal or two-photon microscopy, if microglia can be labelled with an appropriate fluorophore. With a fluorophore coupled to appropriate regulators on other cell types, this modelling could be used to measure the interaction of microglia with retinal ganglion cells. This technique could provide real-time data on the interactions between microglia and retinal ganglion cells in health

and glaucoma and could provide useful data on the actions of any drugs which hope to mitigate glaucomatous damage by manipulating ganglion cell clearance.

References

Agar, A. *et al*., 2006. Retinal ganglion cell line apoptosis induced by hydrostatic pressure. *Brain research*, 1086(1), pp.191–200.

AGIS, 2000. The advanced glaucoma intervention study (AGIS): 7. the relationship between control of intraocular pressure and visual field deterioration. *American journal of ophthalmology*, 130(4), pp.429–440.

Albon, J. *et al*., 2007. Connective Tissue Structure of the Tree Shrew Optic Nerve and Associated Ageing Changes. *Investigative Ophthalmology*, 48(5), pp.2134–2144.

Allingham, R.R., Liu, Y. & Rhee, D.J., 2009. The genetics of primary open-angle glaucoma: a review. *Experimental eye research*, 88(4), pp.837–44.

Almeida, R.D. *et al*., 2005. Neuroprotection by BDNF against glutamate-induced apoptotic cell death is mediated by ERK and PI3-kinase pathways. *Cell death and differentiation*, 12(10), pp.1329–43.

Anderson, C., 2004. ATP- induced ATP release from astrocytes. *Journal of Neurochemistry*, 88(1), pp.246–256.

Anderson, M.G. *et al*., 2005. High-dose radiation with bone marrow transfer prevents neurodegeneration in an inherited glaucoma. *Proceedings of the National Academy of Sciences of the United States of America*, 102(12), pp.4566–71.

Anderson, M.G. *et al*., 2002. Mutations in genes encoding melanosomal proteins cause pigmentary glaucoma in DBA/2J mice. *Nature genetics*, 30(1), pp.81–5.

Badea, T. *et al*., 2002. RGC-32 increases p34CDC2 kinase activity and entry of aortic smooth muscle cells into S-phase. *The Journal of biological chemistry*, 277(1), pp.502–8.

Badea, T.C. *et al*., 1998. Molecular cloning and characterization of RGC-32, a novel gene induced by complement activation in oligodendrocytes. *The Journal of biological chemistry*, 273(41), pp.26977–81.

Beirowski, B. *et al*., 2005. The progressive nature of Wallerian degeneration in wild-type and slow Wallerian degeneration (WldS) nerves. *BMC neuroscience*, 6, p.6.

Beirowski, B. *et al*., 2008. The WldS gene delays axonal but not somatic degeneration in a rat glaucoma model. *European Journal of Neuroscience*, 28(6), pp.1166–1179.

Ben-Achour, S. & Pascual, O., 2010. Glia: the many ways to modulate synaptic plasticity. *Neurochemistry international*, 57(4), pp.440–5.

Van Bergen, N.J. *et al*., 2009. Recharacterization of the RGC-5 retinal ganglion cell line. *Investigative ophthalmology & visual science*, 50(9), pp.4267–72.

Bertuzzi, F. *et al*., 2009. Concordance of retinal nerve fiber layer defects between fellow eyes of glaucoma patients measured by optical coherence tomography. *American Journal of Ophthalmology*, 148(1), pp.148–154.

Bork, K. & Barnstedt, S.E., 2001. Treatment of 193 episodes of laryngeal edema with C1 inhibitor concentrate in patients with hereditary angioedema. *Archives of internal medicine*, 161(5), pp.714–8.

Bosco, A., Steele, M.R. & Vetter, M.L., 2011. Early microglia activation in a mouse model of chronic glaucoma. *The Journal of comparative neurology*, 519(4), pp.599–620.

Bruce-Keller, A.J., 1999. Microglial-neuronal interactions in synaptic damage and recovery. *Journal of neuroscience research*, 58(1), pp.191–201.

Burgoyne, C.F., 2011. A biomechanical paradigm for axonal insult within the optic nerve head in aging and glaucoma. *Experimental Eye Research*, 93(2), pp.120–132.

Caprioli J, C.A., 2008. Intraocular pressure fluctuation a risk factor for visual field progression at low intraocular pressures in the advanced glaucoma intervention study. *Ophthalmology*, 115(7), pp.1123–1129.e3.

Chidlow, G. *et al*., 2011. The optic nerve head is the site of axonal transport disruption, axonal cytoskeleton damage and putative axonal regeneration failure in a rat model of glaucoma. *Acta neuropathologica*, 121(6), pp.737–51.

Chu, Y. *et al*., 2010. Enhanced synaptic connectivity and epilepsy in C1q knockout mice. *Proceedings of the National Academy of Sciences of the United States of America*, 107(17), pp.7975–80.

Collier, R.J. *et al*., 2011. Complement deposition and microglial activation in the outer retina in light-induced retinopathy: inhibition by a 5-HT1A agonist. *Investigative ophthalmology & visual science*, 52(11), pp.8108–16.

Cone, F.E. *et al*., 2010. Differential susceptibility to experimental glaucoma among 3 mouse strains using bead and viscoelastic injection. *Experimental eye research*, 91(3), pp.415–24.

Cook, C. & Foster, P., 2012. Epidemiology of glaucoma: what's new? *Canadian Journal of Ophthalmology / Journal Canadien d'Ophtalmologie*, 47(3), pp.223–226.

Copland, D. a *et al*., 2010. Systemic and local anti-C5 therapy reduces the disease severity in experimental autoimmune uveoretinitis. *Clinical and experimental immunology*, 159(3), pp.303–14.

Creel, D. & Giolli, R. a, 1976. Retinogeniculate projections in albino and ocularly hypopigmented rats. *The Journal of comparative neurology*, 166(4), pp.445–55.

Crish, S.D. *et al*., 2010. Distal axonopathy with structural persistence in glaucomatous neurodegeneration. *Proceedings of the National Academy of Sciences of the United States of America*, 107(11), pp.5196–201.

Davalos, D. *et al*., 2005. ATP mediates rapid microglial response to local brain injury in vivo. *Nature neuroscience*, 8(6), pp.752–8.

DeLuise, V.P. & Anderson, D.R., 1983. Primary infantile glaucoma (congenital glaucoma). *Survey of ophthalmology*, 28(1), pp.1–19.

Dolga, A.M. *et al*., 2008. TNF-alpha-mediates neuroprotection against glutamate-induced excitotoxicity via NF-kappaB-dependent up-regulation of K2.2 channels. *Journal of neurochemistry*, 107(4), pp.1158–67.

Edelhauser, H.F. *et al*., 1975. Intraocular irrigating solutions. Their effect on the corneal endothelium. *Archives of ophthalmology*, 93(8), pp.648–657.

Farrar, S.M. *et al*., 1989. Risk factors for the development and severity of glaucoma in the pigment dispersion syndrome. *American journal of ophthalmology*, 108(3), pp.223–229.

Fileta, J.B. *et al*., 2008. Efficient estimation of retinal ganglion cell number: a stereological approach. *Journal of neuroscience methods*, 170(1), pp.1–8.

Fivgas, G.D. & Beck, A.D., 1997. Angle-closure glaucoma in a 10-year-old girl. *American journal of ophthalmology*, 124(2), pp.251–253.

Fonseca, M.I. *et al*., 2004. Absence of C1q leads to less neuropathology in transgenic mouse models of Alzheimer's disease. *The Journal of neuroscience : the official journal of the Society for Neuroscience*, 24(29), pp.6457–65.

Fonseca, M.I. *et al*., 2011. Contribution of complement activation pathways to neuropathology differs among mouse models of Alzheimer's disease. *Journal of neuroinflammation*, 8(1), p.4.

Fonseca, M.I. *et al*., 2009. Treatment with a C5aR antagonist decreases pathology and enhances behavioral performance in murine models of Alzheimer's disease. *Journal of immunology (Baltimore, Md. : 1950)*, 183(2), pp.1375–83.

Fortune, B. *et al*., 2011. Deformation of the rodent optic nerve head and peripapillary structures during acute intraocular pressure elevation. *Investigative ophthalmology & visual science*, 52(9), pp.6651–61.

Franco, P.J. *et al*., 2008. Effect of Bacterial Lipopolysaccharide on Ischemic Damage in the Rat Retina. *Investigative Ophthalmology*, 49(10), pp.4604–4612.

Fraser, D. a, Pisalyaput, K. & Tenner, A.J., 2010. C1q enhances microglial clearance of apoptotic neurons and neuronal blebs, and modulates subsequent inflammatory cytokine production. *Journal of neurochemistry*, 112(3), pp.733–43.

Gagnon, J., 1984. Structure and Activation of Complement Components C2 and Factor B. *Philosophical Transactions of the Royal Society B: Biological Sciences*, 306(1129), pp.301–309.

Goldknopf, I.L. *et al*., 2006. Complement C3c and related protein biomarkers in amyotrophic lateral sclerosis and Parkinson's disease. *Biochemical and biophysical research communications*, 342(4), pp.1034–9.

Gonzalez, S.F. *et al*., 2010. Complement-dependent transport of antigen into B cell follicles. *Journal of immunology (Baltimore, Md. : 1950)*, 185(5), pp.2659–64.

Groh, M.J. *et al*., 1996. Influence of age on retinal and optic nerve head blood circulation. *Ophthalmology*, 103(3), pp.529–534.

Gu, B.J. *et al*., 2011. P2X7 Is a Scavenger Receptor for Apoptotic Cells in the Absence of Its Ligand, Extracellular ATP. *Journal of immunology (Baltimore, Md. : 1950)*.

Guo, Y. *et al*., 2010. Retinal Cell Responses to Elevated Intraocular Pressure : A Gene Array Comparison between the Whole Retina and Retinal Ganglion Cell Layer. *Investigative Ophthalmology*.

Gutierrez, H. & Davies, A.M., 2007. A fast and accurate procedure for deriving the Sholl profile in quantitative studies of neuronal morphology. *Journal of neuroscience methods*, 163(1), pp.24–30.

Harold, D. *et al*., 2009. Genome-wide association study identifies variants at CLU and PICALM associated with Alzheimer ' s disease. *Nature Genetics*, 41(10), pp.1088–1093.

Heijl, A. Leske, MC. Bengtsson, B. Hyman, L. Bengtsson, B. Hussein, M., 2002. Reduction of intraocular pressure and glaucoma progression - Results from the early manifest clinical trial. *Arch Ophthalmol*, 120(10), pp.1268–79.

Hernandez, M.R. *et al*., 1989. Age-related changes in the extracellular matrix of the human optic nerve head. *American journal of ophthalmology*, 107(5), pp.476–484.

Hernandez, M.R. *et al*., 2000. Hydrostatic pressure stimulates synthesis of elastin in cultured optic nerve head astrocytes. *Glia*, 32(2), pp.122–136.

Hernandez, M.R., 2000. The optic nerve head in glaucoma: role of astrocytes in tissue remodeling. *Progress in retinal and eye research*, 19(3), pp.297–321.

Hernandez, M.R., Agapova, O.A. & Yang, P., 2002. Differential Gene Expression in Astrocytes from Human Normal and Glaucomatous Optic Nerve Head Analyzed by cDNA Microarray. *Cultures*, 64(September 2001), pp.45– 64.

Hide, I. *et al*., 2000. Extracellular ATP triggers tumor necrosis factor-alpha release from rat microglia. *Journal of neurochemistry*, 75(3), pp.965–72.

Hila, S., Soane, L. & Koski, C., 2001. Sublytic C5b-9-Stimulated Schwann Cell Survival Through PI 3-Kinase- Mediated Phosphorylation of BAD. *Glia*, 67(February), pp.58 – 67.

Hiraoka, M. *et al*., 2012. Ischaemia in the Zinn-Haller circle and glaucomatous optic neuropathy in macaque monkeys. *The British journal of ophthalmology*, 96(4), pp.597–603.

Howell, G.R. *et al*., 2007. Axons of retinal ganglion cells are insulted in the optic nerve early in DBA/2J glaucoma. *The Journal of cell biology*, 179(7), pp.1523–37.

Howell, G.R. *et al*., 2013. Deficiency of complement component 5 ameliorates glaucoma in DBA/2J mice. *Journal of neuroinflammation*, 10(1), p.76.

Howell, G.R. *et al*., 2011a. Molecular clustering identifies complement and endothelin induction as early events in a mouse model of glaucoma. , 121(4).

Howell, G.R. *et al*., 2011b. Molecular clustering identifies complement and endothelin induction as early events in a mouse model of glaucoma. , 121(4).

Howell, G.R., Libby, R.T. & John, S.W.M., 2008. Mouse genetic models: an ideal system for understanding glaucomatous neurodegeneration and neuroprotection. In N. N. O. Carlo Nucci Luciano Cerulli & G. Bagetta, eds. *Glaucoma: An Open Window to Neurodegeneration and Neuroprotection*. Progress in Brain Research. Elsevier, pp. 303–321.

Huang, P., Zhang, S.S.-M. & Zhang, C., 2009. The two sides of cytokine signaling and glaucomatous optic neuropathy. *Journal of ocular biology, diseases, and informatics*, 2(2), pp.78–83.

Huang, Y. *et al*., 2008. Differential roles of phosphatidylinositol 3-kinase/akt pathway in retinal ganglion cell survival in rats with or without acute ocular hypertension. *Neuroscience*, 153(1), pp.214–25.

Huang, Y. *et al*., 2008. Roles of PI3K and JAK pathways in viability of retinal ganglion cells after acute elevation of intraocular pressure in rats with different autoimmune backgrounds. *BMC neuroscience*, 9, p.78.

Hughes, A., 1979. A schematic eye for the rat. *Vision research*, 19(5), pp.569–588.

Ishikawa, M. *et al*., 2010. Effects of acutely elevated hydrostatic pressure in a rat ex vivo retinal preparation. *Investigative ophthalmology & visual science*, 51(12), pp.6414–23.

Jakobs, T.C. *et al*., 2005. Retinal ganglion cell degeneration is topological but not cell type specific in DBA/2J mice. *The Journal of cell biology*, 171(2), pp.313–25.

Kacani, L. *et al*., 2001. C5a and C5a(desArg) enhance the susceptibility of monocyte-derived macrophages to HIV infection. *Journal of immunology (Baltimore, Md. : 1950)*, 166(5), pp.3410–5.

Khalyfa, A. *et al*., 2007. Microarray reveals complement components are regulated in the serum-deprived rat retinal ganglion cell line. *Ambio*, (August 2006), pp.293–308.

Kim, B.S.U. *et al*., 2001. Targeted Disruption of the Myocilin Gene (Myoc) Suggests that Human Glaucoma-Causing Mutations Are Gain of Function. *Society*, 21(22), pp.7707–7713.

Ko, M.L. *et al*., 2001. Patterns of retinal ganglion cell survival after brain-derived neurotrophic factor administration in hypertensive eyes of rats. *Neuroscience letters*, 305(2), pp.139–42.

Kuehn, M.H. *et al*., 2008. Disruption of the complement cascade delays retinal ganglion cell death following retinal ischemia-reperfusion. *Experimental Eye Research*, 87, pp.89–95.

Kuehn, M.H. *et al*., 2006. Retinal synthesis and deposition of complement components induced by ocular hypertension. *Experimental Eye Research*, 83, pp.620–628.

Lambert, J.-C. *et al*., 2009. Genome-wide association study identifies variants at CLU and CR1 associated with Alzheimer's disease. *Nature genetics*, 41(10), pp.1094–9.

Langerman, D.W., 1994. Architectural design of a self-sealing corneal tunnel, single-hinge incision. *Journal of cataract and refractive surgery*, 20(1), pp.84–8.

Langmann, T., 2007. Microglia activation in retinal degeneration. *Journal of leukocyte biology*, 81(6), pp.1345–51.

Lees, V.W., Lukey, C. & Orr, R., 1993. CRITTER: A database for managing research animals. *The Canadian veterinary journal. La revue vétérinaire canadienne*, 34(1), pp.28–32.

Leonard A Levin, Siv F. E. Nilsson, James Ver Hoeve, Samuel Wu, Paul L. Kaufman, A.A., 2011. *Adler's Physiology of the Eye*,

Li, S. *et al*., 2008. Enhanced survival of melanopsin-expressing retinal ganglion cells after injury is associated with the PI3 K/Akt pathway. *Cellular and molecular …*, pp.1095–1107.

Libby, R.T. *et al*., 2005. Inherited glaucoma in DBA/2J mice: Pertinent disease features for studying the neurodegeneration. *Visual Neuroscience*, 22(05), pp.637–648.

Lindberg, J.G., 1989. Clinical investigations on depigmentation of the pupillary border and translucency of the iris in cases of senile cataract and in normal eyes in elderly persons. *Acta ophthalmologica. Supplement*, 190, pp.1–96.

Martinez-de-la-Casa, J., 2009. Comparison of rebound tonometer and Goldmann handheld applanation tonometer in congenital glaucoma. *… of glaucoma*, 18(1), pp.49–52.

Merino, S. *et al*., 1998. Activation of the Complement Classical Pathway (C1q Binding) by Mesophilic Aeromonas hydrophila Outer Membrane Protein. *Infection and Immunity* , 66 (8), pp.3825–3831.

Miyahara, T., 2003. Gene Microarray Analysis of Experimental Glaucomatous Retina from Cynomologous Monkey. *Investigative Ophthalmology & Visual Science*, 44(10), pp.4347–4356.

Monge, J.C. *et al*., 1995. Complement in glomerular C5b-9 activates cytosolic epithelial cells phospholipase A2 in glomerular epithelial cells. *The american Physiological society*, 95, pp.739–749.

Morgan, B.P. & Harris, C.L., 2003. Complement therapeutics ; history and current progress. , 40, pp.159–170.

La Morgia, C. *et al*., 2010. Melanopsin retinal ganglion cells are resistant to neurodegeneration in mitochondrial optic neuropathies. *Brain : a journal of neurology*, pp.2426–2438.

Morrison, J. *et al*., 1995. Structure and composition of the rodent lamina cribrosa. *Experimental eye research*, 60(2), pp.127–35.

Morrison, John C. Moore, C G. Deppmeier Lisa M H. Gold, Bruce G. Meshul Charles K. Johnson, E.C., 1997. A Rat Model of Chronic Pressure-induced Optic Nerve Damage. *Blood*, pp.85–96.

Mossakowska, D. *et al*., 1999. Structure-activity relationships within the N-terminal short consensus repeats (SCR) of human CR1 (C3b/C4b receptor, CD35): SCR 3 plays a critical role in inhibition of the classical and alternative pathways of complement activation. *European journal of immunology*, 29(6), pp.1955–65.

Munaut, C., Lambert, V. & Noël, A., 2001. Presence of oestrogen receptor type β in human retina. *British journal of Ophthalmol ogy*, 85, pp.877–882.

Neely, M.D., Stanwood, G.D. & Deutch, A.Y., 2009. Combination of diOlistic labeling with retrograde tract tracing and immunohistochemistry. *Journal of Neuroscience Methods*, 184, pp.332–336.

Nikolskaya, T. *et al*., 2009. Network analysis of human glaucomatous optic nerve head astrocytes. *BMC medical genomics*, 2, p.24.

Nilsson, U. & Müller-Eberhard, H., 1967. Deficiency of the fifth component of complement in mice with an inherited complement defect. *The Journal of experimental …*.

Nolte, C. *et al*., 1996. Complement 5a controls motility of murine microglial cells in vitro via activation of an inhibitory G-protein and the rearrangement of the actin cytoskeleton. *Neuroscience*.

Pease, M., Hammond, J. & Quigley, H., 2006. Manometric calibration and comparison of TonoLab and TonoPen tonometers in rats with experimental glaucoma and in normal mice. *Journal of glaucoma*, 15(6), pp.512–519.

Peitsch, M.C. & Tschopp, J., 1991. Assembly of macromolecular pores by immune defense systems. *Current opinion in cell biology*, 3(4), pp.710–6.

Perry, V.H. & O'Connor, V., 2008a. C1q: the perfect complement for a synaptic feast? *Nature reviews. Neuroscience*, 9(11), pp.807–11.

Perry, V.H. & O'Connor, V., 2008b. C1q: the perfect complement for a synaptic feast? *Nature reviews. Neuroscience*, 9(11), pp.807–11.

Prashar, A. *et al*., 2007. Measurement of intraocular pressure (IOP) in chickens using a rebound tonometer : Quantitative evaluation of variance due to position inaccuracies. *Experimental Eye Research*, 85, pp.563–571.

Quigley, H. a & Broman, a T., 2006a. The number of people with glaucoma worldwide in 2010 and 2020. *The British journal of ophthalmology*, 90(3), pp.262–7.

Quigley, H. a & Broman, a T., 2006b. The number of people with glaucoma worldwide in 2010 and 2020. *The British journal of ophthalmology*, 90(3), pp.262–7.

Quigley, H., Addicks, E. & Green, W., 1982. Optic nerve damage in human glaucoma: III. quantitative correlation of nerve fiber loss and visual field defect in glaucoma, ischemic neuropathy, papilledema, and toxic neuropathy. *Archives of Ophthalmology*, 100(1), pp.135–146.

Quigley, H. & Anderson, D., 1976. The dynamics and location of axonal transport blockade by acute intraocular pressure elevation in primate optic nerve. *Investigative Ophthalmology & Visual Science*, pp.606–616.

Quigley, H.A. *et al*., 2000. Retrograde Axonal Transport of BDNF in Retinal Ganglion Cells Is Blocked by Acute IOP Elevation in Rats. *Investigative Ophthalmology*, 41(11), pp.3460–3466.

Quigley, H.A. & Addicks, E.M., 1980a. Chronic experimental glaucoma in primates. *Methods*, pp.126–136.

Quigley, H.A. & Addicks, E.M., 1980b. Chronic experimental glaucoma in primates. *Transport*.

Ramaglia, V. *et al*., 2007. The Membrane Attack Complex of the Complement System Is Essential for Rapid Wallerian Degeneration. , 27(29), pp.7663–7672.

Reigada, D. *et al*., 2009. the Retina : Possible Role for Pannexin Hemichannels. *Control*, 157(2), pp.396–404.

Resnikoff, S. *et al*., 2004. Policy and Practice Global data on visual impairment in the year 2002. *Bulletin of the World Health Organization*, 012831(04).

Rhodes, K.E. & Fawcett, J.W., 2004. Chondroitin sulphate proteoglycans: preventing plasticity or protecting the CNS? *Journal of anatomy*, 204(1), pp.33–48.

Robin AL, P.I.P., 1982. Argon laser peripheral iridotomies in the treatment of primary angle closure glaucoma: Long-term follow-up. *Archives of Ophthalmology*, 100(6), pp.919–923.

Roos, A. & Daha, M.R., 2002. Antibody-mediated activation of the classical complement pathway in xenograft rejection. *Transplant immunology*, 9(2-4), pp.257–70.

Rus, H. *et al*., 2006. Complement activation in autoimmune demyelination: dual role in neuroinflammation and neuroprotection. *Journal of neuroimmunology*, 180(1-2), pp.9–16.

Russell, M. S., Burch, R.L., 1959. *The principles of humane experimental technique.*, Methuen.

Salmon, J.F., 1993. Long-Term Intraocular Pressure Control After Nd-YAG Laser Iridotomy in Chronic Angle-Closure Glaucoma. *Journal of glaucoma*, 2(4), pp.291–296.

Samsel, P.A. *et al*., 2011. A novel method for the induction of experimental glaucoma using magnetic microspheres. *Investigative Ophthalmology & Visual Science*, 52(3), pp.1671–1675.

Sappington, R.M. *et al*., 2010. The Microbead Occlusion Model : A Paradigm for Induced Ocular Hypertension in Rats and Mice. *Investigative Ophthalmology*, 51(1).

Schjeide, B.-M.M. *et al*., 2011. The role of clusterin, complement receptor 1, and phosphatidylinositol binding clathrin assembly protein in Alzheimer disease risk and cerebrospinal fluid biomarker levels. *Archives of general psychiatry*, 68(2), pp.207–13.

Shen, Y. *et al*., 2001. Complement activation by neurofibrillary tangles in Alzheimer's disease. *Neuroscience Letters*, 305(3), pp.165–168.

Shepard, A.R. *et al*., 2007. Glaucoma-causing myocilin mutants require the Peroxisomal targeting signal-1 receptor (PTS1R) to elevate intraocular pressure. *Human molecular genetics*, 16(6), pp.609–17.

Singhrao, S.K. *et al*., 1999. Increased complement biosynthesis by microglia and complement activation on neurons in Huntington's disease. *Experimental neurology*, 159(2), pp.362–76.

Soane, L. *et al*., 2010. 3-Kinase/Akt Pathway Through Phosphatidylinositol from Death by Regulating Bad Complex Protects Oligodendrocytes C5b-9 Terminal Complement. *Analysis*.

Souza, D.G. *et al*., 2005. APT070 (Mirococept), a membrane-localised complement inhibitor, inhibits inflammatory responses that follow intestinal ischaemia and reperfusion injury. *British journal of pharmacology*, 145(8), pp.1027–34.

Sperlágh, B. & Illes, P., 2007. Purinergic modulation of microglial cell activation. *Purinergic signalling*, 3(1-2), pp.117–27.

Stasi, K. *et al*., 2006. Complement component 1Q (C1Q) upregulation in retina of murine, primate, and human glaucomatous eyes. *Investigative ophthalmology & visual science*, 47(3), pp.1024–9.

Stevens, B. *et al*., 2007. The Classical Complement Cascade Mediates CNS Synapse Elimination. *Cell*, pp.1164–1178.

Stevens, B.E., 2011. Microglia and the complement system: Unveiling novel mechanisms of synaptic pruning in the developing brain. In *SfN 2011*.

Stone, E.M. *et al*., 1997. Identification of a Gene That Causes Primary Open Angle Glaucoma. *Science* , 275 (5300), pp.668–670.

Sun, W., Li, N. & He, S., 2002. Large-scale morphological survey of mouse retinal ganglion cells. *The Journal of comparative neurology*, 451(2), pp.115–26.

Surgucheva, I. *et al*., 2008. Gamma-synuclein as a marker of retinal ganglion cells. *Molecular vision*, 14(April), pp.1540–8.

Takatsuji, K. *et al*., 1988. Selective loss of retinal ganglion cells in albino avian glaucoma. *Investigative ophthalmology & visual science*, 29(6), pp.901–9.

Tamm, E.R., 2002. Myocilin and glaucoma : facts and ideas. *Progress in Retinal and Eye Research*, 21, pp.395–428.

Tegla, C. a *et al*., 2009. Neuroprotective effects of the complement terminal pathway during demyelination: implications for oligodendrocyte survival. *Journal of neuroimmunology*, 213(1-2), pp.3–11.

Tezel, G. *et al*., 2010. Oxidative stress and the regulation of complement activation in human glaucoma. *Investigative ophthalmology & visual science*, 51(10), pp.5071–82.

Tezel, G. & Wax, M.B., 2000. Increased production of tumor necrosis factor-alpha by glial cells exposed to simulated ischemia or elevated hydrostatic pressure induces apoptosis in cocultured retinal ganglion cells. *The Journal of neuroscience : the official journal of the Society for Neuroscience*, 20(23), pp.8693–700.

Thielens, N.M. *et al*., 1999. Structure and functions of the interaction domains of C1r and C1s: keystones of the architecture of the C1 complex. *Immunopharmacology*, 42(1-3), pp.3–13.

Toutenburg, H., 1975. Hollander, M., D. A. Wolfe: Nonparametric statistical methods. John Wiley & Sons, New York-Sydney-Tokyo-Mexico City 1973. 503 S., 9.50. *Biometrische Zeitschrift*, 17(8), p.526.

Tremblay, M.-E. *et al*., 2011. The Role of Microglia in the Healthy Brain. *Journal of Neuroscience*, 31(45), pp.16064–16069.

Tremblay, M.-È., Lowery, R.L. & Majewska, A.K., 2010. Microglial interactions with synapses are modulated by visual experience. *PLoS biology*, 8(11), p.e1000527.

Vecino, E. & Urcola, J.H., 2006. Three experimental glaucoma models in rats : Comparison of the effects of intraocular pressure elevation on retinal ganglion cell size and death. *Animals*, 83.

Wake, H. *et al*., 2009. Resting microglia directly monitor the functional state of synapses in vivo and determine the fate of ischemic terminals. *The Journal of neuroscience : the official journal of the Society for Neuroscience*, 29(13), pp.3974–80.

Weber, a J., Kaufman, P.L. & Hubbard, W.C., 1998a. Morphology of single ganglion cells in the glaucomatous primate retina. *Investigative ophthalmology & visual science*, 39(12), pp.2304–20.

Weber, a J., Kaufman, P.L. & Hubbard, W.C., 1998b. Morphology of single ganglion cells in the glaucomatous primate retina. *Investigative ophthalmology & visual science*, 39(12), pp.2304–20.

Weber, A.J. & Harman, C.D., 2005. Structure – Function Relations of Parasol Cells in the Normal and Glaucomatous Primate Retina. *Investigative Ophthalmology*, 46(9), pp.3197–3207.

Weber, A.J. & Zelenak, D., 2001. Experimental glaucoma in the primate induced by latex microspheres. , 111, pp.39 – 48.

Webster, S., Barr, S.O. & Rogers, J., 1994. Enhanced Aggregation and p Structure of Amyloid p Peptide After Coincubation With ClQ. *Neuroscience Letters*, 448456.

Webster, S.D. *et al*., 2000. Complement component C1q modulates the phagocytosis of Abeta by microglia. *Experimental neurology*, 161(1), pp.127–38.

Weerth, S.H. *et al*., 2003. Complement C5 in experimental autoimmune encephalomyelitis (EAE) facilitates remyelination and prevents gliosis. *The American journal of pathology*, 163(3), pp.1069–80.

Wenzel, A. *et al*., 2005. Molecular mechanisms of light-induced photoreceptor apoptosis and neuroprotection for retinal degeneration. *Progress in retinal and eye research*, 24(2), pp.275–306.

Whitmore, A. V, Libby, R.T. & John, S.W.M., 2005. Glaucoma: Thinking in new ways—a rôle for autonomous axonal self-destruction and other compartmentalised processes? *Progress in Retinal and Eye Research*, 24(6), pp.639–662.

Wu, L., Vadakkan, K.I. & Zhuo, M.I.N., 2007. ATP-Induced Chemotaxis of Microglial Processes Requires P2Y Receptor-Activated Initiation of Outward Potassium Currents. *Image (Rochester, N.Y.)*, 821(February), pp.810–821.

Yamada, T., McGeer, P.L. & McGeer, E.G., 1992. Lewy bodies in Parkinson's disease are recognized by antibodies to complement proteins. *Acta Neuropathologica*, 84(1), pp.100–104.

Yang, P. *et al*., 2004a. DNA microarray analysis of gene expression in human optic nerve head astrocytes in response to hydrostatic pressure. *Physiological genomics*, 17(2), pp.157–69.

Yang, P. *et al*., 2004b. DNA microarray analysis of gene expression in human optic nerve head astrocytes in response to hydrostatic pressure. *Physiological genomics*, 17(2), pp.157–69.

Ying, S.C. *et al*., 1993. Human serum amyloid P component oligomers bind and activate the classical complement pathway via residues 14-26 and 76-92 of the A chain collagen-like region of C1q. *Journal of immunology (Baltimore, Md. : 1950)*, 150(1), pp.169–76.

Zwaka, T.P. *et al*., 2002. Complement and dilated cardiomyopathy: a role of sublytic terminal complement complex-induced tumor necrosis factor-alpha synthesis in cardiac myocytes. *The American journal of pathology*, 161(2), pp.449–57.

Appendices

Appendix 1 – Masking macro

In order to reduce observer bias my images were masked so that I had no knowledge of the source of the image during Sholl analysis. To that end I developed the following macro for the ImageJ platform. The macro effectively masks images by opening each of the images in a specified folder or directory in turn within the system memory, so that the images are not displayed to the user. The user is not displayed the images at any point and is effectively masked themselves, however as I had developed the macro and I was investigating the data I asked a third party to implement the masking macro, for this I must thank Dr Hannah Jones.

Each file is renamed with a random number of a length specified by the user. A key file is generated in the source directory containing all of the original file names and all of the masked file names as well as the date and time the key file was produced in a comma-delimited file. This file can be read by Microsoft Excel which makes incorporation of the unmasked data into results obtained from the masked data straightforward.

The macro does contain an option for 'Remote unmasking' wherein an investigator could automatically rename the masked files using the key file. However I felt this was unnecessary and for my purposes therefore it was not implemented and is not functional.

```
macro "All Files masking[n0]" {

/////First dialog box - this sets the input and output folders, as well
as the length of the random numbers generated and the output file type.
```

```
Dialog.create("First...") ;

Dialog.addMessage("Remove files not for masking from the source folder."+"\n"+"Then select source folder, followed by destination folder") ;

Dialog.addNumber("Length of random numbers", 5) ;

Dialog.addString("Output file type", ".tiff");

Dialog.addCheckbox("Record user name in key file",0);

Dialog.addCheckbox("Filter file types",0);

Dialog.addCheckbox("Produce array files for remote unmasking (Experimental)",0);

Dialog.show();

user = Dialog.getCheckbox();

filter = Dialog.getCheckbox();

io =  Dialog.getCheckbox();

test = 1;

if (user==1) {

      username = getString("User name", "Name");

}

origin = getDirectory("C:\ ");

dest = getDirectory("C:\ ");

lista = getFileList(origin) ;
```

```
exponent = Dialog.getNumber();

power = pow(10,exponent);

file = Dialog.getString();

key = "key";

appendkey = 0;

/////Creates the log file in the source (origin) directory and adds approriate headers, detects if log file is already present and adds an option to overwrite or append if so.  Note the deliminator is a comma. Also checks for key files already present.

panic = File.exists(origin+"key");

if (panic==1) {

     overwrite = getBoolean("There is already a key file present.\nOverwrite?");

     if (overwrite==0) {

          appendkey = getBoolean("Append new key to old file?");

               if (appendkey==0) {

                    key = getString("Select name for new key file", "Key-1");

               }

          }
}

if (appendkey==1) {

     File.append("Masking Number"+","+"Original Name", origin+key);
```

```
	}

else {

	File.saveString("Masking list.  ", origin+key);

}

File.append("\n"+"Masked Number"+","+"Original Name", origin+key);

/////In batch mode, opens each file in the source folder, generates a random number and saves the file as that number in the destination (dest) folder.  Then appends the log file with the original file name (lista[i]) and the random number.

setBatchMode(true) ;

i=0;

oops = "-";

showProgress(i/lista.length);

for (i=0; i<lista.length; i++) {

	showProgress(i/lista.length);

	if (filter==1) {

		keyf = startsWith(lista[i],key);

		tiff = endsWith(lista[i],".tiff");

		tif = endsWith(lista[i],"tif");

		png = endsWith(lista[i],".png");

		jpeg = endsWith(lista[i],".jpeg");

		jpg = endsWith(lista[i],".jpg");
```

```
            bmp = endsWith(lista[i],".bmp");

            lsm = endsWith(lista[i],".lsm");

            gif = endsWith(lista[i],".gif");

            avi = endsWith(lista[i],".avi");

            raw = endsWith(lista[i],".raw");

            txt = endsWith(lista[i],".txt");

            test = keyf+tiff+tif+png+jpeg+jpg+bmp+lsm+gif+avi+raw+txt;

      }

      if (test!=0) {

            open(origin+lista[i]) ;

            if (nImages==0) {

                  oops = oops +"'"+ lista[i] +"'"+   " Is not an image
file and was skipped\n";

                  selectWindow(lista[i]);

                  run ("Close");

            }

            else {

                  num = lista[i] ;

                  ran=(random * power);

                  ran=round(ran);
```

```
                saveAs(file, dest + ran) ;

                File.append(ran+","+num, origin+key);

                if(io==1) {

                      File.append(ran, origin+"Masked Number");

                      File.append(num, origin+"Original Name");

                      }

                close() ;

            }

      } else {

      oops = oops + lista[i] +  " was filtered. \n";

      }

}

mod = File.dateLastModified(origin+key);

if (user==1) {

      File.append("Key file generated on," + mod + "\nUsername," +
username, origin+key);

} else {

      File.append("Key file generated on," + mod, origin+key);

}

call("java.lang.System.gc");
```

```
/////Makes a noise and then tells you it has finished, as well as if it
had to skip any files.


beep() ;


Dialog.create("Status") ;
Dialog.addMessage("Errors = " + oops);
Dialog.addMessage("Finished") ;
Dialog.show() ;


}
```

Appendix 2 – Sholl processing macro

The images obtained from the LSM510 confocal microscope are inherently incompatible with the Sholl analysis Matlab script developed by Gutierrez & Davies (2007), hence I developed the following macro for the ImageJ platform to automatically convert images to 8-bit, jpeg images with a 100µm scale bar, scale bars of other sizes produced aberrant results.

```
macro "Process .LSM files for Gutierez Sholl plugin [n1]" {


///Dialog.create("Source");
///Dialog.addMessage("Select source folder");
///Dialog.addNumber("Start image", 1);
///Dialog.addCheckbox("Scale bar", true);
///Dialog.show();

///sclbr = Dialog.getCheckbox();

///n=Dialog.getNumber();

sclbr=1;

n=1;

origin = getDirectory("C:\ ");

dest = getDirectory("C:\ ");

lista = getFileList(origin) ;

i=0;

for (i=0; i<lista.length; i++) {

open(origin+lista[i]) ;
```

```
run("8-bit");

waitForUser("Check position of Cell") ;

Dialog.create("ROI");
Dialog.addNumber("Start of Stack", 1);
Dialog.addNumber("End of Stack", nSlices);
Dialog.show();

start = Dialog.getNumber;

stop = Dialog.getNumber;

col = Dialog.getString();

title = getTitle();

      run("Input/Output...", "jpeg="+100);
        saveAs("Jpeg", dest + title);

      close();

      call("java.lang.System.gc");

}



selectWindow(pre + title) ;


run("8-bit");

known =(20/zoom);

run("Z    Project...",    "start=start    stop=stop    projection=[Max
Intensity]");
```

```
run("Set Scale...", "distance=2.602 known=known pixel=1 unit=µm global");



if (sclbr==1) {


     run("Scale Bar...", "width=100 height=5 font=18 color=White background=Black location=[Lower Right] bold hide");


}


call("java.lang.System.gc");


 run("Input/Output...", "jpeg="+100);
     saveAs("Jpeg", dest + title);



close();
close();
close();
close();


call("java.lang.System.gc");


}
}



beep();


Dialog.create("Status");
Dialog.addMessage("Finished");
Dialog.show();
```